AKADEMIA GÓRNICZO-HUTNICZA IM. STANISŁAWA STASZICA W KRAKOWIE

DZIEDZINA: NAUK ŚCISŁYCH I PRZYRODNICZYCH

DYSCYPLINA: NAUKI O ZIEMI I ŚRODOWISKU

ROZPRAWA DOKTORSKA

Identyfikacja struktur sejsmogennych na podstawie analizy indukowanej emisji sejsmicznej z wykorzystaniem algorytmów uczenia maszynowego

Autor: mgr inż. **Elżbieta Węglińska**

Promotor rozprawy: prof. dr hab. inż. **Andrzej Leśniak**

Praca wykonana: Akademia Górniczo-Hutnicza im. Stanisława Staszica w Krakowie, Wydział Geologii, Geofizyki i Ochrony Środowiska, Katedra Geoinformatyki i Informatyki Stosowanej

Kraków, 2024

AGH UNIVERSITY OF KRAKOW

FIELD OF NATURAL SCIENCE

SCIENTIFIC DISCIPLINE: EARTH AND RELATED ENVIRONMENTAL SCIENCES

DOCTORAL THESIS

Identification of seismogenic structures based on the analysis of induced seismic emission using machine learning algorithms

Author: **Elżbieta Węglińska**

Supervisor: prof. **Andrzej Leśniak**

Completed in: AGH University of Krakow, Faculty of Geology, Geophysics and Environmental Protection, Department of Geoinformatics and Applied Computer Science

Krakow, 2024

Praca była realizowana i częściowo finansowana w ramach:

- Projektu Inicjatywa Doskonałości - Uczelnia Badawcza, Finansowanie staży zagranicznych młodych pracowników i doktorantów. W ramach projektu uzyskałam finansowanie na krótkoterminowy staż w elektrowni w Soultz-sous-Forets we Francji oraz firmie ES Geothermie (termin realizacji 30.09-2.10.2021)
- Badań statutowych Katedry Geoinformatyki i Informatyki Stosowanej, numer grantu 16.16.140.315

Oświadczenie autora pracy

Oświadczam, że niniejsza rozprawa doktorska została napisana przeze mnie samodzielnie i nie zawiera treści uzyskanych w sposób niezgodny z obowiązującymi przepisami prawa.

Oświadczam ponadto, że przedstawiona praca nie była wcześniej przedmiotem procedur związanych z uzyskaniem stopnia ani tytułu zawodowego na uczelni wyższej.

Oświadczam również, że niniejsza praca jest identyczna z załączoną wersją elektroniczną.

12.06.2024 .... Węglińska ....

Data Podpis autora pracy

Spis treści

Podziękowania

Pragnę złożyć serdeczne podziękowania mojemu Promotorowi, prof. dr hab. inż. Andrzejowi Leśniakowi, za nieocenioną pomoc udzieloną w trakcie przygotowania rozprawy doktorskiej. Dziękuję za ogrom przekazanej mi wiedzy, za wszystkie rozmowy oraz każdą konstruktywną krytykę, które wpłynęły na ostateczny kształt mojej rozprawy. Jestem również wdzięczna za anielską cierpliwość i wsparcie okazane mi podczas wieloletniej opieki naukowej.

W sposób szczególny dziękuję wszystkim współautorom publikacji, które są podstawą niniejszej rozprawy doktorskiej: prof. dr hab. inż. Andrzejowi Leśniakowi, dr Katarzynie Mirek, dr inż. Andrzejowi Pasternackiemu oraz dr inż. Pawłowi Wandyczowi.

Dziękuję również wszystkim pracownikom Katedry Geoinformatyki i Informatyki Stosowanej za stworzenie wspaniałej atmosfery w pracy naukowej. W szczególności dziękuję dr hab. inż. Tomaszowi Dankowi, prof. AGH oraz dr inż. Mateuszowi Zarębie za współpracę przy innych projektach badawczych oraz motywację, które pozytywnie wpłynęły na moją pracę naukową.

Szczególne podziękowania należą się także mojemu Mężowi oraz moim Rodzicom, bez których wsparcia ta praca by nie powstała.

Dziękuję!

Streszczenie

Praca doktorska prezentuje heurystyczną procedurę złożoną z metod służących do identyfikacji struktur sejsmogennych w chmurze zlokalizowanych zjawisk sejsmicznych. Zaproponowana procedura składa się z algorytmów nienadzorowanego uczenia maszynowego oraz optymalizacji statystycznej umożliwiającej zwiększenie dokładności identyfikacji klastrów w chmurze zjawisk sejsmicznych. Znajomość lokalizacji klastrów jest niezbędna do oceny ryzyka sejsmicznego oraz efektywności prac w górnictwie podziemnym oraz przy szczelinowaniu hydraulicznym.

Głównym celem rozprawy doktorskiej jest prezentacja uniwersalności zaproponowanego rozwiązania identyfikacji struktur sejsmogennych dla emisji sejsmicznej wywołanej różnymi czynnikami antropogenicznymi. W rozprawie wskazano na skuteczność metody dla klasteryzacji zjawisk sejsmicznych indukowanych eksploatacją górniczą węgla kamiennego w kopalni Bobrek, szczelinowaniem hydraulicznym na polu geotermalnym Soultz-sous-Forets oraz szczelinowaniem hydraulicznym związanym z wydobyciem gazu łupkowego na polu Wysin. W celu zaprezentowania możliwości proponowanego algorytmu przedstawiono wyniki przetwarzania dla syntetycznego modelu chmury zjawisk sejsmicznych. Utworzenie modelu lokalizacji zjawisk sejsmicznych zostało zainspirowane rzeczywistymi danymi, odzwierciedlającymi faktyczne występowanie zjawisk mikrosejsmicznych podczas szczelinowania hydraulicznego.

Procedura służąca identyfikacji struktur sejsmogennych obejmuje dwie metody: zapadania (ang. *collapsing*) oraz klasteryzację. Metoda zapadania powoduje zmniejszenie rozproszenia chmury zjawisk sejsmicznych, które jest spowodowane przez błędy lokalizacji. Metody klasteryzacji oparte na gęstości danych umożliwiają wyznaczenie obszarów o zwiększonej intensywności występowania zjawisk w stosunku do otoczenia. Dodatkowo, wykorzystano techniki umożliwiające precyzyjne wyznaczenie objętości chmury zjawisk sejsmicznych.

W badaniach pokazano, że zastosowanie metody zapadania oraz klasteryzacji opartej na gęstości zjawisk umożliwia obliczenie dokładniejszej i bardziej realistycznej objętości zaburzonej struktury sejsmogennej. Przetworzenie danych mikrosejsmicznych z kopalni Bobrek pozwoliło zidentyfikować klastry zjawisk sejsmicznych, które są związane zarówno z wcześniej eksploatowanymi pokładami jak i z lokalnymi nieciągłościami tektonicznymi. Dla przetworzonego rozkładu zjawisk sejsmicznych na polu Wysin zidentyfikowano klastry, których kierunek jest bardziej zbliżony do kierunku maksymalnego naprężenia poziomego niż dla orginalnych danych. Wykazano również, że skały mają tendencję do preferencyjnego pękania w obszarach bardziej kruchych. Użycie metody zapadania, klasteryzacji oraz analizy czaso-

przestrzennej ewolucji klastrów na polu Soultz-sous-Forets pozwoliło wskazać zjawiska sejsmiczne potencjalnie związane z hydraulicznym przepływem płynu.

Słowa kluczowe: *sejsmiczność indukowana, struktury sejsmogenne, klasteryzacja, metoda zapadania*

Abstract

The dissertation introduces a heuristic procedure for identifying seismogenic structures in a cloud of localized seismic events. The proposed procedure consists of unsupervised machine learning algorithms and statistical optimization technique to enhance the accuracy of cluster identification in a cloud of seismic events. Understanding the location of clusters is essential for assessing seismic risk and evaluating the effectiveness of operations in underground mining and hydraulic fracturing.

The main objective of the dissertation is to demonstrate the universality of the proposed solution for identifying seismogenic structures in seismic emissions caused by various anthropogenic factors. The dissertation demonstrates the effectiveness of the proposed method for clustering seismic events induced by coal mining operations at the Bobrek mine, hydraulic fracturing at the Soultz-sous-Forets geothermal field, and hydraulic fracturing associated with shale gas production at the Wysin field. To showcase the algorithm's capabilities, the results of processing a synthetic cloud model of seismic events are presented. This synthetic model was inspired by real data reflecting the actual occurrence of microseismic events during hydraulic fracturing.

The procedure for identifying seismogenic structures includes two methods: collapsing and clustering. The collapsing method reduces the scattering of the cloud of seismic events, which is caused by localization errors. Density-based clustering methods allow the determination of areas with increased event intensity relative to the surroundings. Additionally, the research utilized algorithms aimed at precisely determining the volume of the seismic event cloud.

The research demonstrated that the application of the collapsing method and density-based clustering enables the calculation of a more accurate and realistic volume of the disturbed seismogenic structure. Processing microseismic data from the Bobrek mine allowed the identification of seismic event clusters associated with both previously exploited seams and local tectonic discontinuities. For the processed distribution of seismic events in the Wysin field, clusters were identified whose direction is more aligned with the direction of maximum horizontal stress than in the original data. It was also shown that rocks tend to preferentially fracture in more brittle areas. The use of the collapsing method, clustering, and spatiotemporal analysis of cluster evolution in the Soultz-sous-Forêts field identified seismic events potentially associated with hydraulic fluid flow.

Keywords: *induced seismicity, seismogenic structures, clustering, collapsing*

Struktura pracy

Niniejsza rozprawa doktorska składa się z 8 rozdziałów. W rozdziale 1 znajduje się wprowadzenie oraz tezy badawcze. Cel pracy jest omówiony w rozdziale 2. W rozdziale 3 przedstawiono skrótowo metodykę badań. W rozdziale 3.1 omówiono metodę zapadania. Rozdział 3.2 stanowi opis metod identyfikacji struktur sejsmogennych, na które składają się metody klasteryzacji chmury punktów w przestrzeni trójwymiarowej (3D). W rozdziale 3.3 przedstawiono użyte metody obliczania objętości struktury wyznaczonej przez lokalizacje zjawisk sejsmicznych.

Właściwa treść rozprawy doktorskiej została przedstawiona w 4 publikacjach naukowych indeksowanych w bazie Web of Science, które są przedstawione w załącznikach. W rozdziale 4 omówiono publikacje, będące cyklem artykułów naukowych stanowiących realizację postawionych tez badawczych. Rozdział 5 stanowi podsumowanie uzyskanych wyników badań przez doktoranta. Spis pozycji literaturowych znajduje się w rozdziale 6. Oświadczenie współautorów publikacji dotyczące udziału procentowego, jak również wyszczególnienie udziału doktoranta zostały przedstawione w rozdziale 7. Pełna treść artykułów została zamieszczona w formie załączników (rozdział 8).

[Z1] Elżbieta Węglińska, Andrzej Leśniak. 2024. A novel approach to identifying seismogenic structures and estimating reservoir volume based on synthetic cloud of seismicity induced by hydraulic fracturing. Acta Geodaetica et Geophysica, doi: 10.1007/s40328-024-00442-1

[Z2] Andrzej Leśniak, **Elżbieta Śledź**, Katarzyna Mirek. 2020. Detailed Recognition of Seismogenic Structures Activated during Underground Coal Mining: A Case Study from Bobrek Mine, Poland. Energies 13(18), 4622, doi: 10.3390/en13184622

[Z3] Elżbieta Węglińska, Andrzej Leśniak. 2021. Induced Seismicity and Detailed Fracture Mapping as Tools for Evaluating HDR Reservoir Volume. Energies 14(9), 2593, doi: 10.3390/en14092593

[Z4] Elżbieta Węglińska, Andrzej Leśniak, Andrzej Pasternacki, Paweł Wandycz. 2024. Mapping a fracture network formed by hydraulic fracturing in a shale gas reservoir. Geology, Geophysics and Environment 50(3), 213-230, doi: 10.7494/geol.2024.50.3.213

1. Wprowadzenie

Znajomość lokalizacji zjawisk sejsmicznych jest kluczowa dla identyfikacji struktur sejsmogennych. W pracy zaprezentowano integrację metod mających na celu jak najdokładniejsze określenie miejsca występowania tych struktur w górotworze.

W pracy doktorskiej zatytułowanej: **"Identyfikacja struktur sejsmogennych na podstawie analizy indukowanej emisji sejsmicznej z wykorzystaniem algorytmów uczenia maszynowego"** postawiono następujące tezy badawcze:

- Zastosowanie metody zapadania zjawisk mikrosejsmicznych indukowanych podczas szczelinowania oraz eksploatacji podziemnej złóż powoduje zwiększenie dokładności identyfikacji struktur generujących wstrząsy
- Integracja metod zwiększających dokładność lokalizacji z nienadzorowanym uczeniem maszynowym pozwala na zwiększenie możliwości identyfikacji klastrów w chmurze emisji mikrosejsmicznej
- Zapadanie zjawisk mikrosejsmicznych i identyfikacja klastrów z wykorzystaniem metod uczenia maszynowego umożliwia wyznaczenie objętości aktywnej struktury zaburzonej przez proces szczelinowania

W rozprawie doktorskiej pokazano uniwersalność zaproponowanego algorytmu dla emisji sejsmicznej spowodowanej różnymi czynnikami antropogenicznymi. Wykazano, że zaprezentowana metoda identyfikacji struktur sejsmogennych może być skutecznie stosowana w różnych chmurach emisji sejsmicznej. W prezentowanej rozprawie doktorskiej przedstawiono skuteczność metody dla zjawisk sejsmicznych indukowanych eksploatacją górniczą węgla kamiennego (Leśniak i in., 2020; Węglińska i Leśniak, 2022), szczelinowaniem hydraulicznym związanym z udostępnianiem zbiornika geotermalnego (Węglińska i Leśniak, 2021) oraz wydobyciem gazu łupkowego (Węglińska i in., 2024). Praca opiera się na czterech publikacjach, które zostały przedstawione w logicznej kolejności. W pierwszej kolejności omówiono artykuł zawierający analizę z użyciem danych syntetycznych (Węglińska i Leśniak, 2024). Kolejne publikacje dotyczą realizacji tez badawczych dla rzeczywistych chmur emisji sejsmicznych indukowanych górnictwem podziemnym (Leśniak i in., 2020) oraz szczelinowaniem hydraulicznym (Węglińska i Leśniak, 2021; Węglińska i in., 2024).

2. Cel pracy

Prezentacja proponowanej metody identyfikacji struktur sejsmogennych została w pierwszej kolejności zilustrowana w oparciu o dane syntetyczne, co pozwoliło na zaprezentowanie poprawności zastosowanych algorytmów. W dalszej części przedstawiono rezultaty zastosowania tych metod przy eksploatacji górniczej węgla kamiennego, szczelinowaniu hydraulicznym związanym z udostępnianiem złoża geotermalnego oraz wydobyciem gazu łupkowego.

Celem pracy było:

– Zwiększenie dokładności klasteryzacji chmury zlokalizowanych zjawisk sejsmicznych z użyciem metody zapadania

– Identyfikacja klastrów zjawisk sejsmicznych zlokalizowanych przy: eksploatacji węgla kamiennego w kopalni Bobrek w Bytomiu, szczelinowaniu hydraulicznym na polu geotermalnym Soultz-sous-Forets w północno-wschodniej Francji oraz na polu Wysin zlokalizowanym w województwie pomorskim

– Integracja metody zapadania, klasteryzacji opartej na gęstości zjawisk oraz obliczania objętości chmury punktów

Oryginalne osiągnięcia doktorantki:

– Dokonano krytycznego przeglądu literatury światowej omawiającej problematykę identyfikacji struktur sejsmogennych wewnątrz chmury indukowanych zjawisk sejsmicznych

– Zaproponowano algorytm pozwalający na zwiększenie efektywności klasteryzacji wewnątrz chmury emisji mikrosejmicznej

– Zidentyfikowano strefy sejsmogenne na podstawie chmur emisji zarejestrowanych przy: eksploatacji węgla kamiennego w kopalni Bobrek, szczelinowaniu hydraulicznym na polu geotermalnym Soultz-sous-Forets oraz na polu Wysin

– Wykonano porównanie zidentyfikowanych stref sejsmogennych w szczelinowanym otworze Wysin 2H/2Hbis zestawiając je z mapami prawdopodobieństwa występowania danej klasy wskaźnika kruchości

– Zaproponowano metodę automatycznego doboru promienia sąsiedztwa przy klasteryzacji zjawisk sejsmicznych

– Wykonano ocenę efektywności zintegrowanych metod na syntetycznych danych sejsmiczności indukowanej

– Wyznaczono objętość chmury zjawisk sejsmicznych po zwiększeniu rozdzielczości chmury oraz odrzuceniu zjawisk uznanych za szum

3. Podsumowanie metod badawczych

W tym rozdziale omówiono metody zastosowane w trakcie badań. W rozdziale 3.1 przedstawiono metodę zapadania, która jest techniką optymalizacji statystycznej, mającą na celu zwiększenie rozdzielczości chmury zjawisk sejsmicznych. Kolejno w rozdziale 3.2 przedstawiono metody klasteryzacji opartej na gęstości zjawisk- algorytmy DBSCAN i HDBSCAN. Rozdział 3.3 stanowi opis metod służących do wyznaczania objętości chmury zjawisk sejsmicznych - otoczki wypukłej i kształtów alpha.

3.1. Metoda zapadania

Lokalizacja źródeł zjawisk mikrosejsmicznych jest obarczona błędem wynikającym m.in. z uproszczonego modelu prędkości lub błędów w wyznaczeniu czasów lub kierunków przybycia poszczególnych fal sejsmicznych. Powoduje to perturbacje zlokalizowanych źródeł w stosunku do ich rzeczywistych pozycji. Metoda zapadania (ang. *collapsing*) jest techniką optymalizacji statystycznej, która służy zmniejszeniu rozproszenia chmury lokalizacji zjawisk sejsmicznych wynikających z błędów lokalizacji (Jones i Stewart, 1997).

Mimo że metoda zapadania została orginalnie przedstawiona dla wyznaczenia struktur związanych z sejsmicznością wulkaniczną (Jones i Stewart, 1997), może ona być stosowana w każdej chmurze zlokalizowanych zjawisk sejsmicznych, gdy błędy lokalizacji są znane.

Metoda zapadania wykorzystuje informacje o lokalizacjach zjawisk sejsmicznych oraz błędów ich wyznaczenia. Błąd lokalizacji przedstawiany jest w postaci elipsoidy błędu (Havskov i Ottemoller, 2010). Orientacja przestrzenna elipsoidy uzależniona jest od wzajemnego położenia hipocentrów i czujników. Objętość elipsoidy zależy od błędów poszczególnych parametrów dla określonego poziomu ufności.

Idea relokalizacji źródła została schematycznie przedstawiona na Rysunku 3.1. Algorytm działa w następujący sposób:

- Dla każdej lokalizacji źródła (zielony punkt) oblicza się elipsoidę błędu przy założeniu określonego poziomu ufności
- Spośród wszystkich zjawisk leżących wewnątrz danej elipsoidy (niebieskie punkty) wyznacza się środek ciężkości (czerwony krzyżyk)
- Lokalizacja rozpatrywanego zjawiska przesuwana jest w kierunku środka ciężkości

Relokalizacja metodą zapadania źródeł odbywa się w granicach własnych elipsoid błędów, których położenie nie zmienia się. Procedurę zapadania wykonuje się iteracyjnie dopóki populacja translacji nie

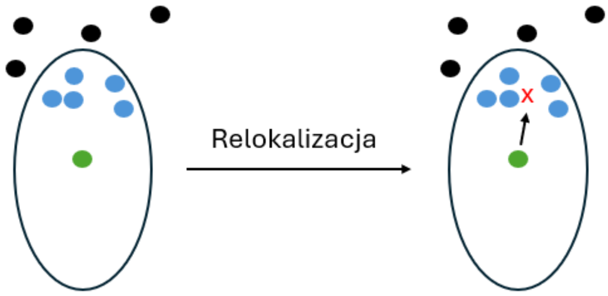

Rysunek 3.1: Schemat relokalizacji źródła wewnątrz elipsoidy błędu

przyjmie formy rozkładu χ^2 z trzema stopniami swobody. W celu weryfikacji tej zależności przeprowadza się test Kołmogorowa-Smirnowa, który porównuje zgodność rozkładu empirycznego z rozkładem teoretycznym χ^2.

Rozmieszczenie zrelokalizowanych źródeł z reguły charakteryzuje się mniejszą dyspersją przestrzenną (Jones i Stewart, 1997).

W literaturze opisano kilka wariantów oryginalnej metody zapadania (Asanuma i in., 2001; Asanuma i in., 2005; Asanuma i in., 2008). W ramach mojej pracy badawczej skupiam się na zastosowaniu jej podstawowej, oryginalnej wersji.

3.2. Metody identyfikacji struktur sejsmogennych

Do identyfikacji struktur sejsmogennych w chmurze zjawisk sejsmicznych wybrano metody, które spełniały następujące kryteria:

– Są dostosowane do trójwymiarowych danych punktowych

– Nie wymagają znajomości z góry założonej liczby klastrów

– Są dostosowane do danych obarczonych szumem

Takie założenia spełniają metody klasteryzacji oparte na gęstości zjawisk, które należą do metod nienadzorowanego uczenia maszynowego. Zgodnie z założeniami tych metod klastry to regiony, w których gęstość punktów jest wyższa niż poza nimi. Jedna z najbardziej znanych metod grupowania gęstościowego to metoda DBSCAN (ang. *Density-based spatial clustering of applications with noise*) zaproponowana w 1996 roku (Ester i in., 1996), wykorzystywana obecnie również w sejsmologii (m.in. (Cesca i in., 2014; Woodward i in., 2018)).

Algorytm DBSCAN posiada dwa parametry wejściowe, od których zależy wynik klasteryzacji:

– Promień sąsiedztwa (oznaczany jako Eps lub ε) - definiuje maksymalną odległość pomiędzy zjawiskami należącymi do tego samego klastra

– Minimalna liczba zjawisk niezbędnych do utworzenia klastra (oznaczana jako MinPts)

Zgodnie z założeniami metody, wartość parametru MinPts powinna być przynajmniej o 1 większa od wymiarowości zbioru danych. Dobór wartości parametru ε jest bardziej problematyczny (m.in. (Karami i Johansson, 2014; Starczewski i in., 2020). Zbyt niska wartość promienia sąsiedztwa może skutkować klasyfikacją znaczącej części zbioru punktów jako szum. Zbyt wysoka wartość promienia może prowadzić do zanikania granic między klastrami, skutkując ich scaleniem i brakiem zdolności do rozróżnienia odrębnych grup danych. W pracy (Węglińska i Leśniak, 2024) zaproponowano metodę automatycznego wyznaczania parametru ε dla danych dotyczących lokalizacji zjawisk sejsmicznych, która zależy od błędów lokalizacji zjawisk. Wartość ε obliczamy jako wartość średnią maksymalnych długości półosi ze wszystkich elipsoid błędu.

Sąsiedztwo jest zbiorem punktów, które leży w odległości mniejszej lub równej ε od danego punktu. Rozróżniamy 3 typy punktów w zbiorze danych: punkty rdzeniowe, punkty graniczne oraz szum. Punkt rdzeniowy to taki punkt, który posiada liczbę sąsiadów większą lub równą wartości MinPts. Punkt graniczny posiada liczbę sąsiadów mniejszą niż MinPts, ale należy do sąsiedztwa innego punktu rdzeniowego. Szumem nazywamy punkt, który nie jest rdzeniowy ani graniczny.

Rozpoczęcie procesu klasteryzacji w metodzie DBSCAN polega na identyfikacji punktów rdzeniowych. Następnie określa się wszystkie punkty w promieniu ε, które spełniają kryterium minimalnej liczby sąsiadów i dodawane są do tworzonego klastra. Wszystkie punkty połączone gęstościowo z punktem rdzeniowym przypisywane są do tego samego klastra.

Często za konkurencyjną metodę uważa się algorytm HDBSCAN (ang. *Hierarchical Density-Based Spatial Clustering of Applications with Noise*) (Campello i in., 2013), który jest modyfikacją metody DBSCAN. Metoda ta wymaga tylko jednego parametru wejściowego. Jest nim minimalna liczba punktów niezbędna do utworzenia klastra. Algorytm HDBSCAN przekształca orginalną metodę DBSCAN w algorytm klasteryzacji hierarchicznej. Buduje on hierarchiczną struturę wszystkich możliwych klastrów dla różnych wartości odległości sąsiedztwa i wyodrębnia klastry o najlepszej stabilności (McInnes i in., 2017). Stabilność klastrów w metodzie HDBSCAN jest parametrem, który świadczy o tym jak długo klaster istnieje w hierarchii zanim zostanie połączony z innym klastrem lub zostanie podzielony. Algorytm HDBSCAN charakteryzuje się większą złożonością obliczeniową niż DBSCAN (Stewart i Al-Khassaweneh, 2022).

3.3. Metody obliczania objętości aktywnej struktury

Rekonstrukcja stref sejsmogennych jest trudna ze względu na dużą złożoność i różnorodność geometrii. Aby móc zobrazować kształt zbioru i obliczyć objętość aktywnej struktury na podstawie lokalizacji zjawisk sejsmicznych użyto algorytmów otoczki wypukłej (ang. *Convex Hull*) (Graham, 1972) i kształtów alpha (α) (ang. *Alpha Shapes*) (Edelsbrunner i Mücke, 1994).

Pierwszym krokiem do rekonstrukcji sieci spękań jest triangulacja Delaunay'a dla wszystkich punktów w przestrzeni. Triangulacja Delaunay'a jest metodą dzielenia zbioru punktów 3D na tetraedry w taki sposób, że żaden punkt nie znajduje się w sferze opisanej na tetraedrze. Na brzegach triangulacji tworzy się otoczkę wypukłą lub kształt alpha.

Otoczkę wypukłą zbioru definiujemy jako najmniejszy wielokąt wypukły zawierający ten zbiór. Granica zbioru jest wielokątem, w którym żadna krawędź graniczna nie przecina się ani nie wyklucza żadnego punktu. Algorytmy wykorzystywane do wyznaczenia otoczki wypukłej to m.in.: algorytm Grahama (Graham, 1972), Jarvisa (Jarvis, 1973), Quickhull (Eddy, 1977; Bykat, 1978; Green i Silverman, 1979; Barber i in., 1996). W prezentowanej pracy doktorskiej używano algorytmu Quickhull.

Kształt alpha (α) jest uogólnieniem otoczki wypukłej dla zbioru punktów (Edelsbrunner i in., 1983). Różni się od otoczki wypukłej tym, że nie musi być wypukły i może zawierać puste przestrzenie (Capinha i Pateiro-López, 2014). Kształt α pozwala odwzorować bardziej złożone kształty niż otoczka wypukła (Edelsbrunner i Mücke, 1994) i pozwala na bardziej precyzyjne dopasowanie do kształtu danych niż kształt utworzony przez otoczkę wypukłą. Parametr α odpowiada za stopień szczegółowości odtworzenia krawędzi zbioru punktów. Dla skończonego zbioru w $\mathbb{R}^3$ α jest liczbą rzeczywistą należącą do przedziału $0 \leq \alpha \leq \infty$. Gdy $\alpha \rightarrow \infty$ mamy do czynienia z otoczką wypukłą.

4. Omówienie publikacji wchodzących w skład rozprawy

Przedstawiona rozprawa doktorska jest wynikiem nowatorskich badań, których wyniki zostały opublikowane w 4 czasopismach naukowych indeksowanych w bazie Web of Science.

[Z1] Węglińska i Leśniak 2024

Elżbieta Węglińska, Andrzej Leśniak. 2024. A novel approach to identifying seismogenic structures and estimating reservoir volume based on synthetic cloud of seismicity induced by hydraulic fracturing. Acta Geodaetica et Geophysica, doi: 10.1007/s40328-024-00442-1

Procentowy udział autorów: Elżbieta Węglińska: 80%, Andrzej Leśniak: 20%

Udział doktoranta polegał na: zaplanowaniu badań, wykonaniu przeglądu literatury, utworzeniu modelu sejsmiczności indukowanej, przygotowaniu figur, napisaniu tekstu manuskryptu, częściowym przygotowaniu kodu, obliczeniu objętości struktur sejsmogennych, analizie i interpretacji uzyskanych wyników.

[Z2] Leśniak i in. 2020

Andrzej Leśniak, **Elżbieta Śledź**, Katarzyna Mirek. 2020. Detailed Recognition of Seismogenic Structures Activated during Underground Coal Mining: A Case Study from Bobrek Mine, Poland. Energies 13(18), 4622, doi: 10.3390/en13184622

Procentowy udział autorów: Andrzej Leśniak: 45% , **Elżbieta Śledź: 35%** , Katarzyna Mirek: 20%
Artykuł został opublikowany pod panieńskim nazwiskiem - Śledź

Udział doktoranta polegał na: przygotowaniu danych, częściowym przygotowaniu kodu i tekstu manuskryptu, realizacji obliczeń metody zapadania, klasteryzacji zjawisk sejsmicznych, analizie map górniczych, przygotowaniu figur, identyfikacji struktur sejsmogennych, analizie wyników i ich interpretacji.

[Z3] Węglińska i Leśniak 2021

Elżbieta Węglińska, Andrzej Leśniak. 2021. Induced Seismicity and Detailed Fracture Mapping as Tools for Evaluating HDR Reservoir Volume. Energies 14(9), 2593, doi: 10.3390/en14092593

Procentowy udział autorów: Elżbieta Węglińska: 60% , Andrzej Leśniak: 40%

Udział doktoranta polegał na: przygotowaniu danych, wykonaniu przeglądu literatury, częściowym przygotowaniu kodu, napisaniu tekstu manuskryptu, realizacji obliczeń metody zapadania, klasteryzacji zjawisk sejsmicznych, czaso-przestrzennej analizie klastrów, przygotowaniu figur, analizie i interpretacji wyników, obliczeniu objętości struktur sejsmogennych

[Z4] Węglińska i in. 2024

Elżbieta Węglińska, Andrzej Leśniak, Andrzej Pasternacki, Paweł Wandycz. 2024. Mapping a fracture network formed by hydraulic fracturing in a shale gas reservoir. Geology, Geophysics and Environment 50(3), 213-230, doi: 10.7494/geol.2024.50.3.213

Procentowy udział autorów: Elżbieta Węglińska: 50%, Andrzej Leśniak: 30%, Andrzej Pasternacki: 10%, Paweł Wandycz: 10%

Udział doktoranta polegał na: przygotowaniu tekstu manuskryptu, wykonaniu przeglądu literatury, przygotowaniu figur, częściowym przygotowaniu kodu, realizacji obliczeń metody zapadania, klasteryzacji zjawisk sejsmicznych, opracowaniu wyników, analizie i interpretacji uzyskanych wyników.

Dodatkowo wyniki zaprezentowane w pracy doktorskiej zostały przedstawione przez doktoranta na międzynarodowych konferencjach naukowych:

Elżbieta Węglińska, Andrzej Leśniak, Andrzej Pasternacki, Paweł Wandycz. Mapping of structures formed by hydraulic fracturing based on microseismic events location. *EGU General Assembly 2023*

Elżbieta Węglińska, Andrzej Leśniak. 2022. Comparison of microseismic locations scatter reduction methods and unsupervised machine learning algorithms for automatic detection of seismogenic structures in a Polish hard coal mine. *Rockbursts and Seismicity in Mines*

Andrzej Leśniak, **Elżbieta Węglińska**, Katarzyna Mirek. 2021. Identification of tectonic structures based on tremors in Bobrek Coal Mine using a collapsing method. *EAGE GeoTech*

Elżbieta Węglińska, Andrzej Leśniak. Enhancing Precision in Seismogenic Structure Identification and Reservoir Volume Estimation Through Synthetic Seismic Cloud Analysis. *39th General Assembly of the European Seismological Commission* [abstrakt przyjęty na konferencję: wrzesień 2024]

4.1. Węglińska E., Leśniak A. 2024

Pierwszym celem badań opublikowanych w artykule było zaproponowanie metody identyfikacji struktur sejsmogennych na podstawie zlokalizowanych zjawisk sejsmicznych mając do dyspozycji hipocentra oraz błędy ich lokalizacji. We wstępie artykułu zrobiono przegląd dotychczasowych metod używanych do wyznaczania klastrów zjawisk sejsmicznych. Przeprowadzono analizę wyłącznie tych metod, które spełniają trzy kluczowe kryteria: są przystosowane do pracy z chmurami punktów trójwymiarowych (3D), nie wymagają wcześniejszego określenia liczby klastrów, a także są zdolne do przetwarzania danych zawierających szum. Te metody zostały również sklasyfikowane w oparciu o rodzaje danych wymaganych do ich wykorzystania.

Drugim celem było przedstawienie metody estymacji objętości aktywnej struktury zaburzonej przez proces szczelinowania. Jedną z metod obliczania objętości stymulowanego zbiornika (SRV) jest wyznaczenie objętości chmury zawierającej wszystkie zjawiska sejsmiczne (Mayerhofer i in., 2010). Jednakże, SRV rzadko odzwierciedla prawdziwą objętość produkcyjną zbiornika (Umar i in., 2021).

W celu przedstawienia efektywności zaproponowanego algorytmu zaprezentowano wyniki na syntetycznym modelu zjawisk sejsmicznych. Aby utworzyć model, początkowo stworzono struktury, które mają symulować pęknięcia wynikające z sejsmiczności podczas szczelinowania hydraulicznego. Zostały one utworzone wzorując się na rzeczywistych strukturach jakie są tworzone podczas eksperymentów szczelinowania hydraulicznego (Maxwell i in., 2015).

W artykule zaproponowano rekonstrukcję sieci spękań w górotworze poprzez integrację metody zapadania (Jones i Stewart, 1997), DBSCAN (Ester i in., 1996) oraz metodę kształtów alpha (Edelsbrunner i Mücke, 1994). Użycie metody zapadania miało na celu zmniejszenie rozproszenia chmury hipocentrów. Na zapadniętej chmurze zjawisk sejsmicznych użyto algorytmu DBSCAN aby znaleźć klastry charakteryzujące się wyższą gęstością zdarzeń w porównaniu z ich otoczeniem. Po odrzuceniu punktów zaklasyfikowanych przez metodę klasteryzacji jako szum, obliczono objętość chmury poprzez wyznaczenie kształtów alpha. Objętość chmury po zastosowaniu zaproponowanej 3-etapowej procedury była 14 razy mniejsza niż objętość orginalnej, nieprzetworzonej chmury. Taka analiza prowadzi do bardziej realistycznej oceny objętości oraz ujawnia liniowe struktury, które odgrywają kluczową rolę w ekstrakcji gazu. W przyszłości umożliwia to także bardziej perspektywiczne lokalizowanie odwiertów oraz podejmowanie decyzji dotyczące stymulacji zbiornika.

W omawianym artykule zaproponowano również metodę automatycznego doboru parametru klasteryzacji ε, która zależy od błędów lokalizacji. Metoda wyznaczenia tego parametru opiera się na błędzie elipsoidy każdego zdarzenia sejsmicznego. Sposób wyznaczenia tego parametru został opisany w rozdziale 3.2 tej rozprawy.

4.2. Leśniak A., Śledź E., Mirek K. 2020

Celem badań była identyfikacja klastrów zjawisk sejsmicznych utworzonych lub reaktywowanych na skutek działalności górniczej związanej z wydobyciem węgla kamiennego w kopalni Bobrek na ścianie 3 pokładu 503. W przypadku zjawisk sejsmicznych indukowanych w trakcie podziemnych robót górniczych, ogólnie rozróżnia się dwa typy zdarzeń sejsmicznych – zdarzenia związane z eksploatacją górniczą oraz zdarzenia pochodzenia górniczo-tektonicznego (Stec, 2007). Aby zidentyfikować te grupy zjawisk możliwie dokładnie, pierwszym krokiem było zwiększenie rozdzielczości chmury zjawisk sejsmicznych za pomocą metody zapadania. Po użyciu tego algorytmu na całym zbiorze danych, chmura reprezentująca hipocentra była bardziej heterogeniczna, co objawia się występowaniem lokalnych zagęszczeń o kształtach podobnych do prostych linii i płaszczyzn o różnych orientacjach.

Aby sprawdzić, czy pojawianie się wstrząsów pokrywa się czasowo z pracami górniczymi, wykonano analizę czaso-przestrzenną. Rozkład hipocentrów został przedstawiony w miesięcznych interwałach wraz z bieżącą pozycją frontu robót. Na podstawie tej analizy zauważono, że liczba zjawisk sejsmicznych znacznie wzrosła w momencie przekroczenia frontu wydobywczego z osią Niecki Bytomskiej.

W celu automatycznego znalezienia klastrów w zapadniętej chmurze zjawisk sejsmicznych, użyto algorytmu HDBSCAN. Zastosowanie tej metody pozwoliło zidentyfikować struktury liniowe i płaszczyznowe. W celu interpretacji lokalizacji utworzonych struktur, w artykule przedstawiono także mapy wcześniej eksploatowanych pokładów jak i lokalizacje chodników. Pionowe struktury liniowe znajdują się poniżej dwóch wcześniej eksploatowanych pokładów. Klastry o prawie pionowym przebiegu mogą być interpretowane jako lokalne nieciągłości tektoniczne, które zostały aktywowane w wyniku działalności górniczej. Ich występowanie było wcześniej postulowane przez Marcaka i Mutke (Marcak i Mutke, 2013) i było kojarzone z występowaniem fleksur w basenie bytomskim. W basenach tego typu można spodziewać się występowania systemów pęknięć o różnej skali o prawie pionowym przebiegu, a zatem prostopadle do osi basenu i wybranego pokładu (Li i in., 2018). Wydzielone struktury poziome cechuje podobne położenie i orientacja przestrzenna do wcześniej eksploatowanych pokładów. Zmniejszenie rozproszenia chmury w tym przypadku umożliwiło na bezpośrednie powiązanie poziomych struktur z chodnikami górniczymi starych, głębszych pokładów eksploatacji węgla.

4.3. Węglińska E., Leśniak A., 2021

Pierwszym celem badań zaprezentowanych w artykule było oszacowanie objętości zbiornika geotermalnego typu HDR (hot dry rock) na podstawie analizy zjawisk mikrosejmicznych zlokalizowanych podczas stymulacji pola Soultz-sous-Forets we wrześniu 1993 roku. Drugim celem było określenie, które ze zjawisk sejsmicznych mogą być bezpośrednio powiązane z przepływem zatłaczanego płynu szczelinującego (określane jako "mokra sejsmiczność") (Maxwell i in., 2015).

W ramach analizy chmury zlokalizowanych zjawisk sejsmicznych, podjęto próbę wydzielenia klastrów. Choć w przeszłości przeprowadzono już wiele badań mających na celu zidentyfikowanie struktur w tej chmurze, to ich wyniki były często fragmentaryczne. Dotychczasowe badania chmury zjawisk sejsmicznych koncentrowały się na znalezieniu dominującego trendu występowania klastrów oraz analizie mechanizmów ich powstawania.

W celu jak najdokładniejszego oszacowania zasięgu zbiornika oraz zidentyfikowania struktur, które mogą być związane z przepływem płynu szczelinującego, zaproponowano 3-etapową procedurę. Pierwszym etapem było wykonanie metody zapadania dla całej chmury zjawisk sejsmicznych w celu zwiększenia jej rozdzielczości. Zjawiska, które nie zostały przesunięte w wyniku tej metody i nie zawierały żadnych zdarzeń w elipsoidzie błędu, zostały uznane za izolowane i zidentyfikowane jako szum. Kolejnym krokiem było wykonanie automatycznej klasteryzacji korzystając z metody DBSCAN. Znalezione klastry reprezentują regiony o wysokiej gęstości występowania zjawisk sejsmicznych. Zakłada się, że prawdopodobnie odzwierciedlają one pęknięcia wywołane przepływem płynu lub zaburzenia naprężeń poza głównymi ścieżkami przepływu. Orientacja wykrytych klastrów wewnątrz chmury mikrosejsmicznej odpowiada kierunkowi N-S do NNW-SSE większości naturalnych pęknięć wykazanych przez Genter i in. (Genter i in., 1997). Największy zidentyfikowany klaster zawiera w przybliżeniu tą samą strukturę, która została opisana jako Evans Line (Evans i in., 2005).

Aby określić, które klastry wykryte przez DBSCAN mają połączenie hydrauliczne, przeprowadzono analizę czasowo-przestrzenną ewolucji klastrów. W ramach tej analizy zbadano różne czynniki, takie jak tempo wzrostu klastra mierzone liczbą zdarzeń zebranych w klastrze, odległość od otworu, rozmiar klastra i czas jego pojawienia się. Zbadano charakter pojawiania się zjawisk w klastrach, rozróżniając te, które pojawiały się stopniowo, od tych pojawiających się nagle. Przyjęto założenie, że stopniowe pojawianie się zdarzeń sejsmicznych wskazuje na związek z przepływem płynu, natomiast nagłe pojawienie się klastra często wiązało się ze zmianami naprężeń tektonicznych. Choć proponowana metoda nie identyfikuje bezpośrednio mokrych zjawisk sejsmicznych, dostarcza kluczowych wskazówek do identyfikacji zdarzeń potencjalnie związanych z hydraulicznym przepływem płynu.

Ostatnim etapem analizy było oszacowanie objętości zbiornika za pomocą algorytmu otoczek wypukłych. Przyjmuje się, że objętość zbiornika możemy obliczyć jako objętość chmury mikrosejsmicznej (Mayerhofer i in., 2010). Chmura ta zawiera zarówno zdarzenia związane z przepływem zatłaczanego płynu, jak również zdarzenia wynikające z wcześniej istniejących naprężeń tektonicznych w danym obszarze. W artykule zaproponowano obliczenie objętości jako sumę objętości wszystkich otoczek wypukłych dla klastrów, które prawdopodobnie są związane z mokrą sejsmicznością. Objętość stymulowanego zbiornika uzyskana z tych klastrów jest około 5 razy mniejsza niż objętość całej orginalnej chmury mikrosejsmicznej. Należy zauważyć, że rzeczywista objętość zaangażowana w przenoszenie ciepła jest nieco większa, ponieważ istnieje połączenie między poszczególnymi klastrami. Algorytm ten nie umożliwia jednak obliczenia objętości ścieżek łączących te klastry, a obliczona objętość reprezentuje minimalną objętość zawierającą prawdopodobny system mokrych szczelin.

4.4. Węglińska E., Leśniak A., Pasternacki A., Wandycz P., 2024

Szczelinowanie hydrauliczne indukuje zdarzenia mikrosejsmiczne (Maxwell, 2013). Na podstawie lokalizacji tych zdarzeń możliwe jest zidentyfikowanie szczelin w górotworze. Mapowanie szczelin jest kluczowe dla oceny skuteczności stymulacji złóż. Aby zbadać orientację pęknięć, konieczne jest zbadanie geometrii rozkładu zdarzeń sejsmicznych (Williams-Stroud i Billingsley, 2010). W artykule została przedstawiona analiza lokalizacji zjawisk mikrosejsmicznych zarejestrowanych podczas szczelinowania hydraulicznego, przeprowadzonego w czerwcu 2016 roku w otworze Wysin-2H/2Hbis. Głównym celem analiz była identyfikacja struktur powstałych w wyniku szczelinowania hydraulicznego oraz porównanie ich orientacji z kierunkiem regionalnego maksymalnego naprężenia poziomego ($S_{H\max}$).

W celu identyfikacji struktur, które mogą zawierać potencjalne szczeliny, w artykule zaproponowano 3-etapową procedurę wyznaczania struktur liniowych. W pierwszym kroku została użyta metoda zapadania, która pozwala na minimalizację rozproszenia zjawisk sejsmicznych, których rozproszenie wynika z błędów lokalizacji. Następnie została użyta metoda klasteryzacji HDBSCAN, która w sposób automatyczny wydziela klastry o zwiększonej gęstości zjawisk w stosunku do otoczenia i rozpoznaje szum. W pracy pokazano wyniki klasteryzacji dla tego samego parametru wejściowego na chmurze zjawisk przed zastosowaniem procedury zapadania (na orginalnych danych) i na chmurze po procedurze. Zidentyfikowane klastry są uważane za możliwe struktury, które pojawiły się w obszarze szczelinowania. Klastry znalezione w orginalnej chmurze zjawisk sejsmicznych nie przedstawiają żadnych oczywistych struktur ze względu na duże rozproszenie zjawisk. Aby zbadać, które klastry zidentyfikowane przez HDBSCAN mogą odpowiadać liniowym strukturom obliczono elipsoidy rozproszenia, czyli elipsoidy o minimalnej objętości, zawierające wszystkie punkty w każdym klastrze. Wyznaczenie elipsoid rozproszenia umożliwia określenie kierunków struktur na podstawie długości półosi elipsoidy. Aby zbadać, czy struktura jest wydłużona w jednym kierunku, oblicza się współczynnik wydłużenia (Zhou i in., 2019) na podstawie długości półosi elipsoid.

W przypadku normalnego reżimu naprężeń, kierunek rozwoju i propagacji pęknięć powinien odpowiadać kierunkowi $S_{H\max}$ (Zoback, 2007). Klastry utworzone po procedurze zapadania mają kierunek bardziej zbliżony do $S_{H\max}$. Asymetria rozwoju pęknięć, która nie była widoczna w rozkładzie zdarzeń przed procedurą zapadania, znacznie wzrosła. W przetworzonej chmurze, jednoskrzydłowa natura rozwoju sieci pęknięć w kierunku NNW jest widoczna, szczególnie w końcowych etapach szczelinowania hydraulicznego.

Aby przeprowadzić walidację wyników, w szczególności metody zapadania, zestawiono lokalizacje zjawisk sejsmicznych z wynikami badań sejsmicznych 3D. Na podstawie parametrów geomechanicznych obliczonych w otworze Wysin-1, określono klasy prawdopodobieństwa wskaźnika kruchości w domenie LMR $(\lambda\rho - \mu\rho)$ (Boyd i in., 2010), a następnie oszacowano prawdopodobieństwo wystąpienia danej klasy wskaźnika kruchości na całej przestrzeni. Mapy te zostały przedstawione dla pierwotnych lokalizacji zdarzeń oraz dla zdarzeń po ich relokalizacji na przekrojach tej samej głębokości. Dla orginalnych zjawisk nie jesteśmy w stanie określić, czy występują one w strefach bardziej kruchych czy plastycznych. Rozkład lokalizacji zjawisk po procedurze zapadania wskazuje, że skały mają tendencję do preferencyjnego pękania w obszarach bardziej kruchych. W kontekście sejsmologicznym, niskie wartości indeksu kruchości mogą również wskazywać na obszary, gdzie generowanych będzie mniej trzęsień ziemi, ale dojdzie do większego nagromadzenia energii. W obszarach o wyższych indeksach kruchości można spodziewać się większej liczby drobnych trzęsień ziemi (Perez-Altamar i in., 2017).

5. Podsumowanie

W pracy doktorskiej zaproponowano orginalne rozwiązanie służące do identyfikacji struktur sejsmogennych w chmurze zlokalizowanych zjawisk sejsmicznych. Wyniki analiz przeprowadzonych przez doktorantkę zostały opublikowane w artykułach, które znajdują się w załącznikach.

Najważniejsze wnioski przedstawione w publikacjach:

1. Zastosowanie metody zapadania umożliwia bardziej jednoznaczne identyfikowanie klastrów w chmurze zjawisk sejsmicznych. Dzięki zmniejszeniu rozproszenia chmury, klasteryzacja jest bardziej efektywna (Węglińska i Leśniak, 2021; Leśniak i in., 2020; Węglińska i Leśniak, 2024; Węglińska i in., 2024).

2. Przetworzenie oryginalnej chmury zjawisk sejsmicznych, indukowanych przez eksploatację węgla kamiennego w kopalni Bobrek, pozwala na identyfikację klastrów zjawisk sejsmicznych, które są związane zarówno z wcześniej eksploatowanymi pokładami, jak i z lokalnymi nieciągłościami tektonicznymi (Leśniak i in., 2020).

3. Zastosowanie metody zapadania oraz klasteryzacji opartej na gęstości zjawisk umożliwia obliczenie dokładniejszej i bardziej realistycznej objętości struktury sejsmogennej. Dzięki zmniejszeniu rozproszenia zjawisk sejsmicznych oraz odrzuceniu zjawisk uznanych za szum, wyznaczona objętość jest mniejsza niż dla danych nieprzetworzonych (Węglińska i Leśniak, 2021; Węglińska i Leśniak, 2024).

4. Wzrasta zgodność orientacji klastrów wyznaczonych w chmurze zjawisk sejsmicznych po procedurze zapadania na polu Wysin z kierunkiem $S_{H\max}$ (Węglińska i in., 2024).

5. Rozkład lokalizacji zjawisk po procedurze zapadania na polu Wysin wskazuje, że skały mają tendencje do preferencyjnego pękania w obszarach bardziej kruchych (Węglińska i in., 2024).

6. Użycie metody zapadania, nienadzorowanego uczenia maszynowego oraz analizy czasowo-przestrzennej ewolucji klastrów na polu Soultz-sous-Forets pozwala wskazać zjawiska sejsmiczne potencjalnie związane z hydraulicznym przepływem płynu (Węglińska i Leśniak, 2021).

6. Literatura

Asanuma H., Ishimoto M., Jones R.H., Phillips W.S i Niitsuma H. (2001). „A Variation of the Collapsing Method to Delineate Structures Inside a Microseismic Cloud". W: *Bulletin of the Seismological Society of America* 91 (1), s. 154–160. DOI: 10.1785/0120000063.

Asanuma H., Kumano Y., Izumi T., Soma N., Niitsuma H. i Baria R (2005). „Monitoring of Reservoir Behavior at Soultz HDR Field by Super-Resolution Microseismic Mapping". W: *In Proceedings of the World Geothermal Congress 2005*. Antalya, Turkey.

Asanuma H., Kumano Y., Niitsuma H., Wyborn D., Schanz U. i Haring M (2008). „Current Status of Microseismic Monitoring Techniques for the Stimulation of HDR/HFR Reservoirs". W: *In Proceedings of the 2008 Australian Geothermal Energy Conference*. Melbourne, Australia, s. 29–36.

Barber C.B., Dobkin D.P. i Huhdanpaa H. (1996). „The quickhull algorithm for convex hulls". W: *ACM Transactions on Mathematical Software* 22 (4), s. 469–483. DOI: 10.1145/235815.235821.

Boyd N.K., Cardenas M. i Galarraga M. (2010). „Improved reservoir characterization using prestack analyses, Eden Yuturi field, Ecuador." W: *SEG Technical Program Expanded Abstracts 2010*. Society of Exploration Geophysicists, s. 2265–2269. DOI: 10.1190/1.3513301.

Bykat A. (1978). „Convex Hull of a Finite Set of Points in Two Dimensions". W: *Information Processing Letters* 7, s. 296–298.

Campello R. J. G. B., Moulavi D. i Sander J. (2013). „Density-Based Clustering Based on Hierarchical Density Estimates". W: *Advances in Knowledge Discovery and Data Mining*. Red. Pei J., Tseng V. S., Cao L., Motoda H. i Xu G. Berlin, Heidelberg: Springer Berlin Heidelberg, s. 160–172. DOI: 10.1007/978-3-642-37456-2_14.

Capinha C. i Pateiro-López B. (2014). „Predicting species distributions in new areas or time periods with alpha-shapes". W: *Ecological Informatics* 24, s. 231–237. DOI: 10.1016/j.ecoinf.2014.06.001.

Cesca S., Sen A.T. i Dahm T. (2014). „Seismicity monitoring by cluster analysis of moment tensors". W: *Geophysical Journal International* 96 (3), s. 1813–1826. DOI: 10.1093/gji/ggt492.

Eddy W.F. (1977). „A New convex Hull Algorithm for Planar Sets". W: *ACM Transactions on Mathematical Software* 3, s. 393–403.

Edelsbrunner H., Kirkpatrick D. i Seidel R. (1983). „On the shape of a set of points in the plane". W: *IEEE Transactions on Information Theory* 29 (4), s. 551–559. DOI: 10.1109/tit.1983.1056714.

Edelsbrunner H. i Mücke E.P. (1994). „Three-dimensional alpha shapes”. W: *ACM Transactions on Graphics* 13 (1), s. 43–72. DOI: 10.1145/174462.156635.

Ester M., Kriegel H.P., Sander J. i Xu X. (1996). „A density-based algorithm for discovering clusters in large spatial databases with noise”. W: *Proceedings of the Second International Conference on Knowledge Discovery and Data Mining*. Portland, Oregon: AAAI Press, s. 226–231. DOI: 10.5555/3001460.3001507.

Evans K.F., Moriya H., Niitsuma H., Jones R.H., Phillips W.S., Genter A., Sausse J., Jung R. i Baria R. (2005). „Microseismicity and permeability enhancement of hydrogeologic structures during massive fluid injections into granite at 3 km depth at Soultz HDR site”. W: *Geophysical Journal International* 160, s. 388–412. DOI: 10.1111/j.1365-246X.2004.02474.x.

Genter A., Castaing C., Dezayes C., Tenzer H., Traineau H. i Villemin T. (1997). „Comparative analysis of direct (core) and indirect (borehole imaging tools) collection of fracture data in the Hot Dry Rock Soultz reservoir (France)”. W: *Journal of Geophysical Research* 102, s. 15419–15431. DOI: 10.1029/97JB00626.

Graham R.L. (1972). „An Efficient Algorithm for Determining the Convex Hull of a Finite Planar Set”. W: *Inf. Process. Lett.* 1, s. 132–133. DOI: 10.1016/0020-0190(72)90045-2.

Green P.J. i Silverman B.W. (1979). „Constructing the Convex Hull of a Set of Points in the Plane”. W: *Computer Journal* 22, s. 262–266.

Havskov J. i Ottemoller L. (2010). *Routine Data Processing in Earthquake Seismology: With Sample Data, Exercises and Software*. Springer.

Jarvis R.A. (1973). „On the identification of the convex hull of a finite set of points in the plane”. W: *Information Processing Letters* 2 (1), s. 18–21. DOI: 10.1016/0020-0190(73)90020-3.

Jones R.H. i Stewart R.C. (1997). „A method for determining significant structures in a cloud of earthquakes”. W: *Journal of Geophysical Research* 102 (B4), s. 8245–8254. DOI: 10.1029/96JB03739.

Karami A. i Johansson R. (2014). „Choosing DBSCAN parameters automatically using Differential Evolution”. W: *International Journal of Computer Applications* 91 (7). DOI: 10.5120/15890-5059.

Leśniak A., Śledź E. i Mirek K. (2020). „Detailed Recognition of Seismogenic Structures Activated during Underground Coal Mining: A Case Study from Bobrek Mine, Poland”. W: *Energies* 13 (18). 4622. DOI: 10.3390/en13184622.

Li Y., Hou G., Hari K.R., Neng Y., Lei G., Tang Y., Zhou L., Sun S. i Zheng C. (2018). „The model of fracture development in the faulted folds: The role of folding and faulting”. W: *Marine and Petroleum Geology* 89, s. 243–251. DOI: 10.1016/j.marpetgeo.2017.05.025.

Marcak H. i Mutke G. (2013). „Seismic activation of tectonic stresses by mining”. W: *Journal of Seismology* 17, s. 1139–1148. DOI: 10.1007/s10950-013-9382-3.

Maxwell S.C. (2013). „Unintentional seismicity induced by hydraulic fracturing”. W: *CSEG Recorder* 38 (8).

Maxwell S.C., Chorney D. i Goodfellow S.D. (2015). „Microseismic geomechanics of hydraulic-fracture networks: Insights into mechanisms of microseismic sources”. W: *Leading Edge* 34, s. 904–910. DOI: 10.1190/tle34080904.1.

Mayerhofer M.J., Lolon E.P., Warpiński N.R., Cipolla C.L., Walser D. i Rightmire C.M. (2010). „What Is Stimulated Reservoir Volume?” W: *SPE Production & Operations* 25 (1), s. 89–98. DOI: 10.2118/119890-PA.

McInnes L., Healy J. i Astels S. (2017). „hdbscan: Hierarchical density based clustering”. W: *Journal of Open Source Software* 2 (11). DOI: 10.21105/joss.00205.

Perez-Altamar R., Alzate J.H., Trumbo A. i Marfurt K. (2017). „Microseismic Calibration of Surface Seismic Brittleness Estimates: Application to a Barnett Shale Survey”. W: *AAPG 2017 Mid-Continent Section Meeting*. Oklahoma City, Oklahoma.

Starczewski A., Goetzen P. i Er M.J. (2020). „New method for automatic determining of the DBSCAN parameters”. W: *Journal of Artificial Intelligence and Soft Computing Research* 10 (3), s. 209–221. DOI: 10.2478/jaiscr-2020-0014.

Stec K. (2007). „Characteristics of seismic activity of the Upper Silesian Coal Basin in Poland”. W: *Geophysical Journal International* 168 (2), s. 757–768. DOI: 10.1111/j.1365-246X.2006.03227.x.

Stewart G. i Al-Khassaweneh M. (2022). „An Implementation of the HDBSCAN* Clustering Algorithm”. W: *Applied Sciences* 12 (5). 2405. DOI: 10.3390/app12052405.

Umar I.A., Negash B.M., Quainoo A.K. i Ayoub M.A. (2021). „An outlook into recent advances on estimation of effective stimulated reservoir volume”. W: *Journal of Natural Gas Science and Engineering* 88. 103822. DOI: 10.1016/j.jngse.2021.103822.

Węglińska E. i Leśniak A. (2021). „Induced Seismicity and Detailed Fracture Mapping as Tools for Evaluating HDR Reservoir Volume”. W: *Energies* 14 (9). 2593. DOI: 10.3390/en14092593.

Węglińska E. i Leśniak A. (2022). „Comparison of Microseismic Locations Scatter Reduction Methods and Unsupervised Machine Learning Algorithms for Automatic Detection of Seismogenic Structures in a Polish Hard Coal Mine”. W: *Proceedings of the 10th international symposium on rockbursts and seismicity in mines*. Tucson,USA.

Węglińska E. i Leśniak A. (2024). „A novel approach to identifying seismogenic structures and estimating reservoir volume based on synthetic cloud of seismicity induced by hydraulic fracturing”. W: *Acta Geodaetica et Geophysica*. DOI: 10.1007/s40328-024-00442-1.

Węglińska E., Leśniak A., Pasternacki A. i Wandycz P. (2024). „Mapping a fracture network formed by hydraulic fracturing in a shale gas reservoir”. W: *Geology, Geophysics and Environment* 50 (3), s. 213–230. DOI: 10.7494/geol.2024.50.3.213.

Williams-Stroud S. i Billingsley R.L. (2010). „Techniques to estimate fracture effectiveness when mapping low-magnitude microseismicity”. W: *SEG Technical Program Expanded Abstracts 2010*. Society of Exploration Geophysicists, s. 2075–2079. DOI: 10.1190/1.3513253.

Woodward K., Wesseloo J. i Potvin Y. (2018). „A spatially focused clustering methodology for mining seismicity”. W: *Engineering Geology* 232, s. 104–113. DOI: 10.1016/j.enggeo.2017.11.015.

Zhou C., Zhang M., Li Y., Lu J. i Chen J. (2019). „Influence of particle shape on aggregate mixture's performance: DEM results”. W: *Road Materials and Pavement Design* 20 (2), s. 399–413. DOI: 10.1080/14680629.2017.1396236.

Zoback M.D. (2007). *Reservoir Geomechanics*. Cambridge University Press.

7. Oświadczenia autorów publikacji naukowych

Kraków, 17.05.2024

Oświadczenie o procentowym udziale autorów publikacji

Tytuł: A novel approach to identifying seismogenic structures and estimating reservoir volume based on synthetic cloud of seismicity induced by hydraulic fracturing

Czasopismo: Acta Geodaetica et Geophysica 2024, doi: 10.1007/s40328-024-00442-1

L.p.	Imię i nazwisko współautora	Zakres merytoryczny	Udział procentowy	Podpis
1.	**mgr inż. Elżbieta Węglińska**	Zaplanowanie badań, utworzenie modelu sejsmiczności indukowanej, realizacja obliczeń metody zapadania, klasteryzacja zjawisk sejsmicznych, obliczenie objętości struktur sejsmogennych, przygotowanie figur, napisanie tekstu manuskryptu, wykonanie przeglądu literatury, analiza i interpretacja uzyskanych wyników, częściowe przygotowanie kodu	80%	Węglińska
2.	prof. dr hab. inż. Andrzej Leśniak	Dyskusja nad wynikami, nadzór merytoryczny, częściowe przygotowanie kodu	20%	[illegible]

Kraków, 17.05.2024

Oświadczenie o procentowym udziale autorów publikacji

Tytuł: Detailed Recognition of Seismogenic Structures Activated during Underground Coal Mining: A Case Study from Bobrek Mine, Poland.

Czasopismo: Energies 2020, 13(18), 4622, doi: 10.3390/en13184622

L.p.	Imię i nazwisko współautora	Zakres merytoryczny	Udział procentowy	Podpis
1.	prof. dr hab. inż. Andrzej Leśniak	Nadzór merytoryczny, dyskusja nad wynikami, częściowe przygotowanie kodu i tekstu manuskryptu	45%	
2.	**mgr inż. Elżbieta Śledź**	Przygotowanie danych, częściowe przygotowanie kodu i tekstu manuskryptu, realizacja obliczeń metody zapadania, klasteryzacja zjawisk sejsmicznych, analiza czaso-przestrzenna zjawisk sejsmicznych, analiza map górniczych, przygotowanie figur, analiza wyników i interpretacja, identyfikacja struktur sejsmogennych	35%	
3.	dr Katarzyna Mirek	Dyskusja nad wynikami, wykonanie opisu i figur dotyczących geologii, pozyskanie danych górniczych	20%	

Kraków, 17.05.2024

Oświadczenie o procentowym udziale autorów publikacji

Tytuł: Induced Seismicity and Detailed Fracture Mapping as Tools for Evaluating HDR Reservoir Volume.

Czasopismo: Energies 2021, 14(9), 2593, doi: 10.3390/en14092593

L.p.	Imię i nazwisko współautora	Zakres merytoryczny	Udział procentowy	Podpis
1.	**mgr inż. Elżbieta Węglińska**	Przygotowanie danych, wykonanie przeglądu literatury, częściowe przygotowanie kodu, napisanie tekstu manuskryptu, realizacja obliczeń metody zapadania, klasteryzacja zjawisk sejsmicznych, czaso-przestrzenna analiza klastrów, przygotowanie figur, analiza wyników i interpretacja, obliczenie objętości struktur sejsmogennych	60%	Węglińska
2.	prof. dr hab. inż. Andrzej Leśniak	Dyskusja nad wynikami, nadzór merytoryczny, częściowe przygotowanie kodu programu	40%	[illegible]

Kraków, 11.06.2024

Oświadczenie o procentowym udziale autorów publikacji

Tytuł: Mapping a fracture network formed by hydraulic fracturing in a shale gas reservoir.

Czasopismo: Geology, Geophysics and Environment 2024, 50(3), 213-230, doi: 10.7494/geol.2024.50.3.213

L.p.	Imię i nazwisko współautora	Zakres merytoryczny	Udział procentowy	Podpis
1.	**mgr inż. Elżbieta Węglińska**	Przygotowanie tekstu manuskryptu, wykonanie przeglądu literatury, przygotowanie figur, częściowe przygotowanie kodu, realizacja obliczeń metody zapadania, klasteryzacja zjawisk sejsmicznych, opracowanie wyników, analiza i interpretacja uzyskanych wyników	50%	Węglińska
2.	prof. dr hab. inż. Andrzej Leśniak	Dyskusja nad wynikami, nadzór merytoryczny, częściowe przygotowanie kodu	30%	Leśniak.
3.	dr inż. Andrzej Pasternacki	Częściowe przygotowanie tekstu manuskryptu, wykonanie map współczynnika kruchości, dyskusja nad wynikami	10%	[illegible]
4.	dr inż. Paweł Wandycz	Przygotowanie danych, częściowe przygotowanie tekstu manuskryptu, przygotowanie figur dotyczących geologii, dyskusja nad wynikami	10%	[illegible]

8. Załączniki

Załącznik 1

Acta Geodaetica et Geophysica
https://doi.org/10.1007/s40328-024-00442-1

ORIGINAL STUDY

A novel approach to identifying seismogenic structures and estimating reservoir volume based on synthetic cloud of seismicity induced by hydraulic fracturing

Elżbieta Węglińska[1] · Andrzej Leśniak[1]

Received: 18 November 2023 / Accepted: 20 March 2024

Abstract

Precise imaging of formed fractures and delineation of a reservoir's boundaries within a scattered seismic cloud is complicated by inaccuracies in event location. Accurate estimate of stimulated reservoir volume (SRV) is key to evaluate fracturing performance. When reservoir volume is assessed based on dispersed locations, values tend to be overestimated. The aim of the article was to calculate SRV via seismicity induced during the course of hydraulic fracturing, solely on the basis of hypocenters and location errors. The methods for three-dimensional (3D) reservoir reconstruction combine the collapsing method, density-based spatial clustering of applications with noise, and alpha-shape estimation technique using synthetic data. The method we proposed for calculating reservoir volume based on the location of microseismic events allows for a more precise and realistic estimation. The SRV obtained using the proposed approach is approximately 14 times smaller than that obtained from the original cloud.

Article highlights

- The paper presents a new approach to more precisely identify seismogenic structures and estimate reservoir volume.
- The study introduces a methodology that significantly reduces the overestimation of the stimulated reservoir volume.
- To assess reservoir details and identify structures, only locations and errors of micro-seismic events were utilized.

Keywords Stimulated reservoir volume · Induced seismicity · Seismogenic structures · Collapsing · DBSCAN

✉ Elżbieta Węglińska
weglinska@agh.edu.pl

1 Department of Geoinformatics and Applied Computer Science, AGH University of Krakow, Krakow, Poland

1 Introduction

In studies of tectonic and seismic risks, accurately determining the position and shape of seismogenic structures is essential (Wu and Zhao 2013). Several widely used clustering techniques have been applied in the analysis of seismic activity. Various cluster identification methods have been categorized according to the features required for their implementation. Only those that met the following assumptions, i.e. have been adapted to a three-dimensional (3D) point cloud, do not require the number of clusters requested and deal with noise in the data, were selected.

The foundational techniques for clustering seismic events predominantly rely on either spatial coordinates of the events or their temporal attributes. Frohlich (1987) proposed a clustering approach based on the incidence of aftershocks and the temporal clustering of nearby deep earthquake events. Ouillon et al. (2008) introduced an enhanced pattern recognition technique that reconstructs the 3D structure of active fault networks using spatial locations of earthquakes by refining the traditional k-means clustering method so as to take into account the full spatial covariance tensor, which produces fault-like, anisotropic clusters and determines the best plane segments representing the data's spatial structure. To detect faults Ouillon and Sornette (2011) clustered events using only the locations of seismic events, assuming that earthquakes indicate the presence of such tectonic structures. They began by distinguishing between clustered seismic events and uncorrelated seismicity based on the distribution of tetrahedra volumes created by the closest neighboring events in original and randomised catalogs. Recognizing the spatial complexity of fault networks, they defined faults as probabilistic anisotropic kernels, incorporating knowledge about discontinuous tectonic deformation and observed geometries of faults and earthquake clusters. Kamer et al. (2020) used the bottom-up clustering method, which first involves creating each point as a separate cluster and then reducing complexity by means of optimally merged substructures. Liu et al. (2021) assumed the existence of a spatial relationship between the location of events and the boundaries of the fractures. One possible means of estimating the plane parameters from 3D points containing an unknown amount of noise involves extracting the fracture planes from microseismic events.

A number of methods take into account the coordinates and timing of seismic events. One such approach is the ST-DBSCAN algorithm proposed by Birant and Kut (2007) and applied in seismological data (i.e., Zhang et al. 2022), which is an extension of the density-based spatial clustering of applications with noise (DBSCAN) (Ester et al. 1996) method through the addition of a time dimension, thus enabling spatial-temporal clustering based on spatial distance and time intervals.

Some methods require information about the location, time, and magnitude of seismic events. SM-DBSCAN (Georgoulas et al. 2013) is based on DBSCAN method, which incorporate the idea of accumulated seismic mass to isolate clusters of seismic events in both time and space. The advantage of this approach is that it can find clusters of any shape, while one of its limitations is that outcomes are greatly influenced by the choice of the cumulative seismic mass parameter. Schaefer et al. (2017) introduced the Smart Cluster Method based on the OPTICS technique (Ordering Points to Identify the Clustering Structure) (Ankerst et al. 1999), which modifies search behavior by taking into account such factors as earthquake density, completeness magnitude, and individual earthquake magnitudes. It further refines its approach using spatial anisotropy data as well as both temporal and spatio-temporal sub-clustering.

The clustering focal mechanism devised by Kagan (1991) seeks to distinguish between groups of earthquakes that exhibit varying rupture styles and directions. Kagan's research provided a standard for comparing the similarity of double-couple earthquake focal mechanisms. Custodio et al. (2016) introduced a novel algorithm that simultaneously clusters focal mechanisms and hypocenters, effectively identifying the alignment between hypocenter lineations and focal mechanisms.

Several methods identify structures through the use of waveforms. The utilization of multiplets for clustering purposes has been demonstrated in the literature. Multiplets refer to a group of closely spaced and similar focal mechanism seismic events. Niitsuma et al. (2002) employed multiplet-clustering techniques to analyze the microstructure of a seismic line during the course of hydraulic fracturing. Arrowsmith and Eisner (2006) proposed an algorithm that groups doublets into multiplets with graph theory. In turn, the GrowClust method (Trugman and Shearer 2017) involves simultaneous relocation and clustering based on waveform similarity. Cesca (2020) developed a set of software tools based on the DBSCAN algorithm. This toolkit enables multidimensional clustering that takes into consideration a variety of attributes such as origin time, focal mechanism, and waveform similarity. Petersen et al. (2020) proposed a Clusty toolkit designed to cluster earthquakes using waveforms recorded by a network of seismic stations. This approach takes into account the following data: the earthquake catalogue, waveform data, and station metadata.

A number of methods have also been developed that identify seismogenic structures that are based solely on the location of events and their errors. The collapsing procedure (Jones and Stewart 1997) is a statistical optimization technique that allows for moving events within an ellipsoid, and which is determined on the basis of the location error. This technique increases the resolution of the seismic event cloud that was previously disturbed by the location error. The collapsed cloud of events might better represent the true spatial distribution of event foci without the influence of location errors. Bossu (2000) presented a simplified version of the collapsing method. The assumption is that for a specific hypocenter, any seismic events within its uncertainty ellipsoid are localized to the same structure. Asanuma et al. (2001) proposed a more complex collapsing procedure with location movements influenced by the shape of the distribution within the confidence ellipsoid and which considers three structural types: point, line, and plane. Kamer et al. (2015) proposed a condensation algorithm, i.e. a strategy for reducing the scatter of the seismic event cloud. This method involves condensing events characterized by greater uncertainties onto those with lower uncertainties. The aim of the condensation approach is to shift the entire weight of the worst-located events and remove them from the seismic catalogue. This method reduces the size of the dataset while preserving the spatial information.

This paper presents a novel method for identifying clusters among recorded microseismic events. One of the objectives of this article is to show possible ways of identifying structures with limited available information. The selected methods depend on the data we have, specifically the coordinates of the events and their associated location errors. To test the effectiveness of the methods, we decided to use synthetic data. We employed modeled data consisting of the location of microseismic events and associated errors. In this paper, we propose a reconstructed 3D fracture network that combines the collapsing method (Jones and Stewart 1997), DBSCAN (Ester et al. 1996), with the alpha-shape method (Edelsbrunner and Mücke 1994). The objective of the collapsing technique is to simplify the point cloud, where the positions of specific events are diffused by uncertainties. In addition, we employed the DBSCAN algorithm to identify structures characterized by a higher density of events relative to their surroundings. We also proposed a method for automatically selecting the clustering parameter, which depends on location errors. The alpha-shape algorithm will assist us in determining the volume delineated by seismic event locations. Although the algorithms in question had been previously used separately for different purposes in seismology, our study is the first to integrate these methods for the purpose of delineating seismogenic structures based solely on hypocenters and their associated errors.

Another goal of the research was to provide a more reliable estimate of stimulated reservoir volume (SRV). The volume affected by seismic activity can be estimated as the volume of the microseismic cloud (Mayerhofer et al. 2010). This volume is calculated by examining microseismic events triggered by a combination of hydraulic fractures and reactivated natural fractures. However, SRV rarely represents the true production volume of the reservoir (Umar et al. 2021). During the hydraulic fracturing process, two primary mechanisms are present that may result in the formation or reactivation of natural fractures. These microseismic events can be induced by fluid pressure (referred to as 'wet' microseismicity linked with a fluid-filled fracture network) or by stress factors (distant dry events linked with nonfluid-filled fractures) (Maxwell et al. 2015). By excluding disconnected events when analyzing fracture geometry we can safeguard against the risk of overestimating reservoir efficiency (Maxwell et al. 2015). In our study, we calculated the fractured zone volume by applying the alpha-shape algorithm to a point cloud. Before performing this procedure, we reduced the event dispersion and eliminated points that were deemed noise. We evaluated the volume results derived from the cloud of located events, followed by those from the collapsed cloud, and from the cloud processed using our suggested procedures.

2 Induced seismicity model

Understanding and modelling induced seismicity has become an increasingly vital feature of geoscientific research, particularly in the case of such activities as hydraulic fracturing (Zhao and Young 2009; Rutqvist et al. 2015). To construct an induced seismicity model, we initially created structures (Fig. 1) intended to represent the fractures resulting from seismicity during hydraulic fracturing. The formulation of this model was inspired by actual data from fracturing processes, as is demonstrated by, among others, i.e. Abdulaziz (2013), Erokhin et al. (2013), Święch et al. (2017), Zoback and Kohli (2019). Our model was constructed on the basis of the geomechanical situation caused by hydraulic fracturing (Maxwell et al. 2015). Some events were modelled on structures intended to represent cracks that water had reached during the fracturing process. Events of varying quantity were modeled for each structure. Subsequently, they were dispersed in random directions, with values drawn from a normal distribution that had a mean of 0 and a specified standard deviation. The information about number of events and standard deviation for each structure is shown in Table 1. In addition to the already dispersed cloud of earthquakes, noise was introduced completely randomly within the area delineated by the extreme coordinates of the remaining events. Dispersed events that are added to the model, and which are not related to any fracture, constitute dry events that occur due to changes in mechanical stress. In total, the

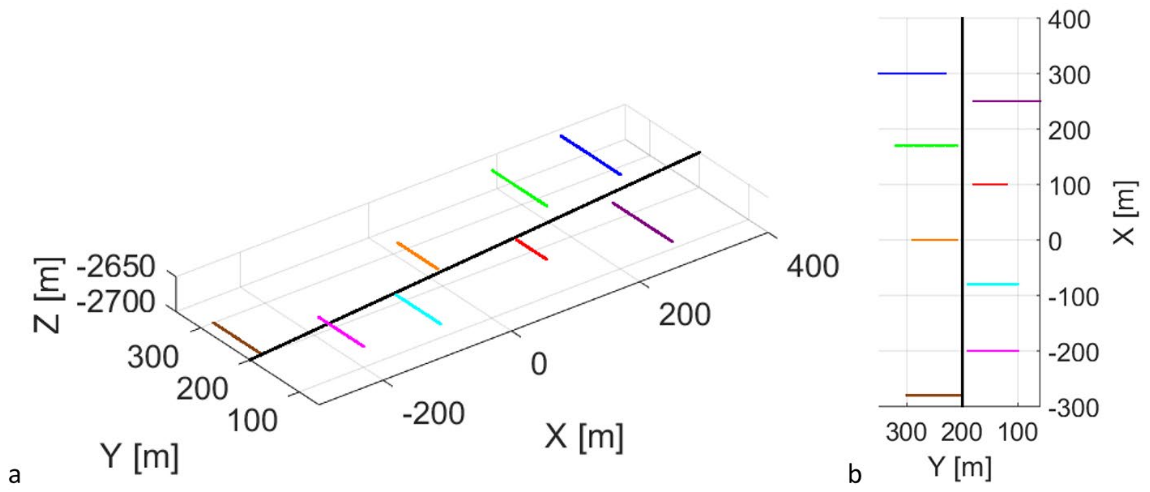

Fig. 1 True fracture network model (a) 3D view; (b) Plane view

Table 1 Number of events and variance for each structure

Fracture Number	1	2	3	4	5	6	7	8	9
Number of events	300	50	30	30	35	35	30	30	40
Standard deviation [m]	15	20	15	15	20	15	15	15	15

model contains 600 events, and is shown in Fig. 2. We assumed that the sensor network (Fig. 3) is similar to the actual positioning of sensors during hydraulic fracturing operations (i.e. Święch et al. (2017), Wandycz et al. (2019). The designed seismic monitoring network consists of 24 three-component geophones placed within a borehole. In Fig. 4, the localization error of each event is represented in the form of an error ellipsoid, as described by Havskow and Ottemoller (2010). The modeling approach mimics the process of obtaining localization errors in procedures for real data. We assume a homogeneous medium, where the spatial orientation of the error ellipsoid depends on spatial configuration of the sensors in relation to the source location and the size depends on the partial errors in the measured values (times and angles of incidence of the P wave). The volume of the ellipsoid illustrates the level of confidence with which the emission source is located within the ellipsoid. In our analysis, the distribution of microseismic events was conceptualized and processed as a three-dimensional point process, thus enabling a more precise spatial characterization and examination of seismogenic structures. Although time and magnitude might appear as intuitive attributes for seismic data clustering, they present certain inherent limitations in our context. It is not accurate to assume that all events occurring on a single fault share the same magnitude. In reality, seismic events manifest on the same structure across a wide range of magnitudes. Typically, one major event occurs followed by a series of smaller ones, which makes clustering based on magnitude unfeasible. Ideally, events of varying magnitude should occur on every structure according to the Gutenberg-Richter distribution (Gutenberg and Richter 1944). In the context of hydraulic fracturing, it is also an oversimplification to assume that events on a single structure occur simultaneously. Rather, at any given moment, events radiate across various structures. Therefore, neither time nor magnitude can serve as reliable attributes for the clustering of our seismic data.

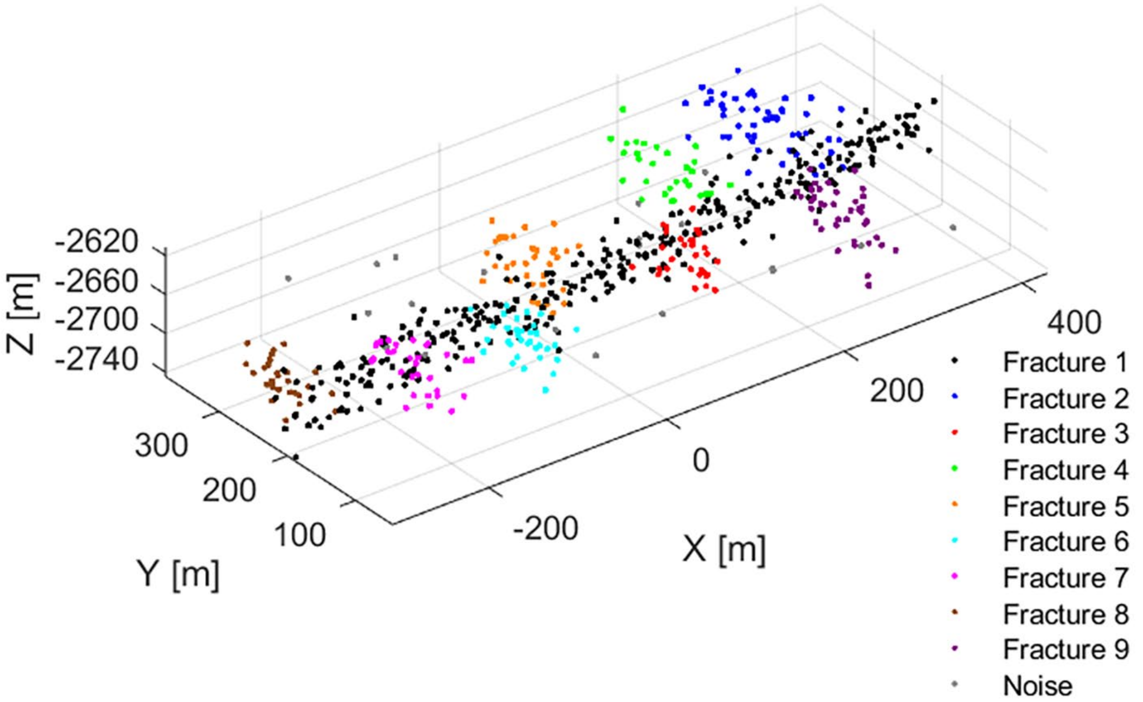

Fig. 2 Cloud of synthetic events used for further analysis

Fig. 3 Simulated events with geophones

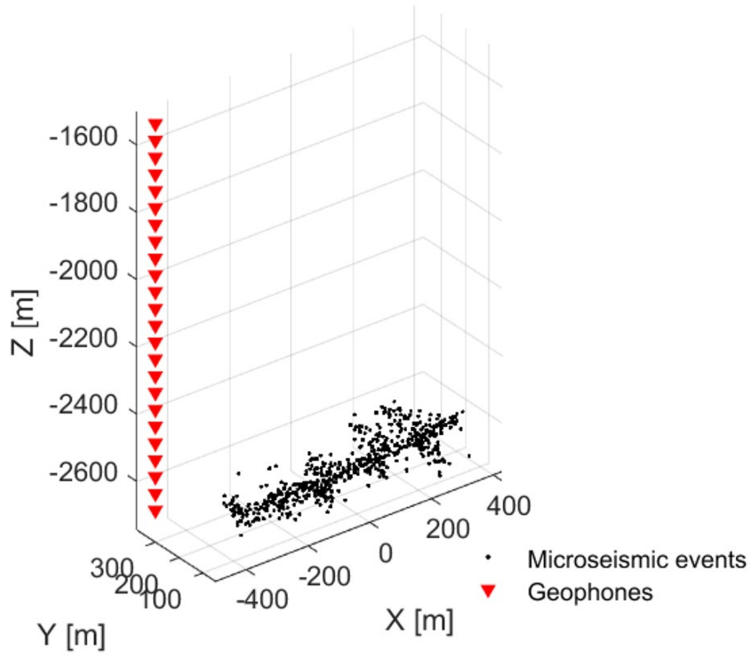

3 Reservoir reconstruction methods

To reconstruct a real model of seismogenic structures and assess the volume of the reservoir, a multistage procedure was proposed, which is presented in Fig. 5. Based on the disturbed locations of seismic events and knowledge of the seismic network, error ellipsoids were calculated for each event. The next step, the collapsing procedure, was performed to enhance the resolution of the seismic cloud and simplify its image. In the collapsed cloud,

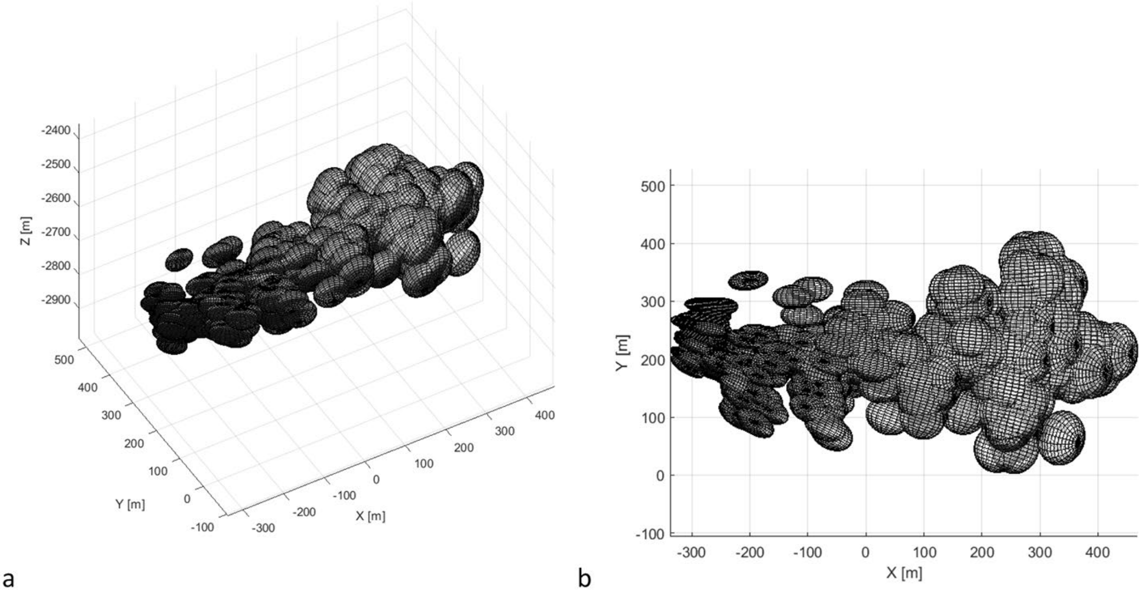

Fig. 4 Error ellipsoid for each event location (a) 3D view; (b) plane view

the authors implemented the DBSCAN algorithm for automatic cluster detection. The final step involved determining the alpha shape for the cloud after eliminating the noise. Details of each procedure will be discussed in the following sections.

3.1 Collapsing

The collapsing method, first introduced in 1997 (Jones and Stewart 1997), continues to be employed as an effective technique for mitigating scatter in seismic event locations. The method was later performed on seismicity accompanying hydrofracturing operations conducted at the Hot Dry Rock site (Fehler et al. 2001), but it can be used wherever we want to simplify the seismic event cloud. Furthermore, the effectiveness of the collapsing method has been demonstrated in various studies (e.g., Leśniak et al. 2020; Li et al. 2019; Węglińska and Leśniak 2021), solidifying its status as a reliable approach to refining seismic event location data.

One basic step that must be taken before embarking on this procedure involves determining any errors associated with the localization process resulting from the simplified structure of the velocity of the propagation medium and the inaccuracy of the selected seismic events. These errors lead to uncertainty regarding the located sources, blurring the true image of the emission cloud. The aim of the collapsing method is not to determine the exact location of events, but rather to focus on refining the spatial distribution and reducing perturbation. It operates as a post-processing step following the initial source location (i.e., Douglas 1967; Waldhauser and Ellsworth 2000; Grigoli et al. 2021).

The key step in the collapsing process involves establishing error ellipsoids for seismic events based on the location method used. Assuming random errors with a normal distribution, the error ellipsoids are determined at a specific significance level, typically at 99.5%. The resulting distribution of collapsed events exhibits greater regularity and reduced spatial dispersion compared to the original perturbed cloud. It reflects a clearer spatial distribution of the tremor foci, less affected by location error. In general, the collapsing method

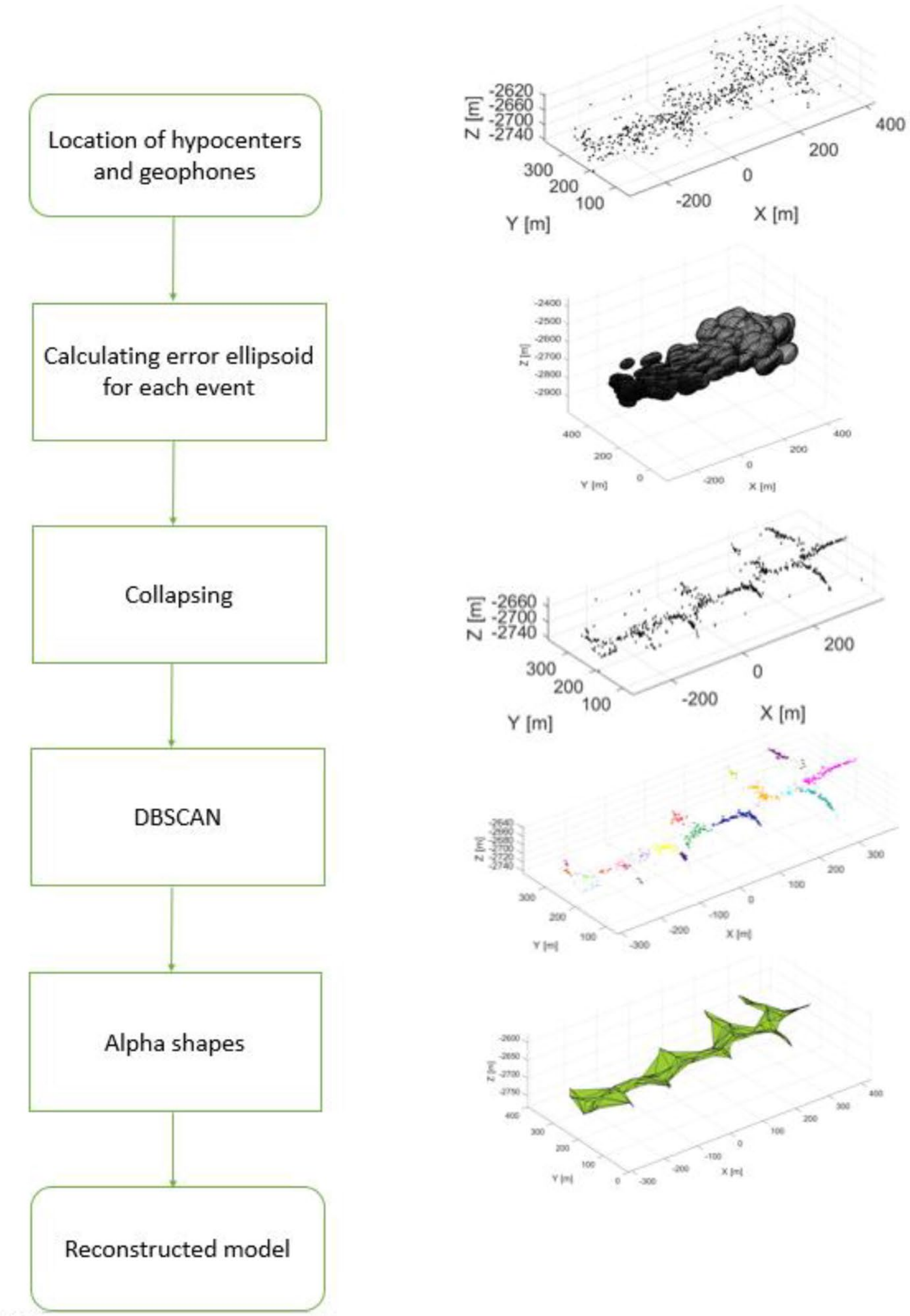

Fig. 5 Flowchart of the reservoir reconstruction. The details of each step are described in the text

significantly improves the resolution of the seismic event cloud by providing more accurate information on the underlying seismic activity. According to Jones and Stewart (1997), the location of events following relocation corresponds, in statistical terms, to the location of events prior to relocation. This means that it offers the simplest representation of the spatial distribution of the sources, while taking into account the location error. The procedure gradually shifts emission sources towards local source densities, but does so, which is important to note, within the boundaries of their respective error ellipsoids established during the source location step. This iterative relocation process continues until the population distribution adopts a chi-square distribution with three degrees of freedom. The results of applying the collapsing method to all events are presented in Fig. 6. The empirical and theoretical distributions are compared in Fig. 6a-c, where the x-axis represent the length of

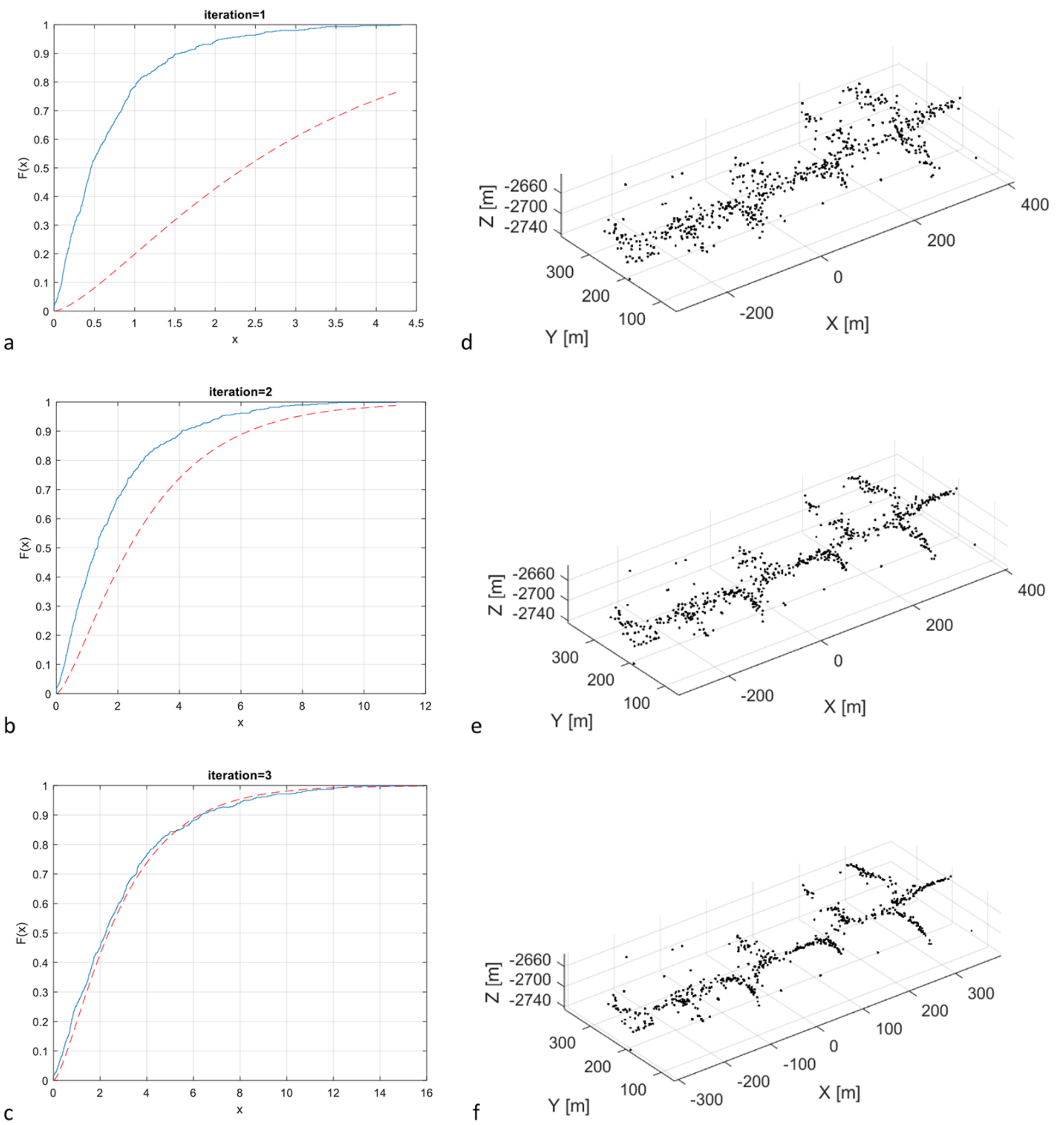

Fig. 6 (a)-(c) comparison of theoretical and empirical distributions, (d)-(f) location of the seismic cloud. The empirical distribution function is represented by the red dashed curve, while the theoretical distribution function is a blue solid curve. The comparison of cumulative distribution functions was prepared for the Kolmogorov-Smirnov test

the displacement vector. The empirical distribution of the displacements obtained during the performed perturbation is presented by red dashed curve. Given that each coordinate of the perturbation vector is a random variable following a normal distribution, the squared length of displacement vector—being the sum of the squared coordinates—adheres to χ^2 distribution with three degrees of freedom. This assertion can be substantiated through the Kolmogorov-Smirnov statistical test. In this test, we compare the empirical cumulative distribution function against the theoretical cumulative distribution function of the chi-square distribution, thereby validating the distribution characteristics of the perturbation vector's length. The distribution of events in each iterative step is presented in Fig. 6d-f.

3.2 Clustering

DBSCAN (Ester et al. 1996) is a widely applied clustering algorithm in many areas, including seismology (i.e. Cesca et al. 2014; Woodward et al. 2018). It is known for its ability to identify clusters of varying shapes and its explicit characterization of noise. It has been demonstrated to be robust to outliers, which is particularly beneficial when handling noisy seismic data. The operation of the DBSCAN algorithm requires specifying two crucial parameters: the ε value, which defines the neighborhood distance, and the minimum number of points (minPts) needed to form a cluster. In the DBSCAN algorithm, a point's density is determined by counting the number of points within distance ε of that point's location. Points can be assigned to one of three categories: the core point, the border point, or noise. Points that have densities exceeding the minPts threshold are categorized as core points. All observations that meet the criteria are combined with each other to form a single group. Observations that are not core points but lie within distance ε are included in existing groups. Points that belong to a group and have less than minPts within ε are labelled as border points. If a data point lacks any neighbouring data points within the epsilon radius it is considered noise. The result of the method is largely dependent on the parameters selected. According to the authors of the method, we choose the minimum number of points in a cluster as the data dimension plus one. However, there is always a problem when it comes to choosing the best ε parameter (i.e. Karami and Johansson 2014; Starczewski et al. 2020). In our study, we proposed a heuristic for selecting clustering parameter ε. The radius within which we look for the minimum number of points will depend on the data in such a way that there is no need to manipulate the results. Our idea of choosing this value will be determined as follows: based on the error ellipsoid of each seismic event we calculated the semi-axes of the ellipsoid and took the average value from the maximum semi-axis of each error ellipsoid. The procedure for calculating this parameter is as follows:

Given error ellipsoid E_i for each seismic event i , let a_i ,b_i ,c_i denote the semi-axes of E_i . The maximum semi-axis for a given event i is M_i , such that:

$$M_i = \max\left(a_i, b_i, c_i\right) \tag{1}$$

The average of these maximum semi-axes across all seismic events (N being the total number of events) then can be calculated as follows:

$$\varepsilon = E_{avg} = \frac{1}{N}\sum_{i=1}^{N} M_i \tag{2}$$

In this way, ε provides a statistically grounded measure for selecting the radius within which we seek the minimum number of points for clustering. The unit of the ε match the unit of distance in the dataset.

For our model data, we adopted a minimum number of 4 points for a cluster and calculated the ε parameter as 11 m.

The clustering results for parameters minPts = 4 and ε = 11 are presented in the earthquake cloud, both before (Fig. 7) and after the collapsing procedure (Fig. 8). The cluster sizes for both clouds are presented in Table 2 (for the original data) and Table 3 (for the collapsed data).

Prior to the collapsing algorithm, clustering analysis of the seismic cloud identified 11 clusters ranging in size between 4 and 9, and classified 543 points as noise. For the same clustering parameters, 25 clusters were identified in the cloud after collapsing, ranging in size from 4 to 76, and 108 points were classified as noise. Applying clustering with the same parameters to both clouds of events makes it possible to observe that prior to the cloud's collapsing, the algorithm was unable to distinguish the modeled structures. In the collapsed cloud, the structures are clearly visible. It should be emphasized that not all identified clusters represent modeled fractures. These clusters also contain events occurring on the long structure (structure 1), which partially includes events from the horizontal drilling borehole. On the other hand, there are clusters separated by DBSCAN that contain only events from induced fractures.

3.3 Alpha shapes

The final stage of the analysis detailed in this article involved estimating the stimulated reservoir volume using the Alpha Shape algorithm (Edelsbrunner et al. 1994). Generally, the dimensions of the microseismic cloud are used to assess the stimulated reservoir volume (SRV). This parameter helps assess the efficiency of the hydraulic fracturing process, understood as the size of the generated fracture network (Mayerhofer et al. 2010). The accuracy of

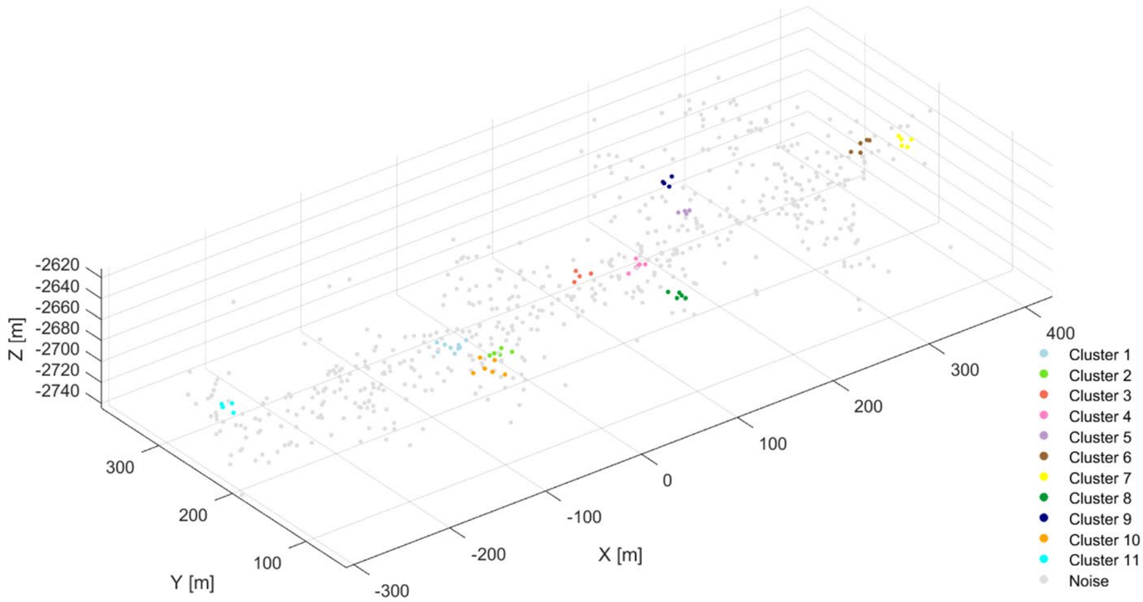

Fig. 7 Cluster identification using the DBSCAN algorithm for original locations of seismic events

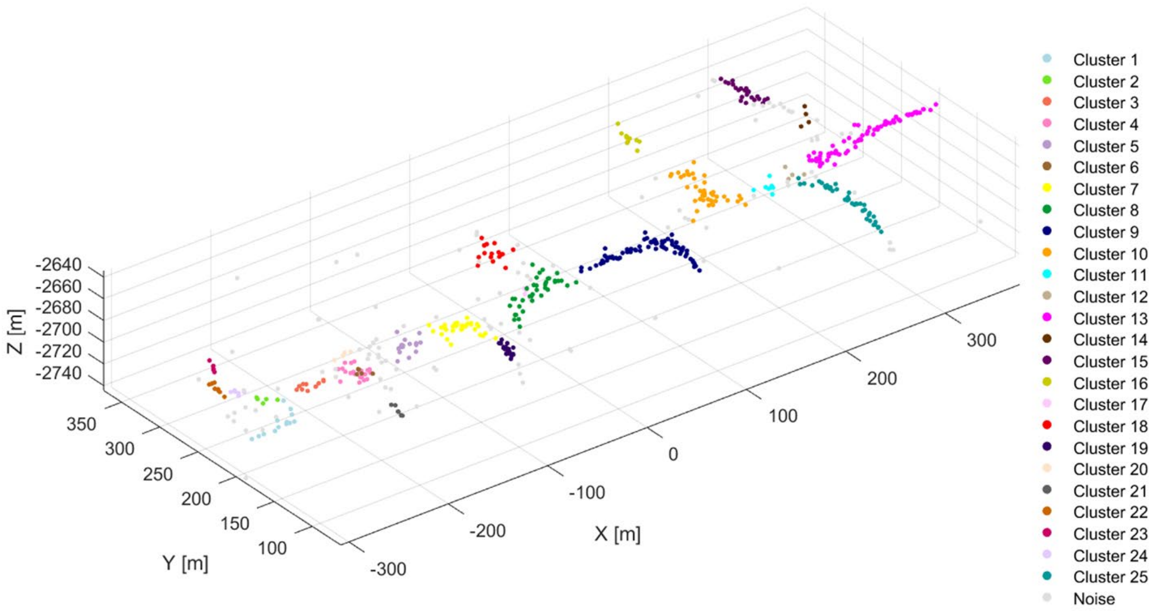

Fig. 8 Cluster identification using the DBSCAN algorithm for collapsed locations of seismic events

the SRV is directly contingent upon the quality of the microseismic data collected (Yang et al. 2018). However, the assemblage of microseismic locations tends to be diffused and scattered due to location inaccuracies, which then results in an overestimation of regions with microseismic activity (Maxwell et al. 2015). This analysis was carried out to demonstrate how important it is to reduce the scattering of point clouds for assessing the volume of the fractured zone.

The Alpha Shape is a generalization of the Convex Hull algorithm (Graham 1972). Alpha Shapes have the ability to cover nonconvex shapes and structures that contain voids. These shapes offer a more accurate representation of the true configuration of a point cloud, particularly when the distribution of data points lacks regularity or the global form deviates from convexity. This makes Alpha Shapes a sophisticated tool for accurately capturing and rendering complex geometrical data patterns. The alpha parameter in the Alpha Shape is a crucial value that determines the level of detail in the shape of a point cloud. Alpha is a positive real number that specifies the radius of the disks (1/alpha) utilized to explore a set of points in order to construct the shape (Edelsbrunner et al. 1983; Edelsbrunner and Mücke 1994). The alpha parameter was selected in such a way as to calculate the volume of the cloud as accurately as possible, while including all registered events. For our data, the alpha value is 55. For each of the three event clouds, alpha shapes were calculated using the same alpha parameter. Figure 9a illustrates the alpha shapes of the initial microseismic cloud. The volume of each cloud is listed in Table 4. The volume of the primary cloud, delineated by the microseismic events, is 5.4995e+06 m^3. Figure 9b shows the alpha shapes for the collapsed cloud and the calculated volume is 1.3496e+06 m^3. When the collapsed cloud is denoised after the DBSCAN procedure, the volume of the cloud is 4.0720e+05 m^3. The alpha shapes for the collapsed and clustered cloud are shown in Fig. 9c.

The volume of the reservoir determined by the locations of seismic events has visibly decreased. It is important to point out that the final reservoir model includes events that are noise, which were randomly located close to events from the borehole axis or fractures

Table 2 Cluster size for original locations of seismic events

Cluster Number	Noise	1	2	3	4	5	6	7	8	9	10	11
Nr of points	543	9	5	4	6	4	5	5	5	4	6	4

Table 3 Cluster size for collapsed locations of seismic events

Cluster Number	Noise	1	2	3	4	5	6	7	8	9	10	11	12
Nr of points	108	13	5	11	21	16	5	35	37	76	44	9	4
Cluster Number	**13**	**14**	**15**	**16**	**17**	**18**	**19**	**20**	**21**	**22**	**23**	**24**	**25**
Nr of points	66	4	23	13	4	17	20	4	6	8	6	7	38

and were collapsed. For this reason, the volume calculated on the basis of the final model might also be overestimated, but not as significantly as when not employing the proposed procedure.

4 Discussion

The results presented in the previous section demonstrate the application of our proposed algorithm. Despite the many methods used in seismology to delineate seismogenic structures, no algorithm has to date been devised that can identify structures when only locations and their errors are available. Although each of the above methods has been used individually, their combination allows for the more unambiguous identification of seismogenic structures. The approach proposed by the authors aims to find clusters of seismic events. This methodology incontestably simplifies the cloud and subsequent clustering, and all the parameters needed for the algorithms are calculated on the basis of error ellipsoids of each event.

One fact that needs to be emphasized is the importance of simplifying the cloud of seismic events dispersed by location errors. As introduced earlier, there are two methods of event dispersion reduction: the collapsing method and condensation. Węglińska and Leśniak (2022) employed unsupervised machine learning methods to compare the effect of both methods on the cloud of seismic events. Their study demonstrated that the collapsing method is much more effective in simplifying the cloud, which is why we adopted this approach in our study.

To highlight the difference between the clustering of the original cloud and the collapsed version, the clustering results were evaluated in both cases. Cluster validation techniques provide a measure of confidence in the results and offer insights into the reliability and stability of the formed groupings. One parameter that can provide information on the clustering quality is the percentage of points considered as noise. A high noise percentage typically indicates a higher level of outliers or irrelevant data points, which can interfere with the accuracy and reliability of cluster formation. As such, careful manipulation of this parameter is necessary to ensure the effectiveness of clustering techniques, particularly when dealing with complex and heterogeneous datasets. In the original cloud, the percentage of points recognized as noise was 90.5%, while in the case of the collapsed cloud it was only 18%.

The Density-Based Clustering Validation (DBCV) index, introduced by Moulavi et al. (2014), serves as a metric for evaluating the quality of clustering. It does this by analyzing two key aspects: intra-cluster density and inter-cluster separation. Intra-cluster density refers to the compactness of points within a cluster, with closer points indicating higher density. Conversely, inter-cluster separation examines the extent of distinction between clusters, where higher values denote well-delineated clusters. The objective of the DBCV index is to achieve minimal intra-cluster distances while ensuring maximal separation between different clusters. The high DBCV index value signifies well-defined clusters that are both internally cohesive and distinctly separate from one another, an indication of an effective clustering arrangement. For the data cloud prior to the collapsing process, the DBCV index stands at 0.09, indicating a lower distinction and density. After collapsing, the index improves significantly to 0.66, reflecting a more robust clustering with clear delineation and internal density.

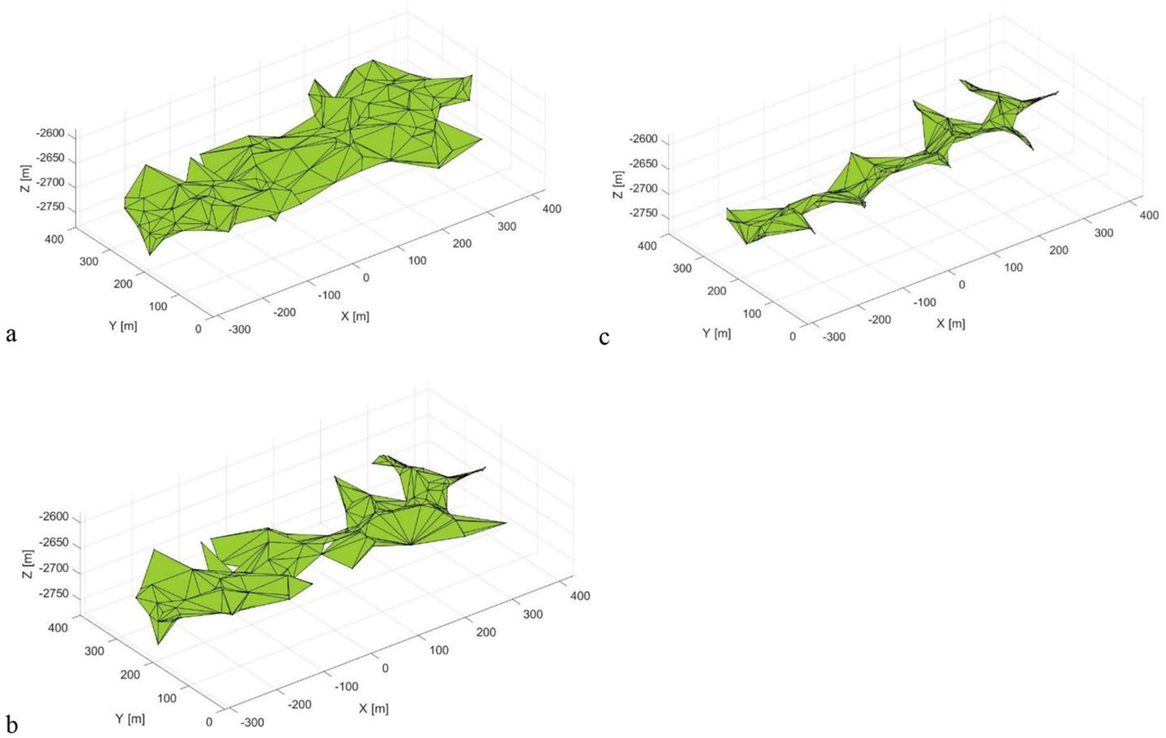

Fig. 9 Alpha shapes for (a) the original cloud of disturbed events; (b) the collapsed cloud; (c) the collapsed cloud after DBSCAN

Table 4 Calculated volume of each cloud based on Alpha Shape

Cloud of seismic events	Original	Collapsed	Collapsed and clustered
Volume [m^3]	5.4995e+06	1.3496e+06	4.0720e+05

We presented an algorithm for identifying structures and calculating SRV based on the locations of induced seismicity and the errors in their determination. To evaluate the effectiveness of the proposed method, an alpha shapes projection is presented along with the highlighted original structures in Fig. 10. After executing a three-step procedure, the reservoir area is reduced to its main structures. This enables the establishment of a more pessimistic scenario when estimating the size of the deposit.

As mentioned in Chap. 2, we solely utilized a geometrical model without taking into account the magnitude and timing of the events. Using time, although informative for understanding the sequence of seismic activity, may not directly influence the delineation of SRV. In real data, time data allows for the correlation of seismic events with specific stages of the hydraulic fracturing operation, such as the pumping phases. In real induced seismicity data, the SRV can be influenced by the magnitude of seismic events because higher magnitude events can be detected over greater distances due to their stronger signals (Zimmer 2011).

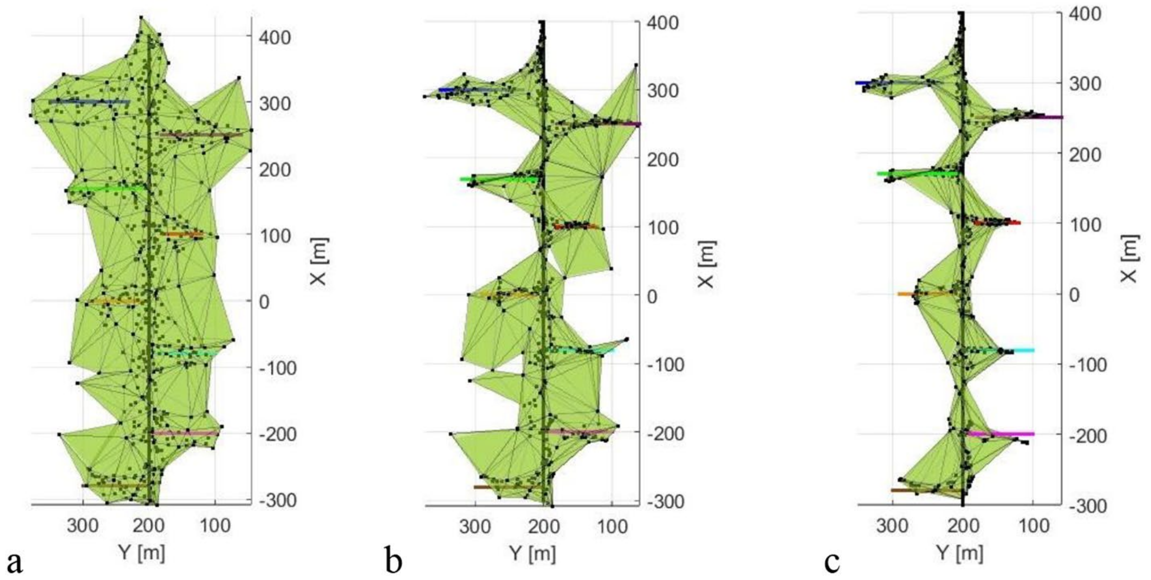

Fig. 10 Plane view of alpha shapes for (a) the original cloud of disturbed events; (b) the collapsed cloud; (c) the collapsed cloud after DBSCAN. The colorful lines represent the fracture network model

5 Conclusions

Ensuring accurate imaging of formed fractures and reconstructing the extent of the reservoir within a dispersed seismic cloud both pose a challenge due to inaccuracies in event location. We proposed a three-step procedure for identifying seismogenic structures with limited available information as well as for calculating a fractured zone. Our analysis was based solely on the located hypocenters and their location errors. By employing the collapsing method we were able to simplify the pattern of the seismic event cloud. We demonstrated that applying this method beforehand facilitated our efforts to identify structures in subsequent steps. Clustering made it possible to separate those areas with increased event intensity relative to the surrounding area and noise. We presented a method for automatically selecting clustering parameter based on the size of errors that occur in the data. This made it possible to differentiate clusters without the user's intervention in the clustering parameters.

The method we proposed for calculating the reservoir volume based on microseismic event location allows for a more precise and realistic estimation. This helps avoid overestimating the volume of the reservoir. We showed that after simplifying the cloud using the collapsing method, the estimated reservoir volume is 4 times smaller than that calculated for the original cloud of events. The volume of the collapsed cloud, after discarding noise identified by DBSCAN, is 14 times smaller than the original cloud. The area of the reservoir after using three-step procedure is being reduced to its main fissures, when connectivity exists. Our refined analysis, which leads to a more realistic volume estimation, reveals linear structures that play a crucial role in gas extraction. It also allows for better well location in the future and safer decisions regarding reservoir stimulation.

Although our approach was inspired by the experimental setups of hydraulic fracturing, particularly those used for shale gas exploration, this technology can be applied anywhere that hydraulic fracturing is conducted, or wherever there is a need to identify structures based on seismic events.

Author contributions Conceptualization: Elżbieta Węglińska and Andrzej Leśniak; Data curation: Elżbieta Węglińska; Methodology: Elżbieta Węglińska and Andrzej Leśniak; Formal analysis: Elżbieta Węglińska; Investigation: Elżbieta Węglińska and Andrzej Leśniak; Project administration: Elżbieta Węglińska; Software: Elżbieta Węglińska and Andrzej Leśniak; Supervision: Andrzej Leśniak; Visualisation: Elżbieta Węglińska; Writing-original draft: Elżbieta Węglińska; Writing-review&editing: Elżbieta Węglińska and Andrzej Leśniak.

Funding This research is funded by the AGH University of Krakow as a part of the statutory project.

Declarations

Competing interests The authors declare no financial or non-financial conflict of interest.

References

Abdulaziz MA (2013) Microseismic Imaging of Hydraulically Induced-Fractures in Gas reservoirs: a Case Study in Barnett Shale GasReservoir, Texas, USA. Open J Geol 3:361–369. https://doi.org/10.4236/ojg.2013.35041

Ankerst M, Breunig MM, Kriegel HP, Sander J (1999) OPTICS: Ordering Points To Identify the Clustering Structure. In Proc. ACM SIGMOD'99 Int. Conf. on Management of Data, Philadelphia PA

Arrowsmith SJ, Eisner L (2006) A technique for identifying microseismic multiplets and application to the Valhall field, North Sea. Geophysics 71(2):V31–V40. https://doi.org/10.1190/1.2187804

Asanuma H, Ishimoto M, Jones RH, Phillips WS, Niitsuma H (2001) A variation of the collapsing method to Delineate structures inside a Microseismic Cloud. Bull Seismol Soc Am 91(1):154–160. https://doi.org/10.1785/0120000063

Birant D, Kut A (2007) ST-DBSCAN: an algorithm for clustering spatial–temporal data. Data Knowl Eng 60:208–221. https://doi.org/10.1016/j.datak.2006.01.013

Bossu R (2000) A simple approach to constrain the position and the geometry of seismogenic structures: application to the Karthala volcano (Grande Comores Island, Mozambique Channel. J Seismolog 4:41–48. https://doi.org/10.1023/A:1009890909336

Cesca S (2020) Seiscloud, a tool for density-based seismicity clustering and visualization. J Seismolog 24(3):443–457. https://doi.org/10.1007/s10950-020-09921-8

Cesca S, Sen AT, Dahm T (2014) Seismicity monitoring by cluster analysis of moment tensors. Geophys J Int 96(3):1813–1826. https://doi.org/10.1093/gji/ggt492

Custódio S, Lima V, Vales D, Cesca S, Carrilho F (2016) Imaging active faulting in a region of distributed deformation from the joint clustering of focal mechanisms and hypocentres: application to the azores–western Mediterranean region. Tectonophysics 676:70–89. https://doi.org/10.1016/j.tecto.2016.03.013

Douglas A (1967) Joint epicentre determination. Nature 215:47–48. https://doi.org/10.1038/215047a0

Edelsbrunner H, Mücke EP (1994) Three-dimensional alpha shapes. ACM Trans Graphics 13(1):43–72. https://doi.org/10.1145/174462.156635

Edelsbrunner H, Kirkpatrick D, Seidel R (1983) On the shape of a set of points in the plane. EEE Trans Inform Theory 29(4):551–559. https://doi.org/10.1109/TIT.1983.1056714

Erokhin GN, Baranov VD, Kremlev AN, Rodin SV (2013) Compact Surface Microseismic Monitoring Technology. EAGE and SPE Joint Workshop: Geoscience Monitoring of the Field Development Process 2013:1–5, https://doi.org/10.3997/2214-4609.201701918

Ester M, Kriegel HP, Sander J, Xu X (1996) A density-based algorithm for discovering clusters in large spatial databases with noise. Proc. KDD 96(34):226–231

Fehler M, Jupe A, Asanuma H (2001) More Than Cloud: new techniques for characterizing reservoir structure using induced seismicity. Lead Edge 20(3):324–328. https://doi.org/10.1190/1.1438942

Frohlich C (1987) Aftershocks and temporal clustering of deep earthquakes. J Geophys Research: Solid Earth 92(B13):13944–13956. https://doi.org/10.1029/JB092iB13p13944

Georgoulas G, Konstantaras A, Katsifarakis E, Stylios CD, Maravelakis E, Vachtsevanos GJ (2013) Seismic-mass density-based algorithm for spatio-temporal clustering. Expert Syst Appl 40(10):4183–4189. https://doi.org/10.1016/j.eswa.2013.01.028

Graham RL (1972) An efficient algorithm for determining the Convex Hull of a Finite Planar Set. Inform Process Lett 1(4):132–133

Grigoli F, Ellsworth W, Zhang M, Mousavi M, Cesca S, Satriano C, Beroza G, Wiemer S (2021) Relative earthquake location procedure for clustered seismicity with a single station. Geophys J Int 225(1):608–626. https://doi.org/10.1093/gji/ggaa607
Gutenberg B, Richter CF (1944) Frequency of earthquakes in California. Bull Seismol Soc Am 34(4):185–188. https://doi.org/10.1785/BSSA0340040185
Havskow J, Ottemoller L (2010) Routine data processing in earthquake seismology. Springer
Jones RH, Stewart RC (1997) A method for determining significant structures in a cloud of earthquakes. J Geophys Research: Solid Earth 102:8245–8254. https://doi.org/10.1029/96jb03739
Kagan YY (1991) 3-D rotation of double-couple earthquake sources. Geophys J Int 106(3):709–716. https://doi.org/10.1111/j.1365-246X.1991.tb06343.x
Kamer Y, Ouillon G, Sornette D, Woessner J (2015) Condensation of earthquake location distributions: optimal spatial information encoding and application to multifractal analysis of south Californian seismicity. Phys Rev E 92:022808. https://doi.org/10.1103/PhysRevE.92.022808
Kamer Y, Ouillon G, Sornette D (2020) Fault network reconstruction using agglomerative clustering: applications to southern Californian seismicity. https://doi.org/10.5194/nhess-2020-231 (preprint; last revised January 2023)
Karami A, Johansson R (2014) Choosing DBSCAN parameters automatically using Differential Evolution. Int J Comput Appl 91(7). https://doi.org/10.5120/15890-5059
Leśniak A, Śledź E, Mirek K (2020) Detailed Recognition of Seismogenic Structures Activated during Underground Coal Mining: a Case Study from Bobrek Mine. Pol Energies 13:4622. https://doi.org/10.3390/en13184622
Li KL, Abril C, Gudmundsson O, Gudmundsson GB (2019) Seismicity of the Hengill area, SW Iceland: details revealed by catalog relocation and collapsing. J Volcanol Geoth Res 376:15–26. https://doi.org/10.1016/j.jvolgeores.2019.03.008
Liu X, Jin Y, Lin B, Zhang Q, Wei S (2021) An integrated 3D fracture network reconstruction method based on microseismic events. J Nat Gas Sci Eng 95:104182. https://doi.org/10.1016/j.jngse.2021.104182
Maxwell SC, Chorney D, Goodfellow SD (2015) Microseismic geomechanics of hydraulic-fracture networks: insights into mechanisms of microseismic sources. Lead Edge 34:904–910. https://doi.org/10.1190/tle34080904.1
Mayerhofer MJ, Lolon EP, Warpiński NR, Cipolla CL, Walser D, Rightmire CM (2010) SPE Prod Oper 25(1):89–98. https://doi.org/10.2118/119890-PA. What Is Stimulated Reservoir Volume?SPE-119890-PA
Moulavi D, Jaskowiak PA, Campello RJGB, Zimek A, Sander J (2014) Proceedings of the 2014 SIAM International Conference on Data Mining 839–847
Niitsuma H, Moriya H, Asanuma H, Evans K, Jones R, Jung R, Baria R (2002) Detecting hydraulically created permeable structures in the soultz hdr site by super resolution seismic mapping techniques, Proceedings 24th NZ Geothermal Workshop 2002
Ouillon G, Sornette D (2011) Segmentation of fault networks determined from spatial clustering of earthquakes. J Geophys Res 116:B02306. https://doi.org/10.1029/2010JB007752
Ouillon G, Ducorbier C, Sornette D (2008) Automatic reconstruction of fault networks from seismicity catalogs: three-dimensional optimal anisotropic dynamic clustering. J Geophys Res 113:B01306. https://doi.org/10.1029/2007JB005032
Petersen GM, Niemz P, Cesca S, Mouslopoulou V, Bocchini G-M (2020) Clusty, the waveform-based network similarity clustering toolbox: Concept and application to image complex faulting offshore Zakynthos (Greece). Geophys J Int 224(3):2044–2059. https://doi.org/10.1093/gji/ggaa568
Rutqvist J, Rinaldi AP, Cappa F, Moridis GJ (2015) Modeling of fault activation and seismicity by injection directly into a fault zone associated with hydraulic fracturing of shale-gas reservoirs. J Petrol Sci Eng 127:377–386. https://doi.org/10.1016/j.petrol.2015.01.019
Schaefer AM, Daniell JE, Wenzel F (2017) The smart cluster method. J Seismolog 21(4):965–985. https://doi.org/10.1007/s10950-017-9646-4
Starczewski A, Goetzen P, Er MJ, New method for automatic determining of the Dbscan parameters (2020) A. J Artif Intell Soft Comput Res 10(3):209–221. https://doi.org/10.2478/jaiscr-2020-0014
Święch E, Wandycz P, Eisner L, Pasternacki A, Maćkowski T, Downhole microseismic monitoring of shale deposits: case study from NORTHERN POLAND (2017) Acta Geodyn Geomater 14(187):297–304. https://doi.org/10.13168/AGG.2017.0012
Trugman DT, Shearer PM (2017) GrowClust: a hierarchical clustering algorithm for relative Earthquake Relocation, with application to the Spanish Springs and Sheldon, Nevada, Earthquake sequences. Seismol Res Lett 88(2A):379–391. https://doi.org/10.1785/0220160188
Umar IA, Negash BM, Quainoo AK, Ayoub MA (2021) An outlook into recent advances on estimation of effective stimulated reservoir volume. J Nat Gas Sci Eng 88:103822. https://doi.org/10.1016/j.jngse.2021.103822

Waldhauser F, Ellsworth WL (2000) A double-difference earthquake location algorithm: Method and application to the northern Hayward fault. Calif Bull Seismological Soc Am 90(6):1353–1368. https://doi.org/10.1785/0120000006

Wandycz P, Święch E, Eisner L, Pasternacki A, Wcisło M, Maćkowski T (2019) Estimation of the quality factor based on the microseismicity recordings from Northern Poland. Acta Geophys 67:2005–2014. https://doi.org/10.1007/s11600-019-00362-7

Węglińska E, Leśniak A (2021) Induced Seismicity and detailed fracture mapping as tools for evaluating HDR Reservoir volume. Energies 14:2593. https://doi.org/10.3390/en14092593

Węglińska E, Leśniak A (2022) Comparison of Microseismic Locations Scatter Reduction Methods and Unsupervised Machine Learning Algorithms for Automatic Detection of Seismogenic Structures in a Polish Hard Coal Mine. Proceedings of the 10th international symposium on rockbursts and seismicity in mines, Tucson, USA

Woodward K, Wesseloo J, Potvin Y (2018) A spatially focused clustering methodology for mining seismicity. Eng Geol 232:104–113. https://doi.org/10.1016/j.enggeo.2017.11.015

Wu W-N, Zhao L (2013) Delineating seismogenic structures by a revised best estimate method: application to the Taiwan orogenic belt. J Seismolog 17(2):545–556. https://doi.org/10.1007/s10950-012-9336-1

Yang S, Yi Y, Lei Z, Zhang Y, Harris NB, Chen Z (2018) Improving predictability of stimulated reservoir volume from different geological perspectives. Mar Pet Geol 95:219–227. https://doi.org/10.1016/j.marpetgeo.2018.04.018

Zhang P, Li X, Chen J (2022) Prediction Method for Mine Earthquake in Time sequence based on clustering analysis. Appl Sci 12(21):11101. https://doi.org/10.3390/app122111101

Zhao XP, Young RP Numerical Simulation of Seismicity Induced by Hydraulic Fracturing in Naturally Fractured Reservoirs. Paper presented at the SPE Annual Technical Conference and, Exhibition (2009) New Orleans, Louisiana, October 2009. https://doi.org/10.2118/124690-MS

Zimmer U (2011) Calculating Stimulated Reservoir Volume (SRV) with Consideration of Uncertainties in Microseismic-Event Locations. Paper presented at the Canadian Unconventional Resources Conference, Calgary, Alberta, Canada, November 2011. https://doi.org/10.2118/148610-MS

Zoback M, Kohli A (2019) Induced Shear Slip during Hydraulic Fracturing. Unconventional Reservoir Geomechanics: Shale Gas, tight oil, and Induced Seismicity. Cambridge University Press, Cambridge, pp 301–321

Załącznik 2

energies

MDPI

Article

Detailed Recognition of Seismogenic Structures Activated during Underground Coal Mining: A Case Study from Bobrek Mine, Poland

Andrzej Leśniak, Elżbieta Śledź * and Katarzyna Mirek

Department of Geoinformatics and Applied Computer Science, Faculty of Geology, Geophysics and Environmental Protection, AGH University of Science and Technology, 30-065 Kraków, Poland; lesniak@agh.edu.pl (A.L.); kmirek@agh.edu.pl (K.M.)

* Correspondence: esledz@agh.edu.pl

Received: 13 July 2020; Accepted: 2 September 2020; Published: 5 September 2020

check for updates

Abstract: In rock mass disturbed by mining activity, distortions in the stress balance may lead to seismic energy being emitted in reactivated seismogenic structures. One way of increasing the imaging resolution of these seismically active structures is through relocation, which itself can be achieved using the cloud collapsing method. This method partially eliminates perturbations in the location of seismic energy sources concerning the actual positions of these sources. It enables events to be grouped into spatially ordered structures that may correspond to actual tectonic structures, such as fractures, fissures, or faults. We present the results of applying the collapsing method in mining seismology using a cloud of located events recorded during mining activity at one of the coalfaces in the Bobrek hard coal mine. The relocation procedure was applied to all the foci of events recorded during mining activity on face 3/503 between April 2009 and July 2010. In the relocated point cloud, two types of the linear structure responsible for generating events are automatically distinguished using the HDBSCAN algorithm: structures directly related to mining activity and structures associated with local tectonics. The location of the separated structures of the first type corresponds to the range of coalface 3/503 and the shafts delimiting earlier mined seams 507 and 509 located below. The isolated structures of the second type, with almost vertical orientation, are associated with existing zones of discontinuity that become seismically active as a result of mining activity. The identified structures lie near the biggest events recorded, which is evidence that these structures may correspond to real discontinuity zones.

Keywords: mining seismicity; collapsing method; reactivated faults

1. Introduction

Underground mining of mineral resources (e.g., hard coal) or energy resources (e.g., crude oil, natural gas, or geothermal energy) leads to changes in stress distribution in mining areas. These changes can trigger dynamic phenomena in the form of seismic events of varying degrees of energy. In the case of underground hard coal mining, some surveys were conducted in many coal-mining areas and reported in the last several decades, e.g., [1–6]. The research on the registered seismic events was conducted mainly to increase the safety of underground work and minimize the adverse impact on the surface [7]. The registered events were analyzed in terms of the causes of its occurrence and its governing mechanisms. Various ways of categorization of the seismic phenomena accompanying exploitation have been proposed. Alber et al. [8] observed at least three different event types characterized by modes of failure, e.g., fault activation, remnant pillar punching, and beam failure. The other studies suggested the key importance of dynamic and static stresses on the character of induced events [9].

The more general classification is based on the observed bimodal distribution of seismic energy [10–12], which in general indicates two types of seismic phenomena associated with mining. The first type includes low and medium energy seismic events, which most often occur in the immediate vicinity of longwall faces or exploited chambers, usually as a result of mining activity. A characteristic feature of the mechanism behind these phenomena is the high share of non-shear components. The second type comprises medium and high energy phenomena associated with the renewal of old fractures and faults. The shear components dominate in this type of seismic phenomena. Their location is closely connected with the position of renewed seismogenic structures and may be located at a greater distance from coalfaces than the first type of phenomenon [13,14].

In many underground mines, including the Bobrek hard coal mine in southern Poland that is described in the article below, both categories of seismic events occur. Numerous seismic phenomena directly induced by the fracturing of the rock mass occur in areas of mining activity and in the case of this mine are concentrated above the mine coal seam or directly below it. The sources of the second group of phenomena recorded during the course of mining activity are located significantly (over 500 m) below the exploited coal seam. Due to the mechanism of their sources, these phenomena are mainly associated with a fault network whose existence is postulated based on tectonic and structural studies as well as on the genesis of individual geological structures. Their existence and location can only be inferred indirectly from seismic events.

For an effective study of the seismic events, the key factors are the precise location of event sources, identification of their source mechanisms, and separation of internal heterogeneities (clusters) inside the registered cloud of phenomena. The location of seismic sources using master event and double-difference relocation techniques and determination of their mechanism are currently standard techniques and are widely used in mining [15,16]. In turn, the separation of clusters in the cloud of located event sources is a difficult but necessary task to better understand the nature of dynamic phenomena. It enables the separation of spatial structures responsible for intensive seismic events and the location of zones particularly endangered by large seismic phenomena [17–19].

This article is a case study from the Bobrek mine, Poland. Its main goal is to determine the structures responsible for the generation of seismic events. For this purpose, it was necessary to increase the resolution of the cloud of localized seismic sources (so-called seismic cloud). The authors employed a well-known collapsing algorithm to increase the latter's resolution to map the structures responsible for the generation of seismic phenomena [20]. The three-step processing procedure that we proposed involved collapsing a cloud of seismic sources in seam No. 503, evaluation of the time slices of this cloud, as well as automatically isolating active microtectonic structures (e.g., fissures and fractures) recognized in this cloud. As the research shows, this procedure allows phenomena to be grouped into more spatially ordered structures such as lines or planes. These may correspond to actual tectonic structures such as fractures, fissures, or faults.

First, we will discuss the geological structure in the Bytom Basin area in which the Bobrek Coal Mine is located, together with the structural and geomechanical factors that contribute to high seismic activity both in this and in neighboring areas. This part will be followed by a short description of the collapsing method applied to the seismic sources and hierarchical density-based spatial clustering of applications with noise algorithm (HDBSCAN). Due to the significant impact that seismic event location errors have on the collapsing procedure, we also addressed the problem of identifying errors in the location of events recorded during the advance of the coalface. In the next part of the article, the author presents data recorded during the mining of seam 503 as well as the results of their relocation following the application of the collapsing procedure. Based on the above, the next section identifies structures with a simple, linear geometry that are responsible for generating some of the events. These results were then set against the earlier results of seismicity studies in this area. In the discussion, we present the benefits of the analyzed method in studies of mining-induced seismicity, as well as their limitations.

2. Geological Structure and Seismicity in the Area Covered by the Study

The occurrence of mining tremors depends on many factors, including the geological and tectonic structure, the location of the coalface, and past exploitation. The interaction of these factors has a significant impact on the formation of tremors.

The Bytom Basin forms a wide trough along the W-E axis and constitutes part of the Paleozoic Variscan structure, which has been cut up by numerous faults. The Bytom Basin is an asymmetrical and relatively shallow trough with a complex structure. Its axis runs latitudinally from West to East near the north-eastern flank. As a consequence, the layers in this flank have quite steep angles of collapse, which range from 8 to 20 degrees, while in the southern flank they do not exceed 3 degrees. The complex structure of the basin is additionally disturbed by a network of faults, mainly running in NW-SE direction and perpendicular to them, the planes of which have different projections and angles of inclination. Large faults with throw values of between several meters and almost 300 m are accompanied by a network of smaller faults with throw values ranging in size from several dozen centimeters up to approximately 20 m.

The geological profile in the vicinity of the coal seam 503 is shown in Figure 1. Carboniferous formations in the studied area reach a thickness of up to 550 m and contain numerous coal seams of varying thickness, up to a maximum of 12 m. A characteristic feature of the carboniferous period is its cyclical structure expressed by the alternating occurrence of sandstone, silt, claystone, conglomerates, and coal. These rocks differ in terms of their elastic properties and compressive strength. For example, sandstone has higher strength parameters than claystone and coal. One additional factor that has a decisive impact on the geomechanical properties of rocks is tectonics in all its forms (faults, joints, cleavage, and other inhomogeneities), which significantly reduces the strength of the rock massif [21]. Geomechanical parameters: volume density, frictional angle, cohesion, Young's modulus, Poissons's ratio, splitting tensile strength, and tension of geological layers are presented in Table 1.

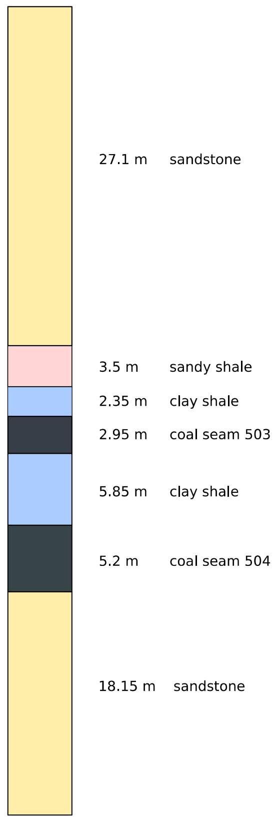

Figure 1. Geological profile in the vicinity of the coal seam 503 (based on data from Bobrek Mine).

Table 1. Geomechanical parameters of geological layers.

	Volume Density	Frictional Angle	Cohesion	Young's Modulus	Poisson's Ratio	Splitting Tensile Strength	Tension
	$\rho[\frac{kg}{m^3}]$	φ [deg]	c [MPa]	E [GPa]	ν [-]	R_r [MPa]	R_c[MPa]
Sandstone	2510	25.3	11.3	18	0.27	3.3	35.7
Sandy shale	2690	25	7.2	11.2	0.24	2.1	22.5
Clay shale	2600	24	6	10	0.25	1.9	19.2
Coal	1290	24	3.3	3.6	0.24	0.5	15.8

In the past, the Bytom Basin had been an area of very intensive hard coal mining. In the 1990s, production was scaled back significantly and exploitation of zinc-lead ore was brought to an end, as a result of which the rate of subsidence decreased together with the number of high-energy events. However, the Bytom Basin is still an area where mining activity continues to have a negative impact on the surface and continues to generate seismic events.

The propensity for rock bursts to occur in a rock mass depends on the geomechanical properties of the rock. It was found, for example, that an area was particularly susceptible to tremors when thick benches of strong rock, such as sandstone or mudstone, are located in the vicinity of a deposit [22]. Another influential factor is old tectonic stresses occurring in the rock, which have led to changes in geomechanical properties, increasing or decreasing their propensity for rock bursts.

In the Upper Silesian Coal Basin, events caused by coal mining activity are concentrated in several areas, one of which is the Bytom Basin. The susceptibility of a rock mass to rock bursts is explained in different ways.

Studies have revealed a close relationship between mining activity and low energy events, while more powerful events are associated with the tectonics of the Upper Silesian Coal Basin. The widespread occurrence of rock bursts in the Bytom Basin was initially explained as being the result of increased stresses in the syncline folds. However, it seems that the higher risk of rock bursts in these basins is due to the compaction of rocks, whereas in the past all three principal tectonic stresses were compressive in character [22].

Stec [12,23] proposed a general classification of the seismic events in this area, which involved dividing them into three groups. The first group consists of events with a slipping and shearing foci mechanism. Events of this type occur during progressive mining as a result of fractures in the seam of thick and compact rock complexes with high rigidity and strength parameters. The second group consists of events characterized by foci with a non-shearing mechanism. Such events are located directly in the coal seam and in the vicinity of active coalfaces. The third group comprises "regional" events, characterized by the highest energy, which usually occur far from areas of active mining activity. Their foci have a slip mechanism that is normal or reversible in character. The most common cause of these events is the interaction of tectonic and residual stresses existing in the analyzed area with mining-induced stresses.

The exploitation area of the Bobrek mine encompasses the region of the Bytom Basin (Figure 2), one of the three areas where the majority of mining events were recorded, including high energy events with local magnitudes of up to 4.0. During the mining of face 3 in seam No. 503 (3/503), the first events were observed in April 2009. The area remained seismically active until 8 July 2010. Most of the recorded events were low energy tremors. However, four higher local magnitude events were also registered: 2.9 (20 May 2009), 3.7 (16 December 2009), 3.0 (5 February 2010), and 2.8 (11 March 2010).

Marcak and Mutke [24] analyzed events recorded by mining seismological stations during mining of coalface 3/503. These authors concluded that tectonic stresses were of key importance in the distribution of seismic events. It was also observed that higher energy events began to occur as the coalface reached the axis of the Bytom Basin. The hypocentres of high energy events were located at a depth of 300 m to 800 m below the mined seam. At the same time, it was noted that once they had passed through the Bytom Basin, the energy produced by these events weakened and the depth of their hypocentres also decreased. The latter still occurred below the mined seam, but at a depth of less than 200 m. Furthermore, the authors showed that high-energy events occurring in the vicinity of the Bytom Basin had a different character to the phenomena typical of the Upper Silesian Coal Basin. The mechanism of these phenomena is associated with slipping in reverse faults, and the nature of the phenomena indicates a relationship between them and tectonics. These results were partially confirmed in the work of Kozłowska et al. [25]. In this article, the authors analyzed a 3.7 local magnitude event that occurred on 16 December 2009, during the course of mining coalface 3/503. The event mechanism indicates a reverse fault with an almost vertical plane. Numerical models that took into account current and past mining activity indicate that the phenomenon is associated with tectonics. However, mining activity affected a change in the stresses present in the local tectonics, which in turn triggered a fault process or the formation of a new fault on the weakening plane.

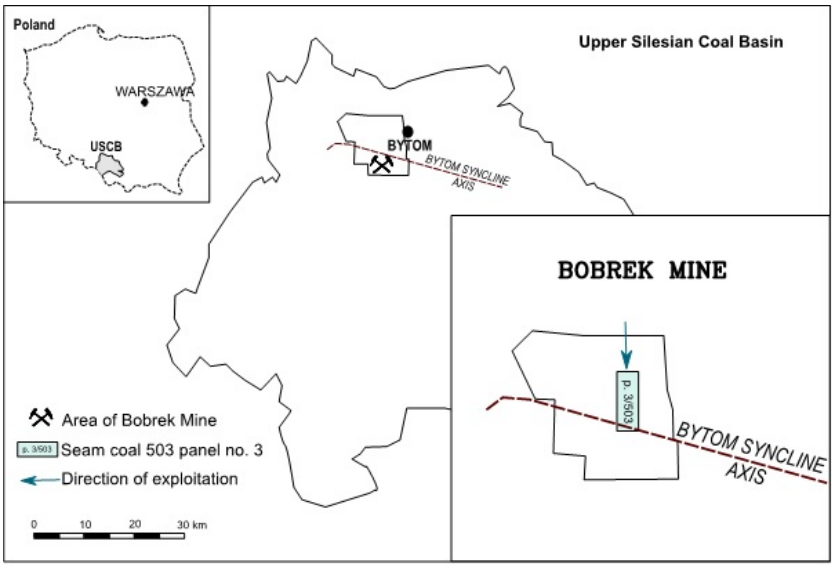

Figure 2. Location of the Bobrek mine area against the background of the Upper Silesian Coal Basin.

3. The Processing Method

To precociously identify seismically active microtectonic structures, the authors proposed applying the collapsing method [20,26,27] followed by automatic detection of clusters in the cloud of collapsed sources using the HDBSCAN method [28]. This two-step procedure is used to help identify the microtectonic structures responsible for the emission of some of the tremors accompanying the stimulation and exploitation of hydrothermal reservoirs and hydrocarbon deposits. The flowchart describing the processing steps is presented in Figure 3.

The location of emission sources involves some level of error, mainly due to the simplified velocity structure of the propagation medium and seismic event picking errors. This causes perturbation of localized sources in relation to the actual positions of these sources and blurs the undisturbed image of the seismic cloud. The purpose of collapsing is to limit at least partially such blurring and reduce perturbation. So, the collapsing is not used for the location of the events' sources. It is recommended as a step implemented after the source location step regardless of the method (single event location, JHD, double difference, and others [29]). It is not used to locate events but to decrease the seismic cloud dispersion and recognize its internal structures [30].

The key to implementing the collapsing procedure is determining the ellipsoid error for seismic events according to the used location method. Assuming that the errors are random with normal distribution and that the measurement is not burdened with a permanent error caused by, for example, defective measuring equipment or significant differences in conditions around the ellipsoid sensors, one can find the error ellipsoids of the located source for a particular significance level α, e.g., 99.5%.

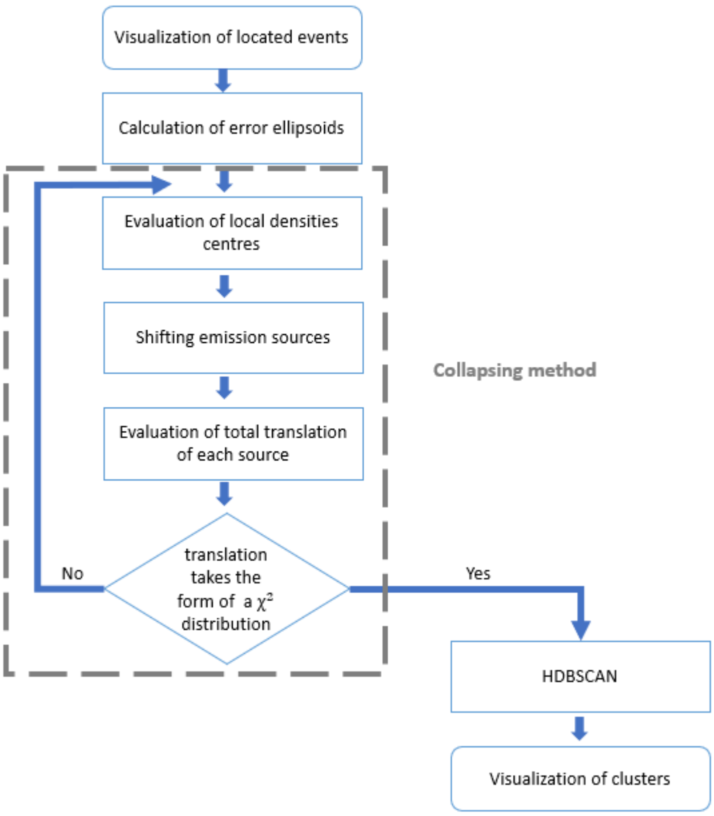

Figure 3. The flowchart of the processing steps. Details of each step are described in the text.

The collapsing procedure gradually shifts events towards local sources' densities. What is important to note is that the relocation of each event takes place within its error ellipsoid, in relation to which the source's location was established. Shifted hypocentres create a new set of locations. The entire relocation procedure is repeated in the same way for each subsequent iterative step until the translation population assumes the form of a chi-square distribution with three degrees of freedom [20]. The relocation of sources takes place within the boundaries of the error ellipsoid, and thus the new distribution of the sources (following the collapsing process) may reflect the actual spatial distribution of the foci of events undisturbed by the location error. This distribution is usually characterized by greater regularity and less spatial dispersion [20]. There are several variations of the original collapsing method. Asanuma et al. proposed a modification of the first version of the collapsing method, where the structure of the cloud depends on the distribution of locations within confidence ellipsoid [31]. Additionally, in the modified collapsing procedure, location movements depend on the dimensionality on the estimated original structures. In other publications, Asanuma et al. presented [30,32] another modification of the collapsing method that uses mutual coherency of waveforms and establishes the similarity of events. Here in the paper, we use the original collapsing method.

The HDBSCAN algorithm that is used in the next turn recognizes the clusters, i.e., parts of the seismic cloud with abnormally high densities of the collapsed sources. This algorithm identifies the so-called cluster cores as those seismic sources in the vicinity of which (i.e., closer than the pre-set limit value ε—radius of the neighbourhood) a sufficient (greater than or equal to the pre-set limit value) number of adjacent sources are located. To the cluster cores defined in this way are attached new sources that are closer than the pre-set value from any of the core sources. Sources not qualified for any cluster are referred to as noise.

The method of source clustering described in this way fails when naturally visible clusters have different densities because grouping is performed using the defined limit radius value ε. To avoid this, a number of radius values ε are used in the HDBSCAN algorithm, and the clusters identified by this method are looked at among stable clusters. An additional parameter used in the HDBSCAN algorithm allows to identify as relevant only clusters containing the number of points greater than the set parameter value. This allows to reject unimportant clusters with small numbers. In the last step of the procedure, from among the clusters separated in this way we choose only those characterized by linear geometry. They will depict active, linear tectonic structures, usually of natural origin. Other clusters with a more complex geometry will correspond to source clusters in zones with complex tectonics disturbed by mining activities.

4. Data

Data on the location of events and the progress of mining work in the Bobrek mine used in the article were published on the IS-EPOS platform [33]. A total of 2995 events were recorded and located in the period between April 2009 and July 2010. They were registered as a result of the exploitation of coalface 3/503. The hypocenters of these events occurred at various depths, ranging from 300 m below ground level to more than 2300 m below ground level. The local magnitude of these events ranged between 0 and 3.7. The most powerful event had a local magnitude M_L = 3.7 that occurred on 16 December 2009. This mining-induced tectonic event was associated with the local tectonic structure of the Bytom Syncline [25].

The Bobrek mine seismic network consists of 27 geophones with a recording band above 1 Hz. It is composed of 21 uniaxial and 6 triaxial geophones, all with a sampling frequency of 500 Hz. Most are located at the level of the exploited seam (approximately 750 m below the surface), two at sea level, and one at surface level. During the analyzed period, individual geophones were serviced and repaired. As a consequence, only those geophones that were operational on the day a particular event occurred were included in the location.

The locations were determined using the classical method for locating event sources based on uniaxial (vertical) sensors and triaxial sensors according to the registration times of the first seismic signal. An approximate model of medium velocity in the area of seam 503 was adopted, for which the velocity of longitudinal wave propagation (used for localization) was 3850 m/s. The location of geophones, along with the location of the sources of all registered seismic events, is presented in Figure 4. Coordinates in this figure and the following figures are in the local coordinate system “Sucha Gora” used in the Polish Coal Mines.

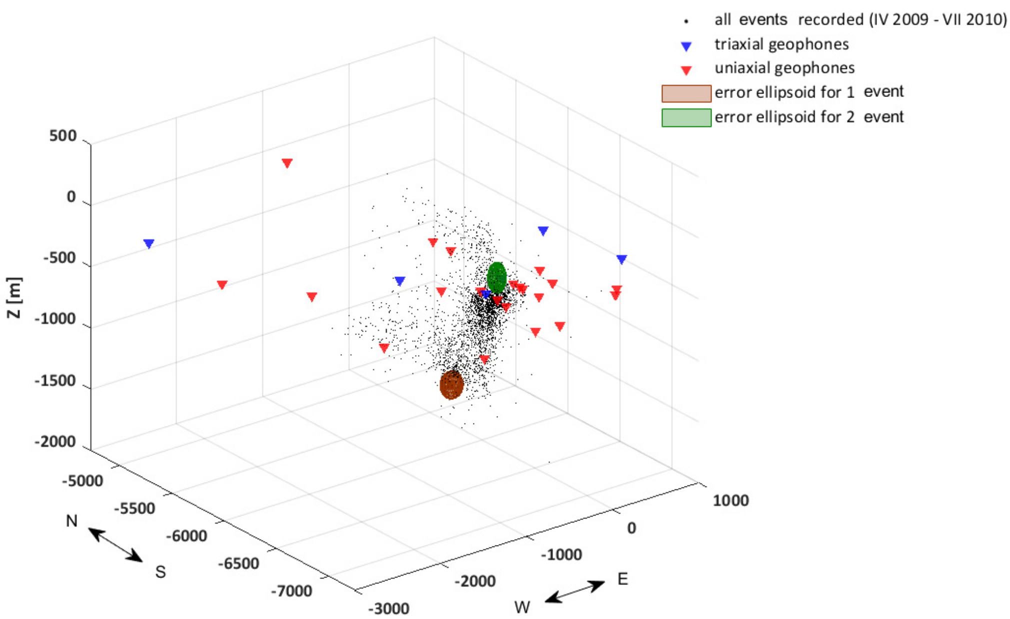

Figure 4. The seismic network of the Bobrek mine with events registered between April 2009 and July 2010. Uniaxial geophones are marked with red triangles and triaxial geophones with blue triangles.

Figure 5 features a histogram showing the seismic activity for each month. This histogram indicates that seismic activity changed during the period in which the mine was in operation. From December 2009 to May 2010, the number of events increased significantly, especially when compared to the months preceding this increase. This coincided with the moment when the active coalface crossed the Bytom basin axis. Additionally, the number of seismic events whose sources were located below and above seam No. 503 were indicated. Face 3 of this seam lies at a depth of approximately 700 m below the surface and, as such, the majority of the events were generated below this depth and only a small (roughly 10%) number occurred above. The number of events below the seam was calculated by taking into account the depth of the coalface at the end of each period. Most of the events occurred below seam 503. During this period, a small number of events were also recorded in the seam roof.

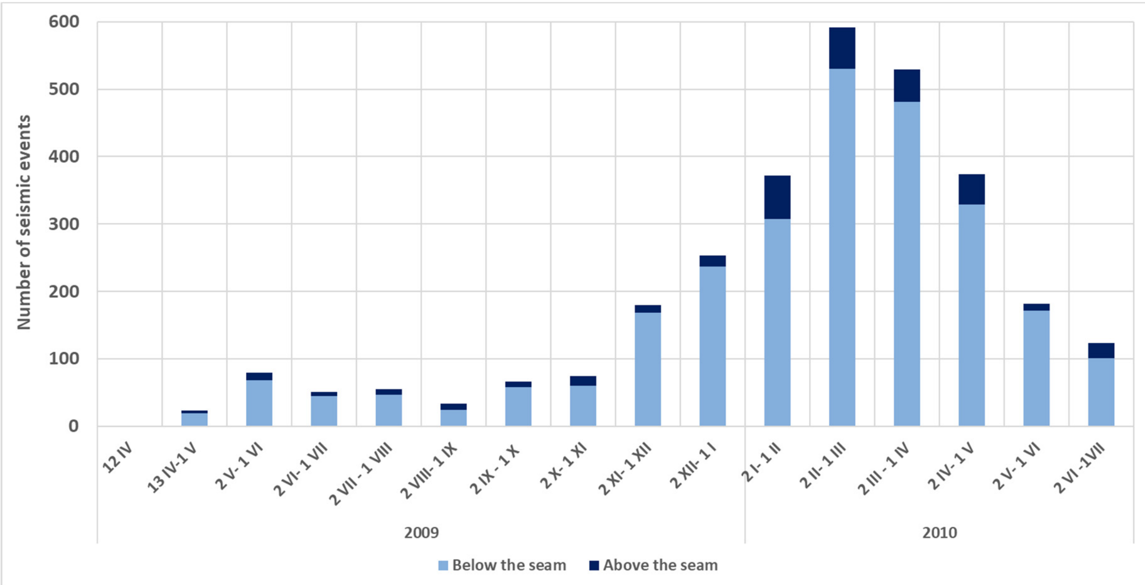

Figure 5. The number of events for each month between April 2009 and July 2010.

As has already been noted [24], the highest energy events took place 300–800 m below the mining level and were located at a short distance from the axis of the Bytom Basin.

The distribution of the event cloud is shown in monthly time intervals together with the current position of the active coalface in Figure 6A–O. The coalface progressed at an average rate of 50 m from month to month. In each sketch, the blue line indicates the position of the coalface at the beginning of the selected time interval, and the red line the position at the end. Additionally, in Figure 6A,O, the green rectangle shows the whole area of mining work. The mining works proceeded from north to south perpendicular to the axis of the Bytom basin. The axis of the Bytom basin was crossed in April 2010, 2 months before mining of the seam came to an end.

It can easily be seen that in the early months of mining activity, seismic events were relatively low and occurred mainly between 500 and 1000 m below the seam. In the next 6 months of mining at the seam, the events were similar to one another in terms of both intensity and the average depth of the source location. Starting from September 2009, there was a significant increase in event intensity as well as a gradual decrease in the location depth of the sources. In the last 2 months of mining activity (Figure 6N,O), events occurred relatively close to the seam, where coal was being mined.

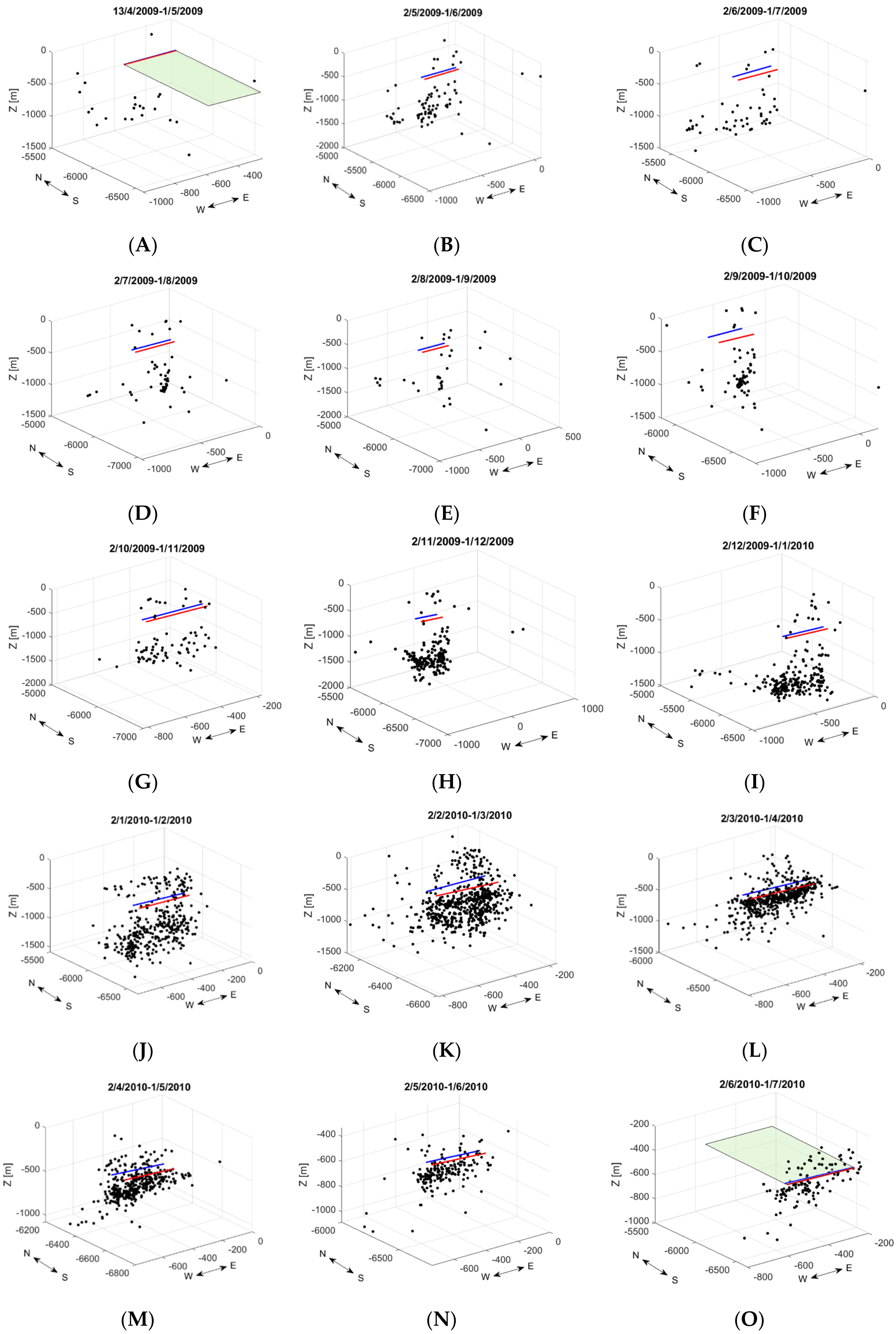

Figure 6. (**A**–**O**) Location of the point cloud in monthly intervals along with the current position of the coalface at the beginning and end of the interval. The green rectangle shows the whole area of mining work.

5. Results

After visualization, the second step of the processing procedure was an evaluation of the error ellipsoids for localized sources [34]. The orientation of the error ellipsoid is determined by the spatial configuration of the sensors in relation to the source location. The size of the ellipsoid is established by the partial errors in the measured parameters. To determine the error ellipsoid, it was assumed that the error in the time of the P wave was, depending on the signal quality, 4 ms. However, greater accuracy was achieved with good quality signals, dropping to as low as 2 ms. The sensor location error parameter was estimated at 0.1 m. In addition to the two types of error mentioned above, the magnitude of the location error is also affected by the simplified velocity model for the center of seismic wave propagation, both in terms of the inaccuracy of the geometric structure and the variable speed values. Sample error ellipsoids for the location of the foci of two events occurring at different depths at the adopted significance level are shown in Figure 4.

All the foci of seismic events recorded during the analyzed period underwent relocation procedure to decrease the dispersion of the cloud.

First, the location of the events after the final fourth iteration is shown in Figure 7. The compatibility of the theoretical and empirical distributions was checked in each iteration using the Kolmogorov–Smirnov test. In the final 4th iteration, the difference between distributions was so small, that the result of the compliance of the empirical distribution with the theoretical distribution test was positive.

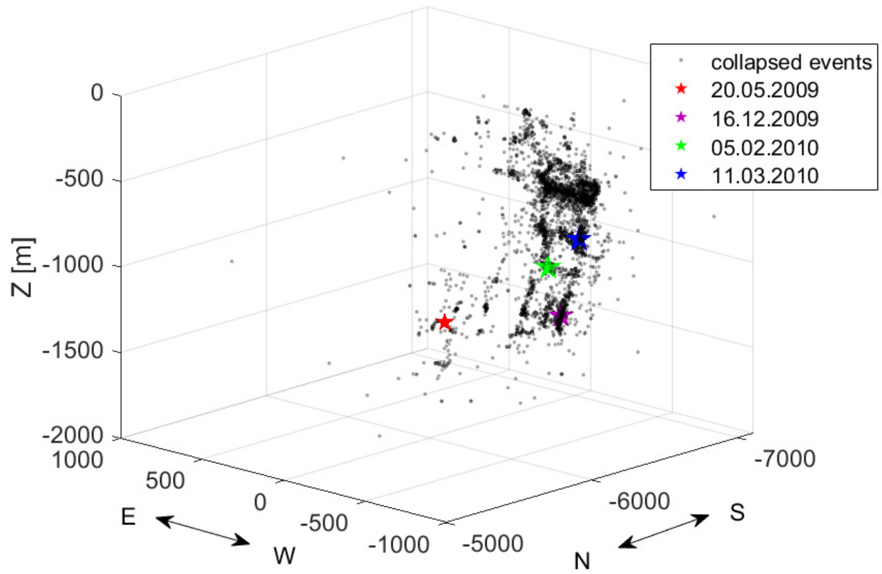

Figure 7. Seismic cloud after collapsing procedure. The figure shows also the location of the foci of the four largest events recorded during mining of the seam.

The event cloud following relocation set against the background of both seam 503 and two deeper, previously mined seams 507 and 509 are shown in Figure 8. Following the collapse of the sources, most phenomena were concentrated below the seam where mining activity was taking place (blue line) in the vicinity of the previously mined seams (lines green and orange). A specific image is likewise formed by the foci of numerous events grouped in narrow zones with a vertical or almost vertical course. They occur near the axis of the Bytom basin, the course of which is marked with red arrows. A relatively small number of events occurred above seam 503. One important trend to note is the sharp drop in the number of events that occurred once the basin axis was crossed, first above the seam, and then below it.

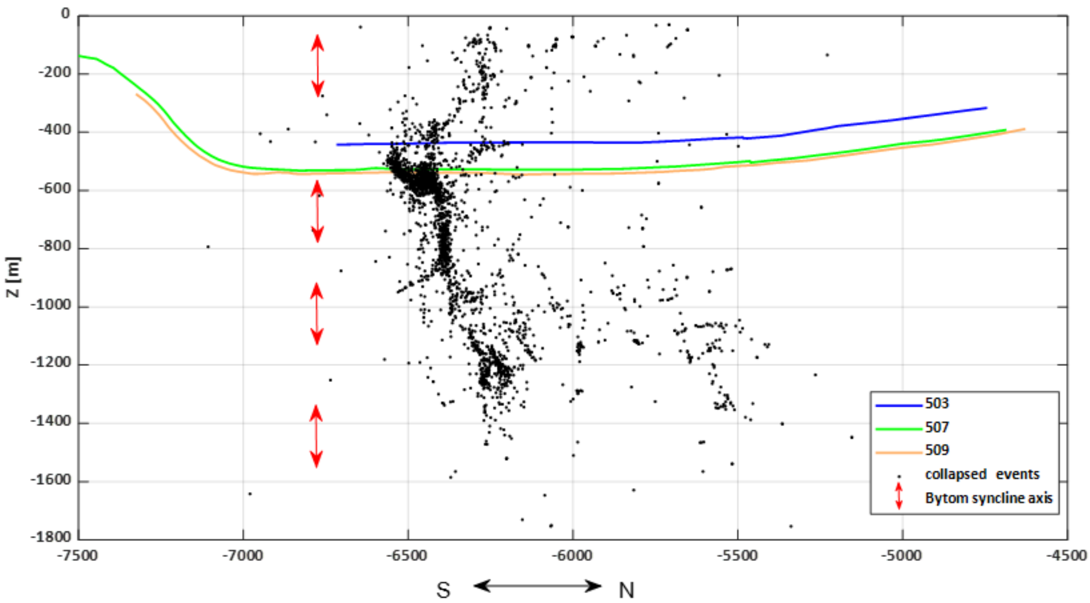

Figure 8. Vertical cross-section of seam 503 and previously mined seams 507 and 509 located below along with the location of event sources after relocation as well as the axis of the Bytom basin.

Generally speaking, following relocation, the cloud representing the foci of events is more heterogeneous, as is manifested in the occurrence of local densities of various shapes. Most often they assume a shape similar to straight lines and planes with different orientations.

Based on the results presented above, an attempt was made to identify clusters using a cloud of seismic events displaced by means of the collapsing method in the data set taken from the entire period of mining activity (Figure 9A,B). The clusters were identified automatically using the HDBSCAN algorithm. In Figure 9A, a light blue color indicates events that were considered as noise— they were not classified in any of the clusters. The other colors represent separate clusters. The goal was to identify distinct groups arranged along straight lines or on planes.

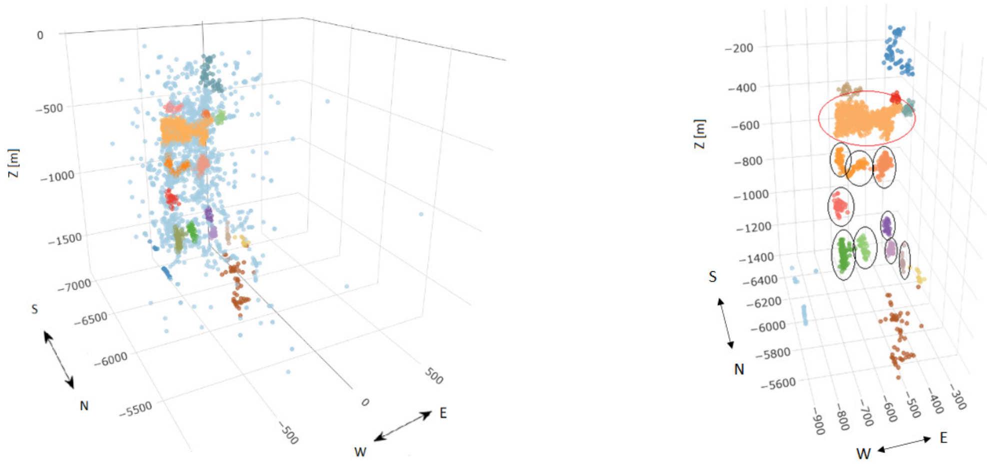

(A) **(B)**

Figure 9. (**A**) Automatic cluster detection using HDBSCAN; (**B**) Clusters that may correspond to tectonic structures (marked with a black ellipse) and directly related to mining activity (marked with a red ellipse).

6. Interpretation

The clusters identified in the seismic cloud by the HDBSCAN method allow the easier interpretation of the possible structures emerged in the mining area. Based on the identified clusters, the linear and planar structures were chosen (Figure 9B). The separated structures are associated with areas characterized by a rectilinear course with an above-average density of events. They are associated with real places of intensive seismic event that run along fracture zones with weakened rock mass. In Figure 9B, clusters marked with a black ellipse with an almost vertical course can be interpreted as local tectonic discontinuities that have been activated as a result of mining activity. Their occurrence was previously postulated by Marcak and Mutke [24] and was associated with the occurrence of flexures (monoclinal fold) in the Bytom basin. In basins of this type, we can expect the occurrence of fracture systems of varying scale with an almost vertical course and thus perpendicular to the axis of the basin and the selected seam [35]. The structures shown in Figure 9 are characterized by a depth of occurrence of between 500 m and 1400 m ppm, i.e., they are located below the two exhausted seams. The results in Figure 9 for the first time allow to directly identify and locate the position of main tectonic structures responsible for an intensive seismic event. It makes the presented findings significant and new. The previously published results only postulated the existence of such structures but because of the significant dispersion of seismic cloud (irrespectively of the method used for source location), it was difficult to identify them.

The cluster marked with a red ellipse with a more or less horizontal direction runs parallel to the active coalface and progress in tandem with its progress. Significantly, they occur deeper than exploited seam 503, namely in the immediate vicinity of exhausted seams 507 and 509. Figure 10 presents, against the backdrop of seams 503, 507, and 509, the location of the collapsed cloud and the range of exploited face 3/503 as well as the location of the shafts delimiting the exploited faces of seams 507 and 509.

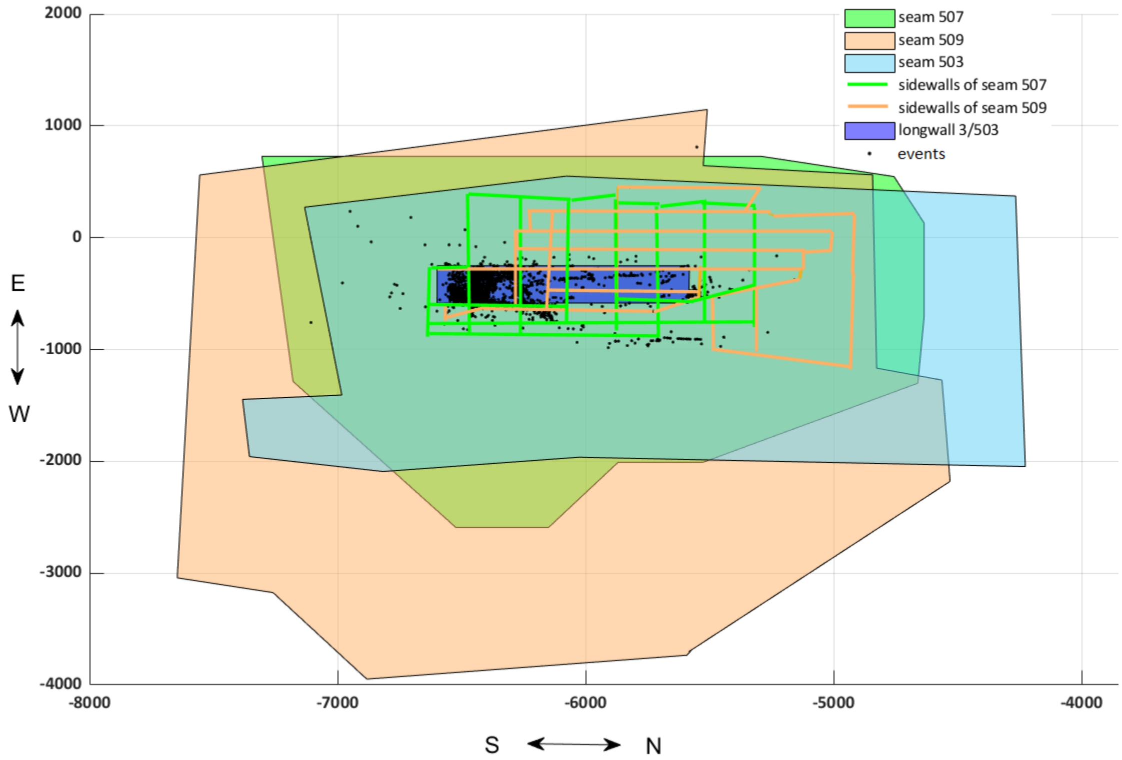

Figure 10. Flat projection of the boundaries of seams 503, 507, and 509; the range of exploited face 3/503; and the location of the shafts delimiting the exploited faces in seams 507 and 509. The black points show the location of the cloud of phenomena following the collapse.

The criterion for selecting these clusters from among the automatic detection clusters was the number of points in the cluster and if they are arranged along straight lines or on planes.

The shafts of exploited seams (lines marked in green and orange) roughly demarcate the zones located below exploited seam 3/503, where the continuity of the rock mass was disturbed as a result of mining activity prior to the exploitation of seam 503. These disturbed zones were the site of an intensive seismic event faithfully depicted by the spatial distribution of seismic event sources (Figure 10). The horizontal structure marked with a red ellipse in the cloud of phenomena in Figure 8 has similar positions and spatial orientations to the shafts of earlier exploited seams 507 and 509. Such compliance is very good for structures closer to seam 509. The reduction of cloud dispersion allowed in this case to directly link the linear seismogenic structures with the mining shafts of old, deeper coal exploitation.

As has already been noted in the case of mining-induced events, two types of seismic events are generally distinguished—mining-induced events and events of mining-tectonic origin [12]. Mining and tectonic seismicity are caused by the interaction between, on the one hand, mining activity, both current and in the past, and, on the other, locally existing seismogenic zones such as faults as well as areas affected by mining activity. Mining seismicity is associated with events located near active mining excavations. The vertical structures isolated from the event cloud were linked above with relatively large fracture zones, which in turn are connected with the flexure of the Bytom basin. These structures include three of the four events with energy greater than 10^7 J registered during mining of face 3/503 (Figure 7).

These events are located at relatively great depths, which indicates that they are of mining-tectonic origin rather than being induced by mining activity alone. They form part of the linear structures in the event cloud isolated in Figure 9, which are located below the shafts surrounding the faces of seams that have been mined. In this, one can directly map the tectonic structure responsible for the generation of the strong events as well as lower energy events generated by such structure.

The above observations suggest that vertical or nearly vertical linear structures identified after collapsing the cloud of phenomena correspond to actual zones of rock mass discontinuity activated during mining. The event recorded during the mining of face 3/503 activated these faults, leading to a series of numerous events with energy emitted over a wide range. In turn, horizontal linear structures located near the exploited seams correspond to the rock mass zones directly affected by the mining of hard coal deposits in the region of the Bytom basin axis. Deeper horizontal structures, which have also been activated by mining and, like vertical structures, occur near the basin axis, may be associated with discontinuities and stress distribution in the synclinal region, as is mentioned by Marcak and Mutke [24].

7. Conclusions

The presented case study from a deep coal mine shows that the applied collapsing method allows to increase the precision of identification of the structures associated with seismic zones in the cloud of seismic event sources. According to the authors of this method, the source cloud after relocation corresponds, in statistical terms, to the original cloud before relocation, in the sense that it provides a picture of the spatial distribution of sources acceptable within the framework of location error. Both distributions clearly differ in their degree of heterogeneity. After the collapse, this heterogeneity increases significantly and, as a rule, there is a clear tendency towards a concentration within the cloud. These clusters are identified with seismically active zones such as systems of fractures and fissures, faults, and areas affected, e.g., by mining activity. Because seismogenic zones are often associated with areas of high-stress concentration, collapsing makes it possible to verify certain hypotheses regarding the distribution of tectonic stress in a deformed rock mass.

Precise imaging of structures in a blurred seismic cloud is difficult and subjective. The collapsing operation makes it possible to reduce the degree of subjectivity when identifying structures and as a consequence increase the reliability of the method itself. The presented example from the Bobrek coal mine fully acknowledges the existence and location of such structures.

The more numerous the set of registered phenomena and the greater the seismic activity, the more effective the collapsing method is. In the case of seismic events registered in underground mines, the main triggering factor is the mining of the deposits. The site where these deposits are mined gradually moves in accordance with the established mining plan. The method used in this article makes a positive result possible if the zones of each seismogenic zone are imaged via at least several dozen phenomena.

The results presented in this article helps to understand why it is necessary to increase the precision when mapping seismogenic zones in a rock mass. On the collapsed cloud, clusters were automatically detected using the HDBSCAN algorithm. As the example presented in this article shows, these mapped zones can be connected with stress concentration sites as well as discontinuities and damaged zones. Compared with other geophysical methods for mapping discontinuities and monitoring dynamic changes in underground mines, seismology supported by appropriately selected processing methods (as shown above) ensures the widest range and increased resolution.

The results presented here will be of great interest to all involved in mining. Understanding the tectonic structures responsible for generating seismic shocks in mines should be crucial because it can help predict future events induced by mining activity and tectonics. They obstruct the coal exploitation process and influence the price of the excavated coal and finally the cost of the produced energy. The presented findings are significant for the safe and efficient extraction of coal in underground mines.

Author Contributions: Conceptualization, A.L. and E.Ś.; Methodology, A.L.; Software, A.L. and E.Ś.; Validation, A.L., E.Ś. and K.M.; Formal Analysis, A.L. and E.Ś.; Investigation, A.L. and E.Ś.; Resources, K.M.; Data Curation, E.Ś.; Writing—Original Draft Preparation, A.L., E.Ś. and K.M.; Writing—Review & Editing, A.L. and E.Ś.; Visualization, A.L. and E.Ś.; Supervision, A.L.; Project Administration, E.Ś.; Funding Acquisition, A.L. All authors have read and agreed to the published version of the manuscript.

Funding: This research received no external funding.

Acknowledgments: Authors thanks to authorities and geology service of Bobrek-Centrum coal mine for the geological and mining data as well as for help during the preparation of the presented article.

Conflicts of Interest: The authors declare no conflict of interest.

References

1. Kusznir, N.J.; Ashwin, D.P.; Bradley, A.G. Mining induced seismicity in the North Staffordshire coalfield, England. *Int. J. Rock Mech. Min. Sci. Geomech. Abstr.* **1980**, *17*, 45–55. [CrossRef]
2. Chouhan, R.K.S. Induced seismicity of Indian coal mines. *Phys. Earth Planet. Int.* **1986**, *44*, 82–86. [CrossRef]
3. Bischoff, M.; Cete, A.; Fritschen, R.; Meier, T. Coal Mining Induced Seismicity in the Ruhr Area, Germany. *Pure Appl. Geophys.* **2010**, *167*, 63–75. [CrossRef]
4. Li, T.; Cai, M.F.; Cai, M. A review of mining-induced seismicity in China. *Int. J. Rock Mech. Min. Sci.* **2007**, *44*, 1149–1171. [CrossRef]
5. Lasocki, S.; Idziak, A. Dominant Directions of Epicenter Distribution of Regional Mining-induced Seismicity Series in Upper Silesian Coal Basin in Poland. In *Seismicity Caused by Mines, Fluid Injections, Reservoirs, and Oil Extraction. Pageoph Topical Volumes*; Talebi, S., Ed.; Birkhäuser: Basel, Switzerland, 1999. [CrossRef]
6. Holub, K. A study of mining-induced seismicity in Czech mines with longwall coal exploitation. *J. Min. Sci.* **2007**, *43*, 32–39. [CrossRef]
7. Abdul-Wahed, M.K.; AlHeib, M.; Senfaute, G. Mining-induced seismicity: Seismic measurement using multiplet approach and numerical modeling. *Int. J. Coal Geol.* **2006**, *66*, 137–146. [CrossRef]
8. Alber, M.; Fritschen, R.; Bischoff, M.; Meier, T. Rock mechanical investigations of seismic events in a deep longwall coal mine. *Int. J. Rock Mech. Min. Sci.* **2009**, *46*, 408–420. [CrossRef]
9. Dou, L.; Mu, Z.; Li, Z.; Cao, A.; Gong, S. Research progress of monitoring, forecasting, and prevention of rockburst in underground coal mining in China. *Int. J. Coal Sci.* **2014**, *1*, 278–288. [CrossRef]
10. Gibowicz, J.S.; Kijko, A. *An Introduction to Mining Seismology*; Academic Press: San Diego, CA, USA, 1994.

11. McGarr, A. Energy budgets of mining-induced earthquakes and their interactions with nearby stopes. *Int. J. Rock Mech. Min.* **2000**, *37*, 437–443. [CrossRef]
12. Stec, K. Characteristics of seismic activity of the Upper Silesian Coal Basin in Poland. *Geophys. J. Int.* **2007**, *168*, 757–768. [CrossRef]
13. Kijko, A.; Drzęźla, B.; Stankiewicz, T. Bimodal character of the distribution of extreme seismic events in Polish mines. *Acta Geophys. Pol.* **1987**, *35*, 157–166.
14. Mendecki, A.J.; Lynch, R.A.; Malovichko, D.A. Routine Micro-Seismic Monitoring in Mines. In Proceedings of the Australian Earthquake Engineering Society 2010 Conference, Perth, Australia, 26–28 November 2010.
15. Schulte-Theis, H.; Joswig, M. Clustering and location of mining induced seismicity in the Ruhr Basin by automated master event comparison based on Dynamic Waveform Matching (DWM). *Comput. Geosci.* **1993**, *19*, 233–241. [CrossRef]
16. Boltz, M.S.; Pankow, K.L.; McCarter, M.K. Fine Details of Mining-Induced Seismicity at the Trail Mountain Coal Mine Using Modified Hypocentral Relocation Techniques. *Seismol. Soc.* **2014**, *104*, 193–203. [CrossRef]
17. Kijko, A.; Funk, C.W. Space-time interaction amongst clusters of mining induced seismicity. *Pure Appl. Geophys.* **1996**, *147*, 277–288. [CrossRef]
18. Leśniak, A.; Isakow, Z. Space–time clustering of seismic events and hazard assessment in the Zabrze-Bielszowice coal mine, Poland. *Int. J. Rock Mech. Min. Sci.* **2009**, *46*, 918–928. [CrossRef]
19. Estay, R.A.; Vallejos, J.A. Space or space—Time clustering? A selection criterion methodology using mining induced seismicity data. In Proceedings of the 9th International Symposium on Rockburts and Seismicity in Mines, Santiago, Chile, 15–17 November 2017.
20. Jones, R.H.; Stewart, R.C. A method for determining significant structures in a cloud of earthquakes. *J. Geophys. Res. Solid Earth* **1997**, *102*, 8245–8254. [CrossRef]
21. Bukowska, M. Laboratory studies of the mechanical properties of coal seam 503 and surrounding rocks in the "Bobrek-Center" mine. In *Characteristics of Stress-Deformation State in Seismic Hazard Based on the Parameters of Seismic Events*; Stec, K., Ed.; Central Mining Institute: Katowice, Poland, 2013; pp. 19–37. (In Polish)
22. Goszcz, A. *Elementy Mechaniki Skał oraz Tąpania w Polskich Kopalniach Węgla i Miedzi*; Wydawnictwo Instytutu Gospodarki Surowcami Mineralnymi i Energią PAN: Kraków, Poland, 1999.
23. Stec, K. Characteristics of the processes taking place at the sources of high energy events occurring in the Upper Silesian Coal Basin in Poland—Regional character. In Proceedings of the 7th International Symposium on Rockbursts and Seismcity in Mines, Dalian, China, 21–23 August 2009; Tang, C., Ed.; Rinton Press: New York, NY, USA; New Jersey, NJ, USA, 2009; pp. 415–426.
24. Marcak, H.; Mutke, G. Seismic activation of tectonic stresses by mining. *J. Seismol.* **2013**, *17*, 1139–1148. [CrossRef]
25. Kozłowska, M.; Orlecka-Sikora, B.; Rudziński, Ł.; Cielesta, S.; Mutke, G. Atypical evolution of seismicity patterns resulting from the coupled natural, human-induced and coseismic stresses in a longwall coal mining environment. *Int. J. Rock Mech. Min.* **2016**, *86*, 5–15. [CrossRef]
26. Fehler, M.; House, L.; Scott Phillips, W. Identifying Structures in Clouds of Induced Microseismic Events. In *SEG Technical Program Expanded Abstracts 1997*; Society of Exploration Geophysicists: Dallas, TX, USA, 1997. [CrossRef]
27. Phillips, W.S.; House, L.S.; Fehler, M.C. Detailed joint structure in a geothermal reservoir from studies of induced microearthquake clusters. *J. Geophys. Res. Solid Earth* **1997**, *102*, 11745–11763. [CrossRef]
28. Campello, R.J.G.B.; Moulavi, D.; Sander, J. Density-Based Clustering Based on Hierarchical Density Estimates. In *Advances in Knowledge Discovery and Data Mining. PAKDD 2013*; Pei, J., Tseng, V.S., Cao, L., Motoda, H., Xu, G., Eds.; Lecture Notes in Computer, Science; Springer: Berlin/Heidelberg, Germany, 2013; Volume 7819.
29. Rudziński, L.; Dębski, W. Extending the double difference location technique-improving hypocenter depth determination. *J. Seismol.* **2013**, *17*, 83–94. [CrossRef]
30. Asanuma, H.; Kumano, Y.; Izumi, T.; Soma, N.; Niitsuma, H.; Baria, R. Monitoring of Reservoir Behavior at Soultz HDR Field by Super-Resolution Microseismic Mapping. In Proceedings of the World Geothermal Congress 2005, Antalya, Turkey, 24–29 April 2005.
31. Asanuma, H.; Ishimoto, M.; Jones, R.H.; Phillips, W.S.; Niitsuma, H. A Variation of the Collapsing Method to Delineate Structures Inside a Microseismic Cloud. *Seismol. Soc. Am. Bull.* **2001**, *91*, 154–160. [CrossRef]

32. Asanuma, H.; Kumano, Y.; Niitsuma, H.; Wyborn, D.; Schanz, U.; Haring, M. Current Status of Microseismic Monitoring Techniques for the Stimulation of HDR/HFR Reservoirs. In Proceedings of the 2008 Australian Geothermal Energy Conference, Melbourne, Australia, 19–22 August 2008; pp. 29–36.
33. IS EPOS. Episode: BOBREK. 2017. Available online: https://tcs.ah-epos.eu/#episode:BOBREK (accessed on 10 January 2020). [CrossRef]
34. Havskov, J.; Ottemoller, L. *Routine Data Processing in Earthquake Seismology: With Sample Data, Exercises and Software*; Springer: Dordrecht, The Netherlands; Heidelberg, Germany; London, UK; New York, NY, USA, 2010.
35. Li, Y.; Hou, G.; Hari, K.R.; Neng, Y.; Lei, G.; Tang, Y.; Zhou, L.; Sun, S.; Zheng, C. The model of fracture development in the faulted folds: The role of folding and faulting. *Mar. Petrol. Geol.* **2018**, *89*, 243–251. [CrossRef]

Załącznik 3

energies

Article

Induced Seismicity and Detailed Fracture Mapping as Tools for Evaluating HDR Reservoir Volume

Elżbieta Węglińska * and Andrzej Leśniak *

Department of Geoinformatics and Applied Computer Science, Faculty of Geology, Geophysics and Environmental Protection, AGH University of Science and Technology, 30-059 Kraków, Poland
* weglinska@agh.edu.pl (E.W.); lesniak@agh.edu.pl (A.L.)

Abstract: The main goal of this paper was to estimate the heat exchange rock mass volume of a hot dry rock (HDR) geothermal reservoir based on microseismicity location. There are two types of recorded microseismicity: induced by flowing fluid (wet microseismicity) and induced by stress mechanisms (dry microseismicity). In this paper, an attempt was made to extract events associated with the injected fluid flow. The authors rejected dry microseismic events with no hydraulic connection with the stimulated fracture network so as to avoid overestimating the reservoir volume. The proposed algorithm, which includes the collapsing method, automatic cluster detection, and spatiotemporal cluster evolution from the injection well, was applied to the microseismic dataset recorded during stimulation of the Soultz-sous-Forets HDR field in September 1993. The stimulated reservoir volume obtained from wet seismicity using convex hulls is approximately five times smaller than the volume obtained from the primary cloud of located events.

Keywords: HDR; induced microseismicity; geothermal reservoir; collapsing; clustering; dbscan; SRV

Citation: Węglińska, E.; Leśniak, A. Induced Seismicity and Detailed Fracture Mapping as Tools for Evaluating HDR Reservoir Volume. *Energies* **2021**, *14*, 2593. https://doi.org/10.3390/en14092593

Academic Editor: Jens Birkholzer

Received: 20 February 2021
Accepted: 28 April 2021
Published: 1 May 2021

1. Introduction

Monitoring microseismicity in geothermal reservoirs is a useful tool for estimating the spatial distribution of fractures and evaluating fluid flow paths [1–3]. When fluid is injected, the fluid pore pressure changes causing a variation in effective stress, which can lead to rock failure [4]. Microseismic events identify the location of fractures generated or reactivated by injection [5]. When interpreting microseismic events recorded during hydraulic fracturing, it is important to understand what mechanism they were caused by [6]. During hydraulic fracturing, two mechanisms can result in the creation or reactivation of natural fractures. Microseismic events can be induced by fluid pressure (i.e., 'wet' microseismicity associated with a wet fracture network) or stress mechanisms (remote dry events associated with dry fractures) [6]. Wet microseismic events occur when the injected water reaches the preexisting fractures causing an increase in the fluid pressure. They are linked with a continuous slip as flow propagates. Dry events are induced by very quickly transferred mechanical stress change. They often occur in the vicinity of the hydraulic fracture tip [6]. The physical details of wet and dry events were studied by Maxwell [6].

One of the goals of hot dry rock (HDR) reservoir analysis is to estimate preferential fluid flow paths. It is important to distinguish dry volumes of a rock mass with a system of fractures that are not in any hydraulic connection with the stimulated fracture network. Excluding disconnected systems of fractures when interpreting fracture geometry can help avoid overestimating HDR reservoir performance [6]. Typically, the size of a microseismic cloud is used to estimate the stimulated reservoir volume (SRV). However, the cloud of microseismic locations is blurred and dispersed due to location errors, which in turn leads to an overestimation of microseismically active regions [6]. In the last few decades, significant improvements have been made to resolve structures within such clouds [7,8].

In this paper, an attempt has been made to evaluate SRV by investigating the volume of wet microseismicity, connected as a result of stimulation. The authors evaluated the percentage of wet events associated with fluid flow. It was assumed that the reservoir volume was directly proportional to the amount of wet microseismicity. The proposed algorithm includes the collapsing method [2], automatic cluster detection, and spatiotemporal cluster evolution from the injection well and was applied to the microseismic dataset recorded during stimulation of the Soultz-sous-Forets HDR field in September 1993. To increase the resolution of a seismic cloud, the collapsing method was applied. Based on relocated events, the seismic events were automatically divided into clusters using density-based spatial clustering of applications with noise algorithm (DBSCAN) [9]. Automatic cluster identification makes it possible to recognize parts of increased intensity of collapsed events—both wet and dry types. The spatiotemporal evolution of detected clusters was investigated to identify both events between which there was a possible hydraulic connection and events in which there was no connection. The latter usually appear as a distant, separated cluster. The convex hull algorithm [10] was used to estimate the SRV.

2. 1993 Soultz EGS Stimulation Injection Test and the Microseismic Data

2.1. The Soultz Geothermal Site

The Soultz-sous-Forets geothermal site is located in northeastern France, along the western edge of the Rhine Graben, a part of the West European Palaeogene Rift System [11]. This region is characterized by the occurrence of high-temperature gradients. The reservoir region in Soultz is situated between 2 to 4 km in granitic rock mass [12]. This granite is classified as an uplifted horst block [13]. It is estimated that the main granite body is a 331 ± 9 million years Hercynian monzogranite [14]. It is composed of phenocrystals of alkali feldspar in a matrix of quartz, plagioclase, biotite, and amphibole [15]. The crystalline basement is overlain by an approximate 1400 m layer of Triassic to Tertiary sediments [5]. More geological details are described in [11,16,17].

The site is located in a minor natural earthquake zone [18]. The region of Soultz has been investigated by many authors using microseismic, geophysical, geological, and hydraulic data [15,19–21]. Analysis of the cores and borehole geophysical logs indicated significant fracturing in the granitic massif with the main orientation of the fracture system NNW-SSE [22,23]. Although most of the fractures are naturally permeable, the permeability values are very low. This is due to sealing with hydrothermal deposits, such as calcite, silica, and clays [24].

Different parameters were used to study the stress field in the region of Soultz [25–28]. The orientation of the maximum horizontal principal stress (SH_{max}) up to a depth of 5 km is in the range of 170° N to 180° N [26], but is characterized by the presence of inhomogeneities in some depth intervals through major fracture zones [29].

2.2. Injection Test

During stimulation of the geothermal reservoir around the GPK-1 well in September 1993, 25,000 m^3 of fresh water was injected at a rate of up to 40 L/s and pressure of up to 10 MPa (Figures 1 and 2) [30]. In the September test, more than 10,000 microseismic events were recorded with three downhole 4-axis detectors (#4550, #4616, and #4601) and a hydrophone deployed in well EPS1 [31]. The frequency band of the detectors ranged from 10 Hz to 1 kHz, and the signals were digitized with a 5 kHz sampling frequency [31]. The borehole was open from the casing shoe at a depth of 2850 m and down to a depth of 3400 m [32]. Major intervals of water flow outlets from the well were located at measured depths of 2850–2900 m, 3090–3100 m, 3230–3240 m, and 3320–3325 m [33]. It was reported [34] that the most intensive seismic activity migrates from the top of the outlet point (2850–

2900) toward deeper levels when the flow rate and the wellhead pressure were increased. The injection created a nearly vertical cloud of microseismicity with the following rough size: 0.5 km in width, 1.2 km in length, and 1.5 km in height [35]. The test revealed that the permeability and transmissivity increased [31,34].

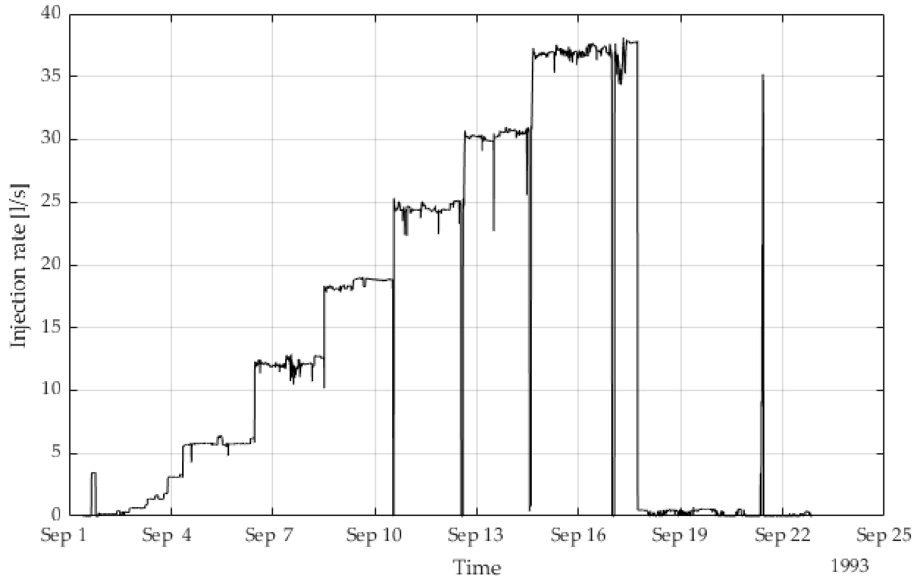

Figure 1. Fluid injection flow rate in GPK-1 Soultz 1993 injection test.

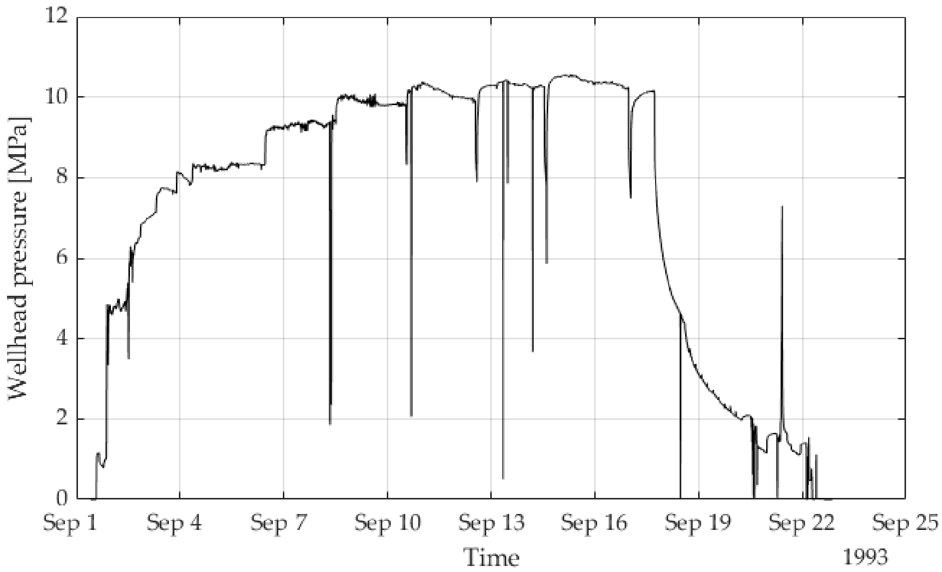

Figure 2. Wellhead pressure of GPK-1 Soultz 1993 injection test.

2.3. Microseismicity

Data on the location of events and seismic stations are available on the IS-EPOS platform [36]. The company CSMA located a total of 10,743 events during the period of 2–22 September 1993. All the coordinates were converted in order to indicate distances from the GPK-1 wellhead. The distances shown on the X-axis indicate the distances from the well to the east and the Y distances to the north. Depths are expressed in true vertical depths. The locations of microseismic events and detectors are presented in Figure 3. The positions of the 4-component detectors are marked with red triangles and a hydrophone with a blue triangle. The direction of the minimum horizontal stress (SH_{min}) is shown in Figure 3B. The moment magnitude of these events ranged between −2.4 to 0.8.

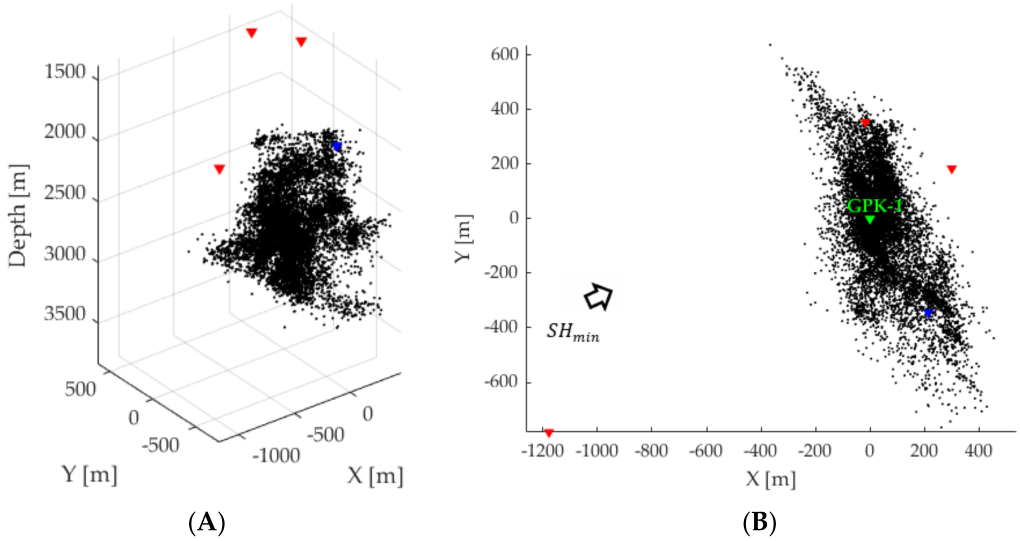

Figure 3. (**A**) Distribution of hypocenters of induced seismicity during the September 1993 injection test (black points) set against the background of the borehole network. The hydrophone is marked with a blue triangle and 4-component detectors with red triangles. (**B**) View from the top with the GPK-1 wellhead marked with a green triangle. The direction of the minimum horizontal stress is represented by SH_{min}.

The event rate was over 1000 per day (Figure 4). The link between the daily number of events and the injection flow rate is clearly demonstrated. Initially, the hypocenters of seismic events were located near the casing shoe at a depth range of 2800–3000 m [32]. At the end of the stimulation, the microseismic cloud reached a distance of 800 m from the injection well [37]. During the first days of the stimulation, seismicity extended downwards and was radially distributed. A few days after the stimulation began, the microseismic cloud expanded vertically and horizontally [32]. The microseismicity cloud grew gradually during the stimulation, with events distributed along subvertical planar structures [21,38,39]. The dominant structural trends inside the cloud range from NW-SE to N-S [32]. Jones et al. [32] mapped depth slices through the seismic data and showed the presence of several distinct strike directions for different sections of the seismic cloud, which suggest variation in the jointing patterns.

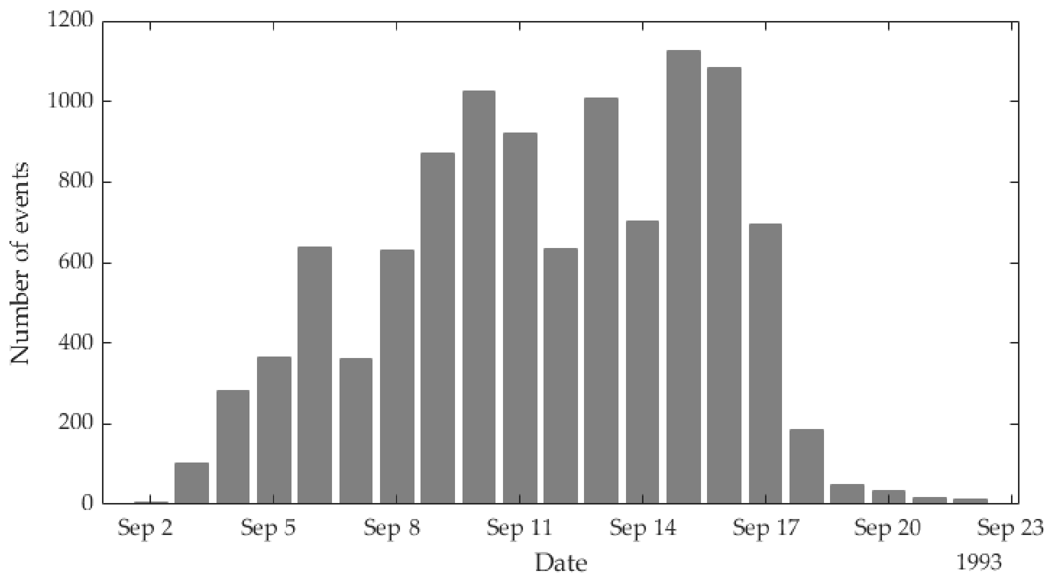

Figure 4. Daily number of microseismic events during the September 1993 test.

A lot of research has been conducted with the aim of finding structures inside this cloud of hypocenters. Most of these studies have been fragmentary in character and have only focused on selected structures. Phillips [3] performed a relative relocation of two chosen clusters and grouped events based on S-waveform shapes. Following their relocation, both clusters collapsed into well-defined patterns, consisting of two intersecting and terminating planar patches. The early activity inside these clusters indicates their link with permeable zones. Moriya et al. [35] analyzed the microseismicity cloud from the September 1993 test using high-resolution mapping methods, including the collapsing method, and the multiplet analysis method. Their analysis, based on microseismic multiplets, revealed that the fracture system was formed by the interconnection of fractures ranging in dimension from 4 to 26 m in the maximum principal direction of the existing tectonic stresses. They also claimed that the permeability of the system is enhanced by shear slippage and linking to more permeable fractures. The next set of results, provided by Moriya et al. [40], were drawn from an analysis of microseismic multiplets using the coherency function. They pointed out that multiplets were usually observed in the initial stage of the experiment. They concluded that seismic activation of fractures was caused by a small increase of pore pressure and extend to over several hundred meters. Evans et al. [21] applied the collapsing method to the cloud of microseismicity and claimed that it contains mainly linear and planar structures. They distinguished structure that appears from the proximity of a flow inlet at the beginning of the injection to 350 m downwards. A collapsed image of this structure suggests that it is tubular in shape due to a ± 50 m horizontal location error. After the application of multiplets and clustering, the structure appears to be a subvertical, NNW-SSE striking fracture zone 10–20 m in width.

So far, research of the cloud of hypocenters recorded during the 1993 stimulation has focused on finding the dominant trend of such structures and their mechanism. In this article, the authors discussed which localized events can be related to the injected fluid flow, which is crucial for determining the performance of a geothermal reservoir.

3. Detailed Fracture Mapping

To accurately identify the extent of the geothermal reservoir and structures that may be related to the injection fluid flow, the authors proposed a 3-step procedure. During each step, some events were rejected from further analysis. Rejected events are treated as noise and authors assumed them to be related to dry fractures with no connection to the main reservoir. They were induced by changes in the pre-existing tectonic stresses.

The first step, i.e., the application of the collapsing procedure, was intended to increase the resolution of the seismic cloud. Following the collapsing method, those events that were too distant location-wise from the others were rejected. In the next step, the authors performed the automatic cluster detection algorithm, i.e., DBSCAN. The clustering result made it possible to reject from further analysis events that occurred in spatial isolation from existing clusters and consider them as noise. The spatiotemporal evolution of detected clusters was studied with the aim of distinguishing between events possibly connected hydraulically and those that occur suddenly and are remote. A flowchart describing wet microseismicity identification is shown in Figure 5. Details of each procedure will be discussed in the following sections. The final step in the analysis is a convex hull algorithm, the purpose of which is to estimate the SRV.

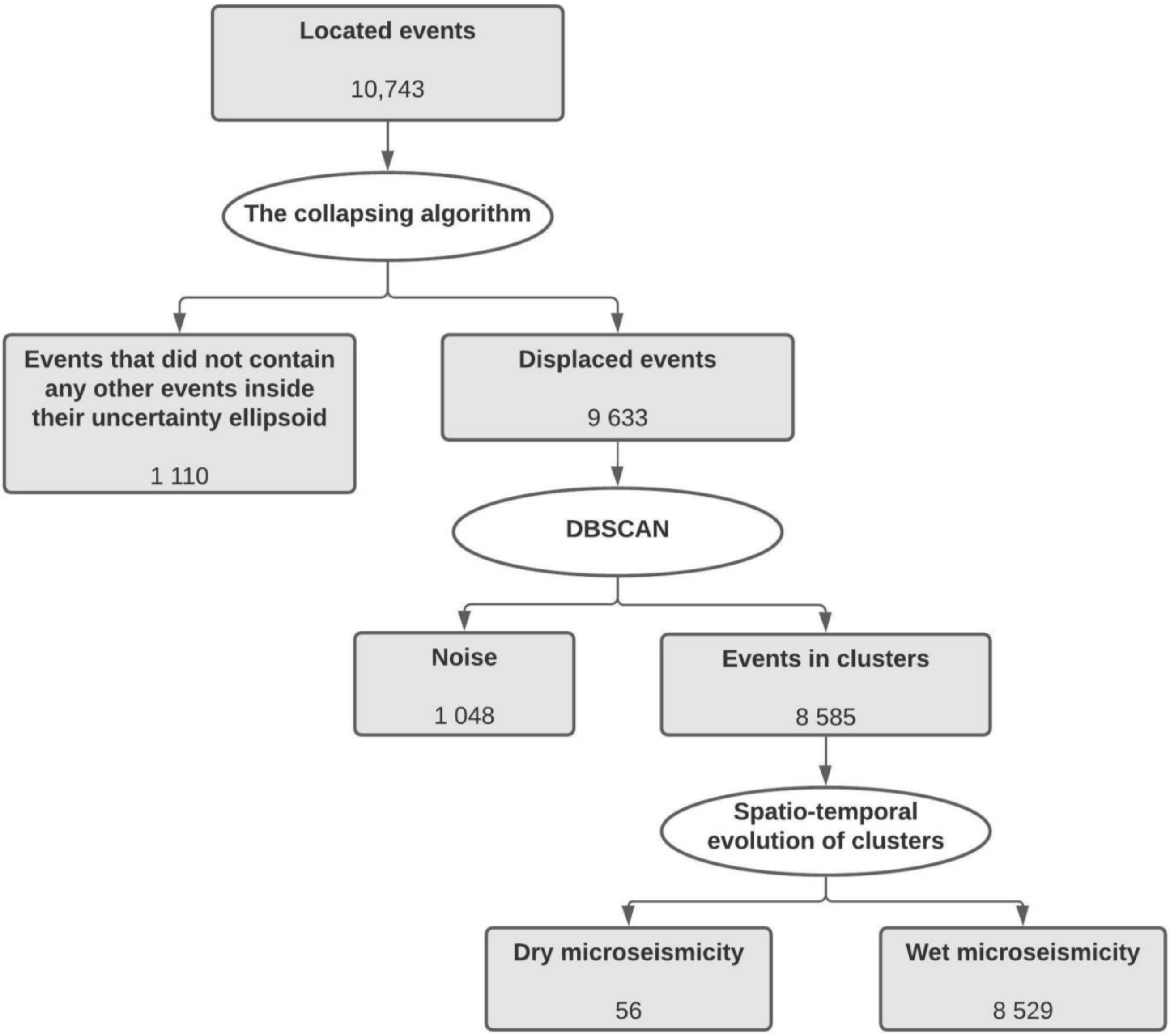

Figure 5. Flowchart describing wet microseismicity identification.

3.1. Collapsing Method

The reservoir structure was assessed by examining induced microseismicity. The first step increasing the resolution of the seismic cloud was the collapsing algorithm. The collapsing method has been used to reduce location error in the seismic cloud since 1997 [2]. This statistical optimization technique simplifies the seismic cloud structure originally blurred by location error. The key step in the collapsing procedure involves establishing the error ellipsoids for all seismic locations. The ellipsoid size is determined by partial errors in the measured parameters. Events are shifted towards local source densities inside their error ellipsoids iteratively until the translation vector takes the form of a χ^2 distribution with 3 degrees of freedom. The distribution of sources after collapsing may reflect the real distribution of the hypocenters not affected by location error. The collapsing procedure exhibited an ability to delineate seismic structures in volcanic seismicity [2], mining seismicity [41], and induced seismicity from geothermal reservoirs [21].

The results of applying the collapsing method to all of the hypocenters recorded during the September 1993 injection test is shown in Figure 6A. If an event did not move during the algorithm, it meant that it did not contain any other events inside their uncertainty ellipsoid. These 1110 events (Figure 6B) were excluded from further analysis. After their relocation, some structures inside the seismic cloud are more distinctive. In general, the collapsed cloud of hypocenters is more heterogeneous. This means that there is a tendency towards events within the cloud to concentrate. To resolve the microseismic structures inside the collapsed cloud, clustering was performed on displaced points (Figure 6C).

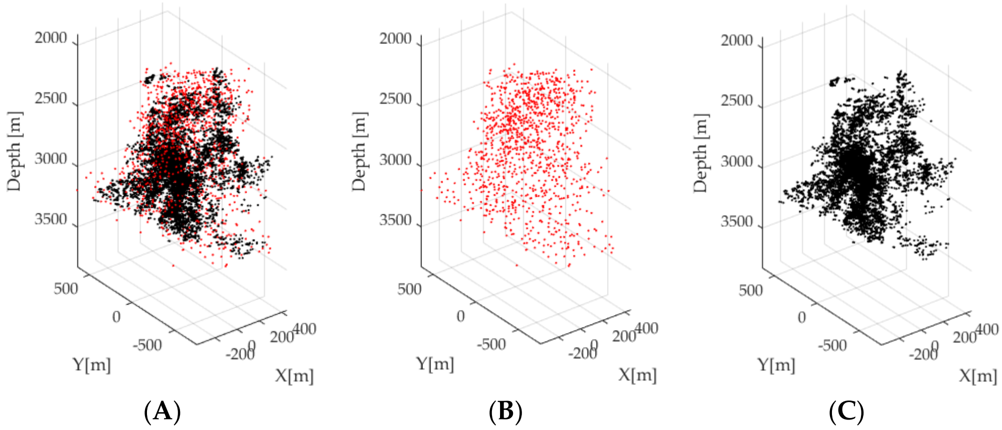

Figure 6. Results of applying the collapsing method on the microseismic cloud. (**A**) All hypocenters of events after the collapsing procedure. The black dots represent events that moved during the collapsing algorithm, while the red dots denote events that did not change their positions. (**B**) Events that did not change their location during the relocation. (**C**) Events that changed their location during the collapsing procedure.

3.2. Density-Based Spatial Clustering of Applications with Noise

According to density-based clustering approaches, clusters are regions where the density of points is much higher than outside the clusters [42]. One of the most commonly used density-based clustering algorithms is density-based spatial clustering of applications with noise (DBSCAN). This algorithm was proposed in 1996 [9] and is still widely used today [43–46]. One of the advantages of this method is the ability to extract clusters of arbitrary shape in dense regions and recognize noise points. The undoubted advantage of the algorithm is that there is no need to specify the number of groups to be found. The algorithm works assuming that points are assigned to the same group if they are density-reachable from each other.

The DBSCAN algorithm requires estimating two parameters: the minimum number of points and the radius. After conducting a clustering series with different parameters, the optimal results were obtained with the assumption that a minimum of 30 events within a neighborhood radius of 50 m constitues a cluster. The neighborhood radius value was chosen based on the distance of the data set using k-nearest neighbour distance graph.

The result of applying the DBSCAN algorithm to the relocated microseismic cloud is presented in Figure 7. The DBSCAN algorithm was able to identify 8 clusters and 1048 noise points. The points marked in gray represent noise and were rejected for further analysis. The points in other colors indicate particular clusters. Detected clusters have different shapes, sizes, and population numbers. The population in each cluster is listed in Table 1. These clusters represent high-density regions of event occurrence. It is assumed that they symbolize fractures created as a result of fluid flow or as disturbances of concentrated stress and pressure away from the fluid flow path. The method of distinguishing between clusters according to wet and dry seismicity is described in the next chapter.

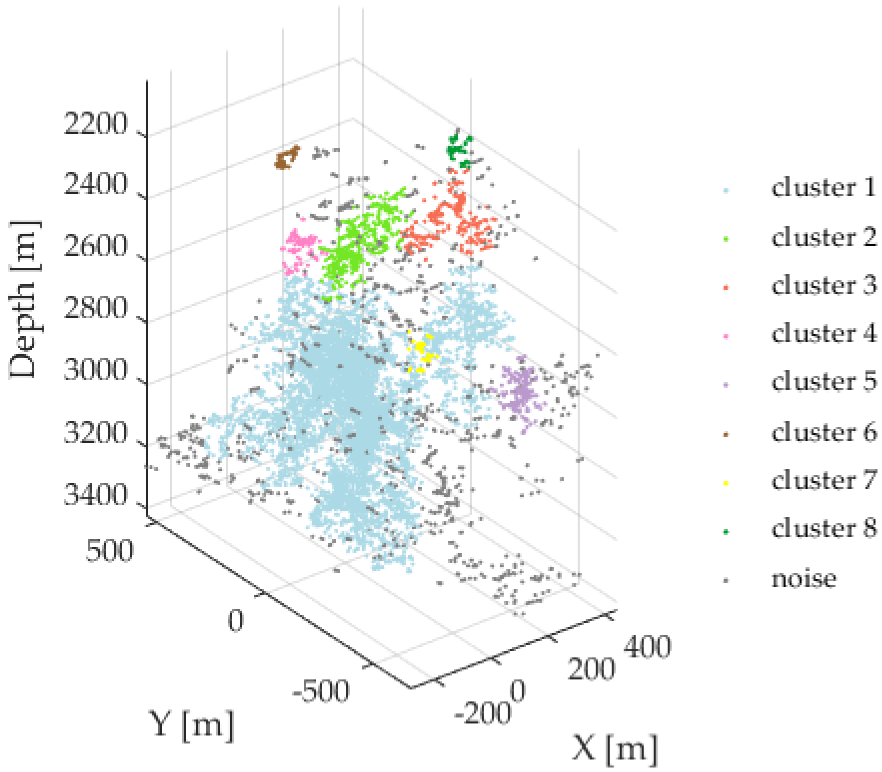

Figure 7. Results of the DBSCAN algorithm, whereby a cluster is deemed to comprise a minimum of 30 events within a neighborhood radius of 50 m.

Table 1. Population in each cluster.

Cluster Number	1	2	3	4	5	6	7	8
Nr of points	7446	449	250	101	185	56	44	54

4. Spatiotemporal Evolution of Clusters

Fracture network connectivity is a key factor shaping generated microseismicity, stimulated rock volume, and production [47]. To find which clusters detected by DBSCAN are possibly hydraulically connected, the spatiotemporal evolution of clusters was analyzed. The spatiotemporal evolution of a collapsed and clustered cumulative microseismic cloud is presented in daily intervals in Figure 8. Additionally, the minimum, maximum, and mean values for injection rate and wellhead pressure for each day are shown. The different colors of the seismic events indicate that they belong to a different cluster.

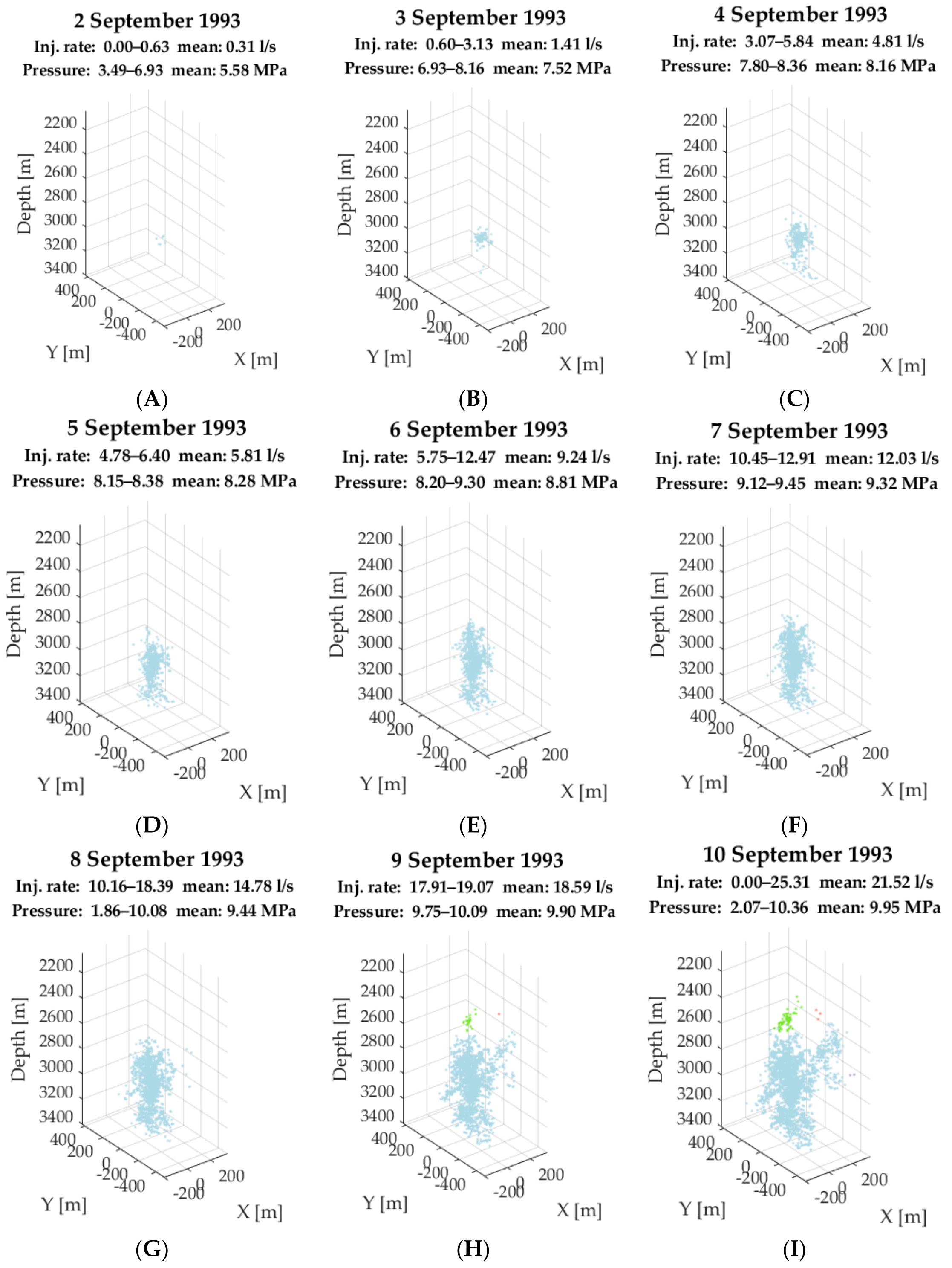
2 September 1993
Inj. rate: 0.00–0.63 mean: 0.31 l/s
Pressure: 3.49–6.93 mean: 5.58 MPa
(A)
3 September 1993
Inj. rate: 0.60–3.13 mean: 1.41 l/s
Pressure: 6.93–8.16 mean: 7.52 MPa
(B)
4 September 1993
Inj. rate: 3.07–5.84 mean: 4.81 l/s
Pressure: 7.80–8.36 mean: 8.16 MPa
(C)
5 September 1993
Inj. rate: 4.78–6.40 mean: 5.81 l/s
Pressure: 8.15–8.38 mean: 8.28 MPa
(D)
6 September 1993
Inj. rate: 5.75–12.47 mean: 9.24 l/s
Pressure: 8.20–9.30 mean: 8.81 MPa
(E)
7 September 1993
Inj. rate: 10.45–12.91 mean: 12.03 l/s
Pressure: 9.12–9.45 mean: 9.32 MPa
(F)
8 September 1993
Inj. rate: 10.16–18.39 mean: 14.78 l/s
Pressure: 1.86–10.08 mean: 9.44 MPa
(G)
9 September 1993
Inj. rate: 17.91–19.07 mean: 18.59 l/s
Pressure: 9.75–10.09 mean: 9.90 MPa
(H)
10 September 1993
Inj. rate: 0.00–25.31 mean: 21.52 l/s
Pressure: 2.07–10.36 mean: 9.95 MPa
(I)

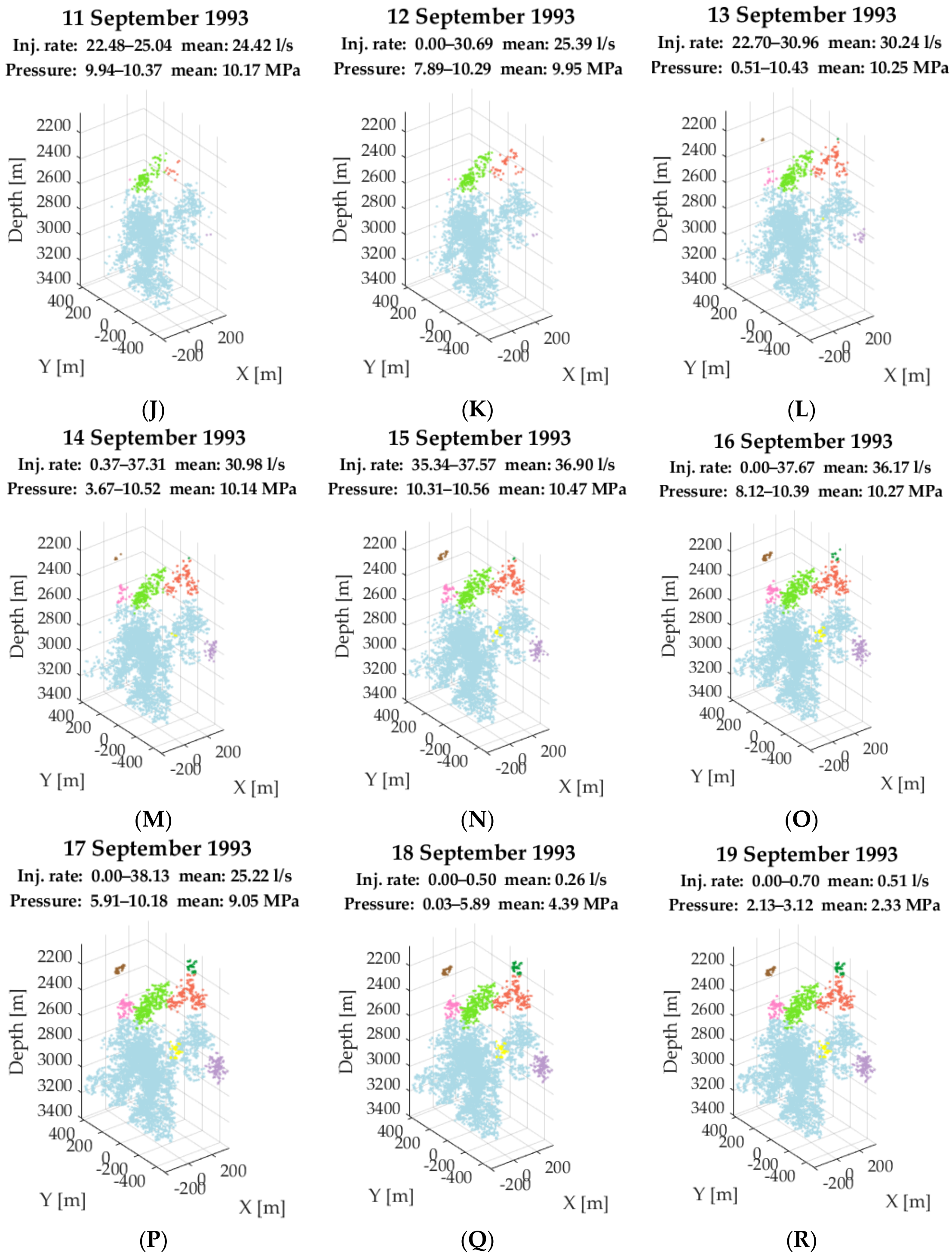

11 September 1993
Inj. rate: 22.48–25.04 mean: 24.42 l/s
Pressure: 9.94–10.37 mean: 10.17 MPa
(J)
12 September 1993
Inj. rate: 0.00–30.69 mean: 25.39 l/s
Pressure: 7.89–10.29 mean: 9.95 MPa
(K)
13 September 1993
Inj. rate: 22.70–30.96 mean: 30.24 l/s
Pressure: 0.51–10.43 mean: 10.25 MPa
(L)
14 September 1993
Inj. rate: 0.37–37.31 mean: 30.98 l/s
Pressure: 3.67–10.52 mean: 10.14 MPa
(M)
15 September 1993
Inj. rate: 35.34–37.57 mean: 36.90 l/s
Pressure: 10.31–10.56 mean: 10.47 MPa
(N)
16 September 1993
Inj. rate: 0.00–37.67 mean: 36.17 l/s
Pressure: 8.12–10.39 mean: 10.27 MPa
(O)
17 September 1993
Inj. rate: 0.00–38.13 mean: 25.22 l/s
Pressure: 5.91–10.18 mean: 9.05 MPa
(P)
18 September 1993
Inj. rate: 0.00–0.50 mean: 0.26 l/s
Pressure: 0.03–5.89 mean: 4.39 MPa
(Q)
19 September 1993
Inj. rate: 0.00–0.70 mean: 0.51 l/s
Pressure: 2.13–3.12 mean: 2.33 MPa
(R)
Depth [m]
Y [m]
X [m]

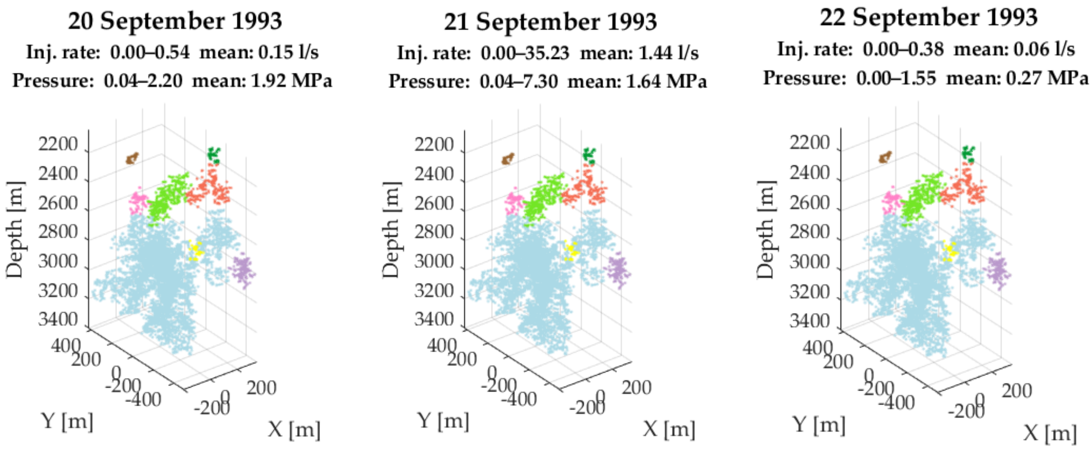

(**S**) (**T**) (**U**)

Figure 8. Three-dimensional view of the spatiotemporal evolution of a cumulative collapsed seismic cloud. The colors of events match the colors representing clusters in Figure 7. The minimum, maximum, and mean values for injection rate and wellhead pressure for each day are shown. (**A**) 2.09.1993 (**B**) 3.09.1993 (**C**) 4.09.1993 (**D**) 5.09.1993 (**E**) 6.09.1993 (**F**) 7.09.1993 (**G**) 8.09.1993 (**H**) 9.09.1993 (**I**) 10.09.1993 (**J**) 11.09.1993 (**K**) 12.09.1993 (**L**) 13.09.1993 (**M**) 14.09.1993 (**N**) 15.09.1993 (**O**) 16.09.1993 (**P**) 17.09.1993 (**Q**) 18.09.1993 (**R**) 19.09.1993 (**S**) 20.09.1993 (**T**) 21.09.1993 (**U**) 22.09.1993.

Various factors were investigated as part of the spatiotemporal analysis: the cluster growth rate measured by the number of events gathered in the cluster, the distance from the injection well, the size of the cluster, and the time of its appearance. The absolute number of daily events divided by clusters is shown in Figure 9. This histogram shows only those events that the DBSCAN algorithm classified into clusters. The clusters growth rate are presented in Figure 10A–H. These graphs show the daily percentage growth of each cluster in relation to the maximum number of events in a given cluster. The colors in Figures 8–10 match the colors representing clusters in Figure 7. The authors analyzed whether events in clusters occur gradually or suddenly. It was assumed that if seismic events appeared gradually, they were related to the fluid flow. However, when the appearance of a cluster was sudden, it tended to be associated with a change in tectonic stress.

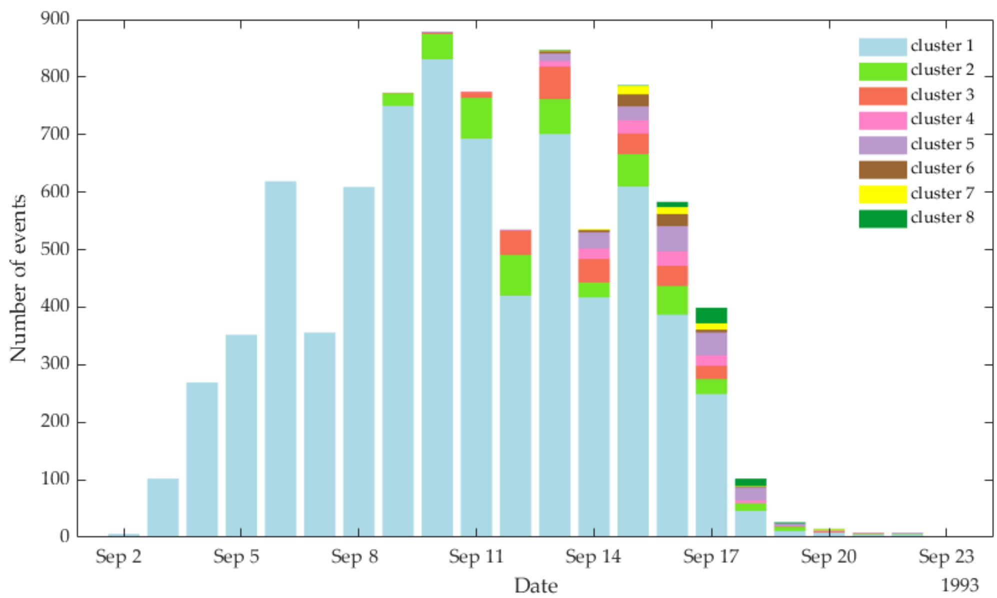

Figure 9. Daily number of seismic events divided by clusters. This bar chart shows only those events that the DBSCAN method classified into clusters.

Each of the detected clusters was analyzed in order of their appearance. The highest number of points is contained in the light blue cluster—about 80% of all points subjected to cluster detection. It is not assumed to be a single fracture. This area consists of many smaller structures that are very close to one another, which may indicate a connection between them. Throughout the stimulation period, this structure grew uniformly on both sides of the well. The first events inside this cluster occurred near the casing shoe at a depth of 2800 m and migrated downwards. After 4 days, events were observed at shallower depths. This structure was approximately 1 km deep, 0.5 km wide, and 0.8 km long. An analysis of the depth of occurrence of the biggest detected cluster, its position in relation to the GPK-1 well (origin of the coordinate system), and the rate of growth, lead to the conclusion that the events inside this cloud occurred as a result of contact with fluid flows.

The second cluster that appears in the seismic cloud is the one marked in light green. It contains less than 5% of all the points that were subject to the automatic clustering algorithm. Its rate of growth is variable, but not rapid. The first events classified as part of this cluster appeared along with an increase in the injection rate. They took place when the largest cluster was growing, and were located very close to it. This may indicate a hydraulic connection between these clusters.

The third cluster, marked in red, containing approximately 2.5% of all clustered events, appeared as an expanded light green cluster after an increase in the injected fluid. This may indicate the presence of a fluid flow path between them.

The next chronological structures are marked in pink and heather. They consist of 1% and 2% of the entire population of points that underwent clustering, respectively. Events inside these structures began to occur after the next injection rate increased and as the range of the biggest cluster with a hydraulic connection to the well increased. This may suggest that these events represent a case of wet seismicity.

The sixth structure farthest from the borehole and which at the same time had one of the fastest growth rates is shown in brown. This cluster has no connection to the well or to the structures that can be permeable. This means that it could not have arisen as a result of flowing water. It can be concluded that events inside this cluster were triggered by tectonic stress changes.

The next cluster, marked in yellow, appeared in its entirety at a time when the injection rate was at its height. It is located in close proximity to the structure which the authors considered wet. The structure composed by these events may be permeable.

The fastest rate of point growth occurred in the dark green cluster. Less than 1% of all the points are located in this structure. The first observed events in this structure occurred when the injection flow rate increased. This fact may indicate that events within that cluster will be classified as wet.

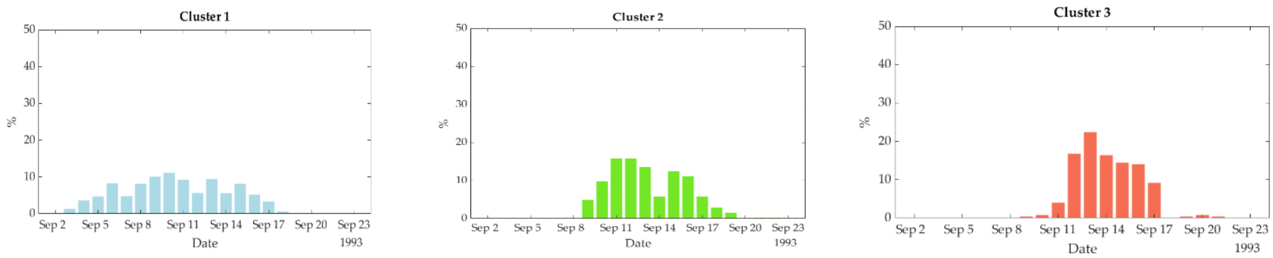

(**A**) (**B**) (**C**)

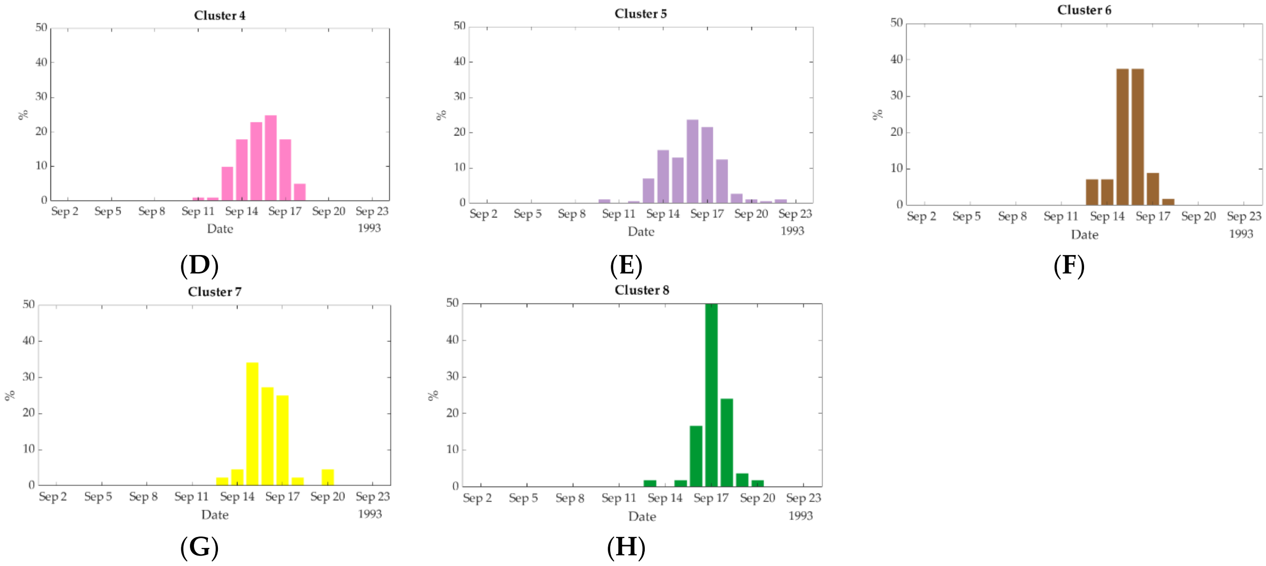

Figure 10. Daily rate of growth of each cluster in relation to the maximum number of events in a given cluster. (**A**) cluster 1, (**B**) cluster 2, (**C**) cluster 3, (**D**) cluster 4, (**E**) cluster 5, (**F**) cluster 6, (**G**) cluster 7, (**H**) cluster 8.

In order to assign to each cluster to its presumed origin—tectonic or directly related to the fluid flow—a spatiotemporal analysis of the evolution of the clusters was performed. The cluster that had rapid growth was temporally and spatially separated and had no close connections with other neighboring clusters; it is probably of tectonic origin due to changes in stress in the rock mass. The clusters inside which the events appeared gradually along with the increasing injection rate are probably related to the fluid flow.

5. Discussion

Despite many studies conducted to find structures within the microseismic cloud recorded during injection in Soultz in 1993, the research presented in this paper was the first attempt to divide the entire cloud into clusters. The authors attempted to determine which of the localized seismic events may be involved in heat transfer. The methodology proposed by the authors does not explicitly identify wet microseismic events but provides a premise for the identification of events that may be associated with the flowing fluid.

It is important to note that the Soultz reservoir is naturally fractured. The big complex structure may be formed of smaller natural discontinuities, which as a result of fracturing combine into larger structures according to the percolation process. These natural discontinuities are potential paths for fluid flow [15]. The orientation of detected clusters inside microseismic cloud appears to be in agreement with the N-S to NNW-SSE direction of most natural fractures demonstrated by Genter et al. [22]. The largest detected cluster (cluster 1) contains approximately the same structure described by Evans et al. [21]. The structure identified as Evans Line [21] ranging from a flow zone to 300 m downwards is considered to be permeable, supporting significant flow.

The distinction between wet and dry microseismic events was based on the spatiotemporal evolution of clusters and the rate of point growth in them. The authors considered the possibility that events inside the brown cluster may have been triggered by stress mechanisms. These events will not contribute to the SRV due to the absence of any hydraulic connection. The remaining detected clusters may indicate the presence of permeable structures. The authors calculated that about 80% of all localized events can be characterized as wet microseismicity. A flowchart describing wet microseismicity identification and the number of events in each processing step is presented in Figure 5.

The last step in the analysis presented in this article involved estimating the stimulated reservoir volume using the convex hull algorithm. The volume engaged by seismic activity can be approximated as a volume of the microseismic cloud [48]. The convex hull of the original microseismic cloud—before the 3-step procedure was performed—is presented in Figure 11A. The volume of the primary cloud defined by the microseismic events is 7.6×10^8 m^3. The authors proposed only calculating the SRV of those clusters that can be in a hydraulic connection with the well. The convex hulls for each cluster are shown in Figure 11B. The authors assumed that the stimulated reservoir volume is the sum of the volumes of all convex hulls. The volumes of each structure are shown in Table 2. The sum of the volumes of the structures identified as possibly permeable is equal to 1.4×10^8 m^3. It is important to note that the real volume engaged with the heat transfer is slightly greater because there is a connection between particular clusters. With this algorithm, it is impossible to calculate the volume of paths connecting individual clusters. The calculated volume is the smallest volume containing the wet fracture system.

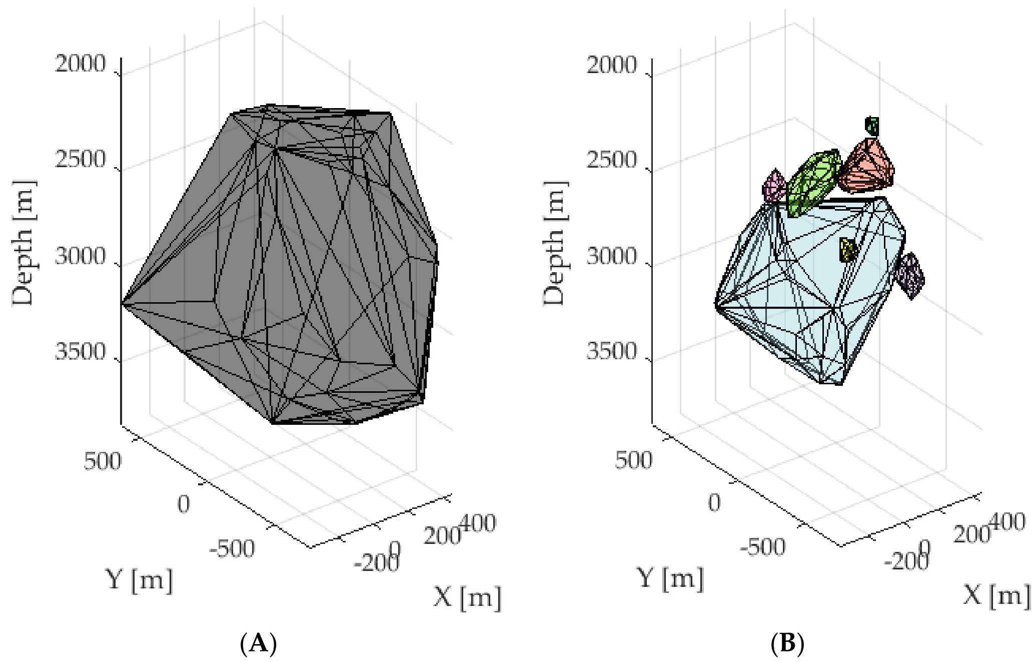

Figure 11. Convex hulls for the clouds of microseismic events (**A**) Convex hull for the microseismic cloud after location. (**B**) Convex hulls for each cluster that can be permeable.

Table 2. Volumes of structures identified as possibly permeable.

Cluster Number	1	2	3	4	5	7	8
Volume [m^3]	1.25×10^8	5.11×10^6	3.63×10^6	6.92×10^5	1.33×10^6	1.66×10^5	2.13×10^5

The dominant source mechanism during hydraulic fracturing is shear slip, which is represented by a double-couple source model. This mechanism is triggered by an increase in the pore pressure reducing normal stress along existing fractures [49]. Some events occur near the tips of generated fractures and are characterized by significant non-shear (tensile opening and closing) components [6]. Although new fractures are inevitably created by a non-shear mechanism during stimulation of the geothermal reservoir and should be related to the volume of the stimulated rock mass, a large number of shear mechanism events are also connected to the fluid flow. Dry microseismic events resulting from the disturbance of stresses are characterized by a shear stress mechanism. However, when only the source mechanism is examined, it cannot be unequivocally determined whether shear or tensile fracturing are associated with wet microseismicity [6,50]. This analysis does not always produce good results. Hence, for this reason a different analysis was performed in this article. Instead of resorting to the source mechanism, only localized seismic events were used to extract wet microseismicity. These events were subject to relocation, clustering, and spatiotemporal evolution.

6. Conclusions

The microseismicity detected during hydraulic stimulation in the Soultz HDR field in September 1993 provides a basis for making a rough estimation of the number of events associated with fluid flow. To calculate the stimulated reservoir volume, the authors proposed an algorithm comprising the collapsing method, DBSCAN automatic cluster detection, and spatiotemporal cluster evolution from the injection well. The use of the collapsing method made it possible to simplify the hypocenter cloud and exclude points that were too distant from others. Clustering provided a platform for detecting areas with an above-average intensity of seismic events. However, this method could not be used to distinguish between wet and dry events. Therefore, the next step was a spatiotemporal analysis of detected clusters. Various factors were investigated in this analysis: the rate of cluster growth measured by the number of events, the distance from the injection well, the size of the cluster, and the time of the appearance. This approach allowed the authors to identify seven clusters containing events that can be related to the wet fracture system. These structures were deemed to be the preferential paths for the fluid flow.

When the volume of a geothermal reservoir is estimated according to the extent of the recorded microseismic events, this volume is overestimated. The microseismicity cloud contains events that are related to the flow of the injected fluid as well as events resulting from pre-existing tectonic stresses in the area. The stimulated reservoir volume obtained from wet systems of fractures, excluding paths connecting individual clusters using convex hulls, is approximately five times smaller than the volume obtained from the entire microseismic cloud.

The method proposed by the authors to identify events directly associated with the hydraulic fracture network can be applied to any geothermal reservoir. Accurately identifying dry fractures is crucial for correctly estimating the volume of a geothermal reservoir containing only hydraulically connected fracture systems. The results presented in the article are significant from the perspective of evaluating HDR reservoir performance.

Author Contributions: Conceptualization, A.L. and E.W.; methodology, A.L. and E.W.; software, A.L. and E.W.; validation, A.L. and E.W.; formal analysis, A.L. and E.W.; investigation, A.L. and E.W.; resources, A.L.; data curation, E.W.; writing—original draft preparation, E.W.; writing—review and editing, A.L. and E.W.; visualization, E.W.; supervision, A.L.; project administration, E.W.; funding acquisition, A.L. All authors have read and agreed to the published version of the manuscript.

Funding: This research is funded by the AGH University of Science and Technology, Statutory Research grant number 16.16.140.315.

Conflicts of Interest: The authors declare no conflict of interest.

References

1. Moriya, H.; Nagano, K.; Niitsuma, H. Precise source location of AE doublets by spectral matrix analysis of triaxial hodogram. *Geophysics* **1994**, *59*, 36–45, doi:10.1190/1.1443532.
2. Jones, R.H.; Stewart, R.C. A method for determining significant structures in a cloud of earthquakes. *J Geophys. Res. Solid Earth* **1997**, *102*, 8245–8254, doi:10.1029/96jb03739.
3. Phillips, W.S. Precise Microearthquake Locations and Fluid Flow in the Geothermal Reservoir at Soultz-sous-Foreˆts, France. *Seismol. Soc. Am. Bull.* **2000**, *90*, 212–228, doi:10.1785/0119990047.
4. Gaucher, E.; Schoenball, M.; Heidbach, O.; Zang, A.; Fokker, P.A.; van Wees, J.D.; Kohl, T. Induced seismicity in geothermal reservoirs: A review of forecasting approaches. *Renew. Sustain. Energy Rev.* **2015**, *52*, 1473–1490, doi:10.1016/j.rser.2015.08.026.
5. Elsass, P.; Aquilina, L.; Beauce, A.; Benderitter, Y.; Fabriol, H.; Genter, A.; Pauwels, H. Deep structures of the Soultz-sous-Forets HDR Site (Alsace, France). In Proceedings of the World Geothermal Congress, Florence, Italy, 18–31 May 1995.
6. Maxwell, S.C.; Chorney, D.; Goodfellow, S.D. Microseismic geomechanics of hydraulic-fracture networks: Insights into mechanisms of microseismic sources. *Lead. Edge* **2015**, *34*, 904–910, doi:10.1190/tle34080904.1.

7. Niitsuma, H.; Fehler, M.; Jones, R.; Wilson, S.; Albright, J.; Green, A.; Baria, R.; Hayashi, K.; Kaieda, H.; Tezuka, K.; et al. Current status of seismic and borehole measurements for HDR/HWR development. *Geothermics* **1999**, *28*, 475–490, doi:10.1016/S0375-6505(99)00024-3.
8. Fehler, M.; Jupe, A.; Asanuma, H. More than cloud: New techniques for characterizing reservoir structure using induced seismicity. *Lead. Edge* **2001**, *20*, 324–328, doi:10.1190/1.1438942.
9. Ester, M.; Kriegel, H.-P.; Sander, J.; Xu, X. A Density-Based Algorithm for Discovering Clusters in Large Spatial Databases with Noise. In Proceedings of the Second International Conference of Knowledge Discovery and Data Mining (KDD'96), Portland, OR, USA, 2–4 August 1996; pp. 226–231, doi:10.5555/3001460.3001507.
10. Barber, C.B.; Dobkin, D.P.; Huhdanpaa, H. The Quickhull Algorithm for Convex Hulls. *ACM Trans. Math. Softw.* **1996**, *22*, doi:10.1145/235815.235821.
11. Aichholzer, C.; Duringer, P.; Orciani, S.; Genter, A. New stratigraphic interpretation of the Soultz-sous-Forêts 30-year-old geothermal wells calibrated on the recent one from Rittershoffen (Upper Rhine Graben, France). *Geotherm. Energy* **2016**, *4*, 1–26.
12. Jung, R.; Rummel, F.; Jupe, A.; Bertozzi, A.; Heinemann, B.; Wallroth, T. Large-scale Hydraulic Injections in the Granitic Basement in the European HDR Programme at Soultz, France. In Proceedings of the 3rd International HDR Forum, Santa Fe, NM, USA, 13–16 May 1996.
13. Helm, J.A. The Natural Seismic Hazard and Induced Seismicity of the European HDR Geothermal Energy Project at Soultz-sous-Forets (Bas-Rhin, France), Ph.D. Thesis, Universite Louis Pasteur, Strasbourg, France, 1996.
14. Alexandrov, P.; Royer, J.-J.; Deloule, É. 331 ± 9 Ma emplacement age of the Soultz monzogranite (Rhine Graben basement) by U/Pb ion-probe zircon dating of samples from 5 km depth. *Ser. IIA Earth Planet. Sci.* **2001**, *332*, 747–754, doi:10.1016/S1251-8050(01)01594-4.
15. Sausse, J.; Genter, A. Types of permeable fractures in granite. *Geol. Soc. Spec. Publ.* **2005**, *240*, 1–14, doi:10.1144/GSL.SP.2005.240.01.01.
16. Dezayes, C.; Genter, A.; Valley, B. Structure of the low permeable naturally fractured geothermal reservoir at Soultz. *Comptes Rendus Geosci.* **2010**, *342*, 517–530, doi:10.1016/j.crte.2009.10.002.
17. Genter, A.; Evans, K.; Cuenot, N.; Fritsch, D.; Sanjuan, B. Contribution of the exploration of deep crystalline fractured reservoir of Soultz to the knowledge of enhanced geothermal systems (EGS). *Comptes Rendus Geosci.* **2010**, *342*, 502–516, doi:10.1016/j.crte.2010.01.006.
18. Majer, E.L.; Baria, R.; Stark, M.; Oates, S.; Bommer, J.; Smith, B.; Asanuma, H. Induced seismicity associated with Enhanced Geothermal Systems. *Geothermics* **2007**, *36*, 185–222, doi:10.1016/j.geothermics.2007.03.003.
19. Bruel, D. Using the migration of the induced seismicity as a constraint for fractured Hot Dry Rock reservoir modelling. *Int. J. Rock Mech. Min. Sci.* **2007**, *44*, 1106–1117, doi:10.1016/j.ijrmms.2007.07.001.
20. Egert, R.; Maziar, G.K.; Held, T.; Kohl, T. Implications on large-scale flow of the fractured EGS reservoir Soultz inferred from hydraulic data and tracer experiments. *Geothermics* **2020**, *84*, 101749, doi:10.1016/j.geothermics.2019.101749.
21. Evans, K.F.; Moriya, H.; Niitsuma, H.; Jones, R.H.; Phillips, W.S.; Genter, A.; Sausse, J.; Jung, R.; Baria, R. Microseismicity and permeability enhancement of hydrogeologic structures during massive fluid injections into granite at 3 km depth at Soultz HDR site. *Geophys. J. Int.* **2005**, *160*, 388–412.
22. Genter, A.; Castaing, C.; Dezayes, C.; Tenzer, H.; Traineau, H.; Villemin, T. Comparative analysis of direct (core) and indirect (borehole imaging tools) collection of fracture data in the Hot Dry Rock Soultz reservoir (France). *J. Geophys. Res.* **1997**, *102*, 15419–15431, doi:10.1029/97JB00626.
23. Charléty, J.; Cuenot, N.; Dorbath, L.; Dorbath, C.; Haessler, H.; Frogneux, M. Large earthquakes during hydraulic stimulations at the geothermal site of Soultz-sous-Forêts. *Int. J. Rock Mech. Min. Sci.* **2007**, *44*, 1091–1105, doi:10.1016/j.ijrmms.2007.06.003.
24. Cuenot, N.; Dorbath, L.; Frogneux, M.; Langet, N. Microseismic Activity Induced Under Circulation Conditions at the EGS Project of Soultz-Sous-Forêts (France). In Proceedings of the World Geothermal Congress, Bali, Indonesia, 25–29 April 2010.
25. Klee, G.; Rummel, F. Hydrofrac Stress Data for the European HDR Research Project Test Size Soultz-Sous-Forets. *Int. J. Rock Mech. Min. Sci. Geomech. Abstr.* **1993**, *30*, 973–976, doi:10.1016/0148-9062(93)90054-H.
26. Dorbath, L.; Evans, K.; Cuenot, N.; Valley, B.; Charléty, J.; Frogneux, M. The stress field at Soultz-sous-Forêts from focal mechanisms of induced seismic events: Cases of the wells GPK2 and GPK3. *Comptes Rendus Geosci.* **2010**, *342*, 600–606, doi:10.1016/j.crte.2009.12.003.
27. Tenzer, H. Fracture mapping and determination of horizontal stress field by borehole measurements in HDR drillholes Soultz & Urach. In Proceedings of the World Geothermal Congress, Florence, Italy, 18–31 May 1995.
28. Bérard, T.; Cornet, F.H. Evidence of thermally induced borehole elongation: A case study at Soultz, France. *Int. J. Rock Mech. Min. Sci.* **2003**, *40*, 1121–1140, doi:10.1016/S1365-1609(03)00118-7.
29. Valley, B.; Evans, K.F. Stress State At Soultz-Sous-Forêts to 5 km depth from wellbore failure and hydraulic observations. In Proceedings of the Thirty-Second Workshop on Geothermal Reservoir Engineering, Stenford, CA, USA, 22–24 January 2007.
30. Niitsuma, H. Detection of Hydraulically Created Permeable Structures In HDR/HWR Reservoir By High Resolution Seismic Mapping Techniques. *Elsevier Geo-Eng. Book Ser.* **2004**, *2*, 73–79, doi:10.1016/S1571-9960(04)80024-7.
31. Baria, R.; Baumgartner, J.; Gerard, A.; Jung, R.; Garnish, J. European HDR research programme at Soultz-sous- Forets (France) 1987–1996. *Geothermics* **1999**, *28*, 655–669, doi:10.1016/S0375-6505(99)00036-X.
32. Jones, R.H.; Beauce, A.; Jupe, A.; Fabriol, H.; Oyer, B.C. Imaging induced microseismicity during the 1993 injection tests at Soultz-sous-Forets France. In Proceedings of the World Geothermal Congress, Florence, Italy, 18–31 May 1995.

33. Baria, R.; Garnish, J.; Baumgartner, J.; Gerard, J.; Reinhard, J. Recent developments in the European HDR Research Programme at Soultz-sous-Forets (France). In Proceedings of the World Geothermal Congress, Florence, Italy, 18–31 May 1995; pp. 2631–2637.
34. Evans, K.F. The effect of the 1993 stimulations of well GPK1 at Soultz on the surrounding rock mass: Evidence for the existence of a connected network of permeable fractures. In Proceedings of the World Geothermal Congress, Kyushu-Tohoku, Japan, 28 May–10 June 2000; pp. 3695–3700.
35. Moriya, H.; Nakazato, K.; Evans, K.F.; Niitsuma, H.; Jones, R.H.; Baria, R. Evaluation of the Soultz HDR System by Precise Mapping Techniques of Induced Microseismic Event. *Geotherm. Resour. Counc. Trans.* **2001**, *25*, 187–190.
36. EOST; GEIE EMC. *Episode: 1993 Stimulation Soultz-sous-Forêts*; EOST— CDGP: Strasbourg, France, 2017; doi:10.25577/SSFS1993.
37. Cauchie, L.; Lengline, O.; Schmittbuhl, J. Seismic asperity size evolution during fluid injection: Case study of the 1993 Soultz-sous-Forets injection. *Geophys. J. Int.* **2020**, *221*, 968–980, doi:10.1093/gji/ggaa051.
38. Moriya, H.; Niitsuma, H.; Baria, R. Multiplet-Clustering Analysis Reveals Structural Details within the Seismic Cloud at the Soultz Geothermal Field, France. *Seismol. Soc. Am. Bull.* **2003**, *93*, 1606–1620, doi:10.1785/0120020072.
39. Cornet, F.H.; Helm, J.; Poitrenaud, H.; Etchecopar, A. Seismic and aseismic slips induced by large-scale fluid injections. *Pure Appl. Geophys.* **1997**, *150*, 563–583, doi:10.1007/978-3-0348-8814-1_12.
40. Moriya, H.; Nakazato, K.; Niitsuma, H.; Baria, R. Detailed Fracture System of the Soultz-sous-Forets HDR Field Evaluated Using Microseismic Multiplet Analysis. *Pure Appl. Geophys.* **2002**, *159*, 517–541, doi:10.1007/978-3-0348-8179-1_22.
41. Leśniak, A.; Śledź, E.; Mirek, K. Detailed Recognition of Seismogenic Structures Activated during Underground Coal Mining: A Case Study from Bobrek Mine, Poland. *Energies* **2020**, *13*, 4622, doi:10.3390/en13184622.
42. Kriegel, H.-P.; Kroger, P.; Sander, J.; Zimek, A. Density-based clustering. *WIREs Data Min. Knowl. Discov.* **2011**, *1*, 231-240, doi:10.1002/widm.30.
43. Çelik, M.; Dadaşer-Çelik, F.; Şakir Dokuz, A. Anomaly detection in temperature data using DBSCAN algorithm. In Proceedings of the International Symposium on Innovations in Intelligent Systems and Applications, Instanbul, Turkey, 15–18 June 2011; pp. 91–95, doi:10.1109/INISTA.2011.5946052.
44. Bodenstein, C.; Götz, M.; Jansen, A.; Scholz, H.; Riedel, M. Automatic Object Detection using DBSCAN for Counting Intoxicated Flies in the FLORIDA Assay. In Proceedings of the 15th IEEE International Conference on Machine Learning and Applications, Anahaim, CA, USA, 18–20 December 2016, doi:10.1109/ICMLA.2016.49.
45. Kazemi-Beydokhti, M.; Abbaspour, R.A.; Mojarab, M. Spatio-Temporal Modeling of Seismic Provinces of Iran Using DBSCAN Algorithm. *Pure Appl. Geophys.* **2017**,174, 1937–1952, doi:10.1007/s00024-017-1507-0.
46. Mosobalaje, O.O.; Orodu, O.D.; Ogbe, D. The Application of DBSCAN Algorithm to Improve Variogram Estimation and Interpretation in Irregularly-Sampled Fields. In Proceedings of the International Conference on Applied Informatics ICAI 2020, Ota, Nigeria, 29–31 October 2020. p. 1277, doi:10.1007/978-3-030-61702-8_20.
47. Zhang, F.; Nagel, N.; Lee, B.; Sanchez-Nagel, M. Fracture Network Connectivity- A Key To Hydraulic Fracturing Effectiveness and Microseismicity Generation. In *Effective and Sustainable Hydraulic Fracturing;* Jeffrey, R., ed.; IntechOpen: Brisbane, Australia, 2013; pp. 591–603, doi:10.5772/56302.
48. Mayerhofer, M.J.; Lolon, E.P.; Warpinski, N.R.; Cipolla, C.L.; Walser, D.; Rightmire, C.M. What Is Stimulated Reservoir Volume? *SPE Prod. Oper.* **2010**, *25*, 89–98, doi:10.2118/119890-PA.
49. Pearson, C. The relationship between microseismicity and high pore pressures during hydraulic stimulation experiments in low permeability granitic rocks. *J. Geophys. Res. Solid Earth* **2010**, *86*, 7855–7864, doi:10.1029/JB086iB09p07855.
50. Rutledge, J.T.; Phillips, W.S. Hydraulic Stimulation of Natural Fractures As Revealed By Induced Microearthquakes, Carthage Cotton Valley Gas Field, East Texas. *Geophysics* **2003**, *68*, 441–452, doi:10.1190/1.1567214.

Załącznik 4

Geology, Geophysics & Environment

2024, vol. 50 (3): 213–230

Mapping a fracture network formed by hydraulic fracturing in a shale gas reservoir

Elżbieta Węglińska[1], Andrzej Leśniak[2], Andrzej Pasternacki[3], Paweł Wandycz[4]

[1] AGH University of Krakow, Faculty of Geology, Geophysics and Environmental Protection, Department of Geoinformatics and Applied Computer Science, Krakow, Poland, e-mail: weglinska@agh.edu.pl (corresponding author), ORCID ID: 0000-0003-0645-6570
[2] AGH University of Krakow, Faculty of Geology, Geophysics and Environmental Protection, Department of Geoinformatics and Applied Computer Science, Krakow, Poland, ORCID ID: 0000-0002-9442-0799
[3] AGH University of Krakow, Poland, Faculty of Geology, Geophysics and Environmental Protection, Department of Energy Resources, Krakow, Poland, ORCID ID: 0000-0002-0934-0277
[4] AGH University of Krakow, Faculty of Geology, Geophysics and Environmental Protection, Department of Energy Resources, Krakow, Poland, ORCID ID: 0000-0002-1145-0184

Received: 24 November 2023; accepted: 8 June 2024; first published online: 21 June 2024

Abstract: Microseismic monitoring is an important technique that can be used to identify fractures in rock mass. The aim of this article is to identify, on the basis of the location of microseismic events, structures formed by hydraulic fracturing in the Wysin-2H/2Hbis horizontal well from the Baltic Basin in northern Poland, and to compare the patterns of these structures with the direction of regional stresses. The authors proposed a novel multi-step workflow for finding these structures. To be able to delineate the structures from microseismic events with greater accuracy, a collapsing algorithm was used. Then, based on the Hierarchical Density-Based Spatial Clustering of Applications with Noise (HDBSCAN) clustering algorithm and the elongation coefficient of each cluster, probable fissures were identified and compared against the maximum horizontal stress direction. In addition, based on the 3D seismic data from the Wysin and the calculated geomechanical parameters in the monitoring well, the probability classes of brittleness indices in the LMR (λρ-μρ) parameter domain were determined. A comparative analysis was performed between the two variants of microseismic event location (before and after the collapsing procedure) and the estimated probability of a given class of brittleness index. The comparison of the event location with the 3D seismic data was used to validate the results before and after collapsing due to the high resolution of the seismic method. It is shown that the collapsed events appeared in more rigid regions, where more energy release is expected.

Keywords: fracture network, shale gas, microseismicity, collapsing, HDBSCAN, Baltic Basin

INTRODUCTION

Hydraulic fracturing (HF) is a technique that allows fractures to be created in a rock formation to stimulate the flow of oil or gas. This process is carried out by pumping fracturing fluid under high pressure into a well to create new fractures or enlarge pre-existing fractures in the rock. Creation of hydraulic fractures or reactivation of existing fractures by hydraulic stimulation induces microseismic events (Maxwell 2013). Based on the location of microseismic events, it is possible to identify fractures in the rock mass. Fracture mapping is key to estimating stimulation effectiveness. To infer the orientation of the cracks, the geometry of the distribution of the seismic events must be investigated (Williams-Stroud & Billingsley 2010). Two types of seismic phenomena have been interpreted as occuring during hydraulic fracturing: wet and dry microseismicity (Maxwell 2014, 2015a, 2015b). In order to correctly interpret the structures formed, it is necessary to distinguish phenomena that are directly created by the flow of fracturing fluid (so-called wet microseismicity). The fracturing operation causes a stress change or stress transfer in the rock mass, resulting in seismic emissions even at large distances from the well (so-called dry microseismicity). It is necessary to distinguish between these two types of events to avoid overestimating the volume of the reservoir, because dry events are not hydraulically connected to pore-pressure induced fracturing.

This paper presents an analysis of microseismic event locations recorded during HF performed from June 9, 2016 to June 18, 2016 in the Wysin-2H/2Hbis horizontal well. The main goal of the paper is to determine the fractures formed by hydraulic fracturing and compare the patterns of these fractures with the direction of regional maximum horizontal stress. The authors developed a novel workflow that uses microseismic event locations to identify linear structures which may be formed by hydraulic fracturing. To minimize the dispersion of the location of events that results from location errors and thus increase the resolution of the cloud of seismic events, a collapsing method (Jones & Stewart 1997) was used. The collapsing procedure produced a more clustered character from scatter event locations. This allows the identification of structures from which seismic emission occurs, such as cracks or fissures in the rock mass. Using the HDBSCAN (Hierarchical Density-Based Spatial Clustering of Applications with Noise) unsupervised machine learning method (Campello et al. 2013), clusters were then identified inside the seismic events cloud that may correspond to fractures formed in the rock mass. The biggest advantages of this method are its ability to identify noise and find clusters of different shapes, and its lack of a need to assume the number of clusters. The structures formed were compared with the direction of maximum horizontal stress. To identify potential fractures from all delineated clusters, only those that are linear were selected by calculating the elongation coefficient based on the semi-axis length of the point dispersion ellipsoid in the cluster.

In this paper we present the results of the relocation of seismic events after using the collapsing procedure; then, automatic detection of clusters using HDBSCAN is presented. Two seismic event locations (variants before and after applying the collapsing procedure) are compared with the regional stress direction. To validate the locations of microseismic events, a comparative analysis is performed between these two variants of the microseismic cloud, and the estimated probability of a given brittleness index is shown.

GEOLOGICAL SETTING

Wysin-2H/2Hbis is a horizontal well located in the village of Wysin in the northern part of Poland (see Fig. 1) in the Peri-Baltic Syneclise (Zaręba & Danek 2018), situated in the western region of a Lower Paleozoic basin, referred to as the Baltic Basin. This basin is part of the northernmost section of the Polish segment on the Baltica continent, which is also known as the East European Craton (EEC) (see Fig. 2). The geological structure of the Baltic Basin includes a sequence of sediments, ranging from Paleozoic (where shale gas and oil exploration is possible) to Mesozoic (EIA 2013). Figure 3 shows the geological sequence of the study area. About 4 km below the surface, there are Cambrian sandstones and shales overlying Ordovician marly limestone, mudstone, and siltstone, and Silurian shales interbedded with dolomitic limestones (Lopez-Comino et al. 2018). The Pelplin Claystone Formation was hydraulically fractured.

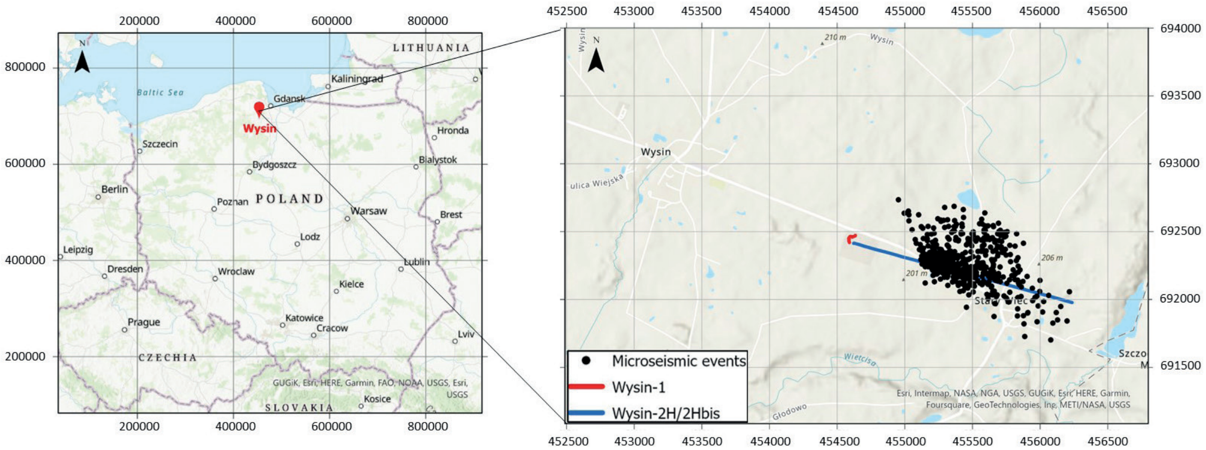

Fig. 1. *Location of Wysin village, Wysin-1 and Wysin-2H/2Hbis wells, and microseismic events located during Wysin-2H/2Hbis hydraulic fracturing*

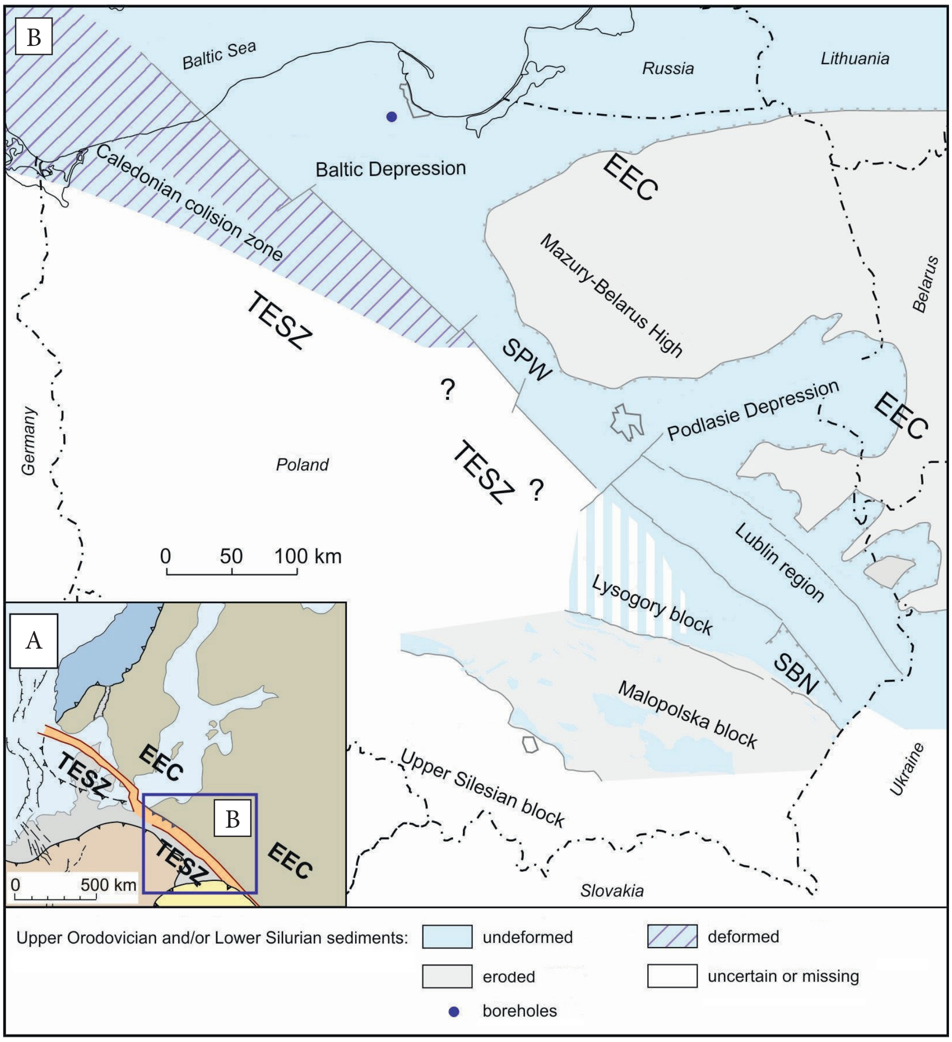

Fig. 2. *Location of Lower Paleozoic sedimentary basins and lateral extend of the Upper Ordovician and/or Lower Silurian shale formations: A) western slope of the East European Craton (EEC) with the background of the main tectonic units of the central and northern Europe; B) location of the Lower Paleozoic sedimentary basins in Poland (Poprawa 2010, modified Wandycz 2022); TESZ – Trans-European Suture Zone, SBN – Biłgoraj-Narol zone*

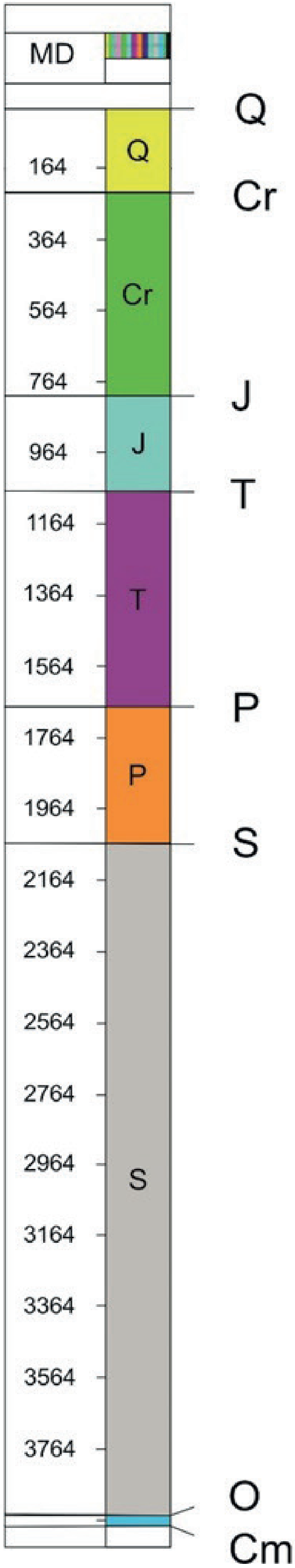

Fig. 3. *Stratigraphic profile in Wysin-1 (Wandycz 2022, modified)*

WYSIN-2H/2HBIS HYDRAULIC FRACTURING

The Wysin-2H/2Hbis experiment consisted of eleven stages during which fracking was performed. In each stage, six perforation shots were carried out. During the hydraulic fracturing operation conducted from June 9 to 18, 2016, 565 microseismic events were located. All coordinates are presented in the PUWG1992 (EPSG 2180) system. Figure 4 shows the Wysin-2H/2Hbis injection well, the location of geophones, and localized seismic events in the various stages of fracturing. The 18 triaxial geophones were deployed in the Wysin-1 vertical monitoring well. The fracturing was carried out using the "plug and perf" method. This method is a HF technique that involves isolating fractured parts of the well from the previously fractured zones using plugs after completion of each stage. The stages located in the SE section, which is the deepest part of the horizontal well, were fractured first. The HF process was conducted between 1600 meters (stage 1) and 500 meters (stage 11) from the monitoring array deployed in Wysin-1 well (Wandycz et al. 2019).

Wysin-1 is a vertical hydraulic fracturing monitoring well with a total depth of 4,040 m (Zaręba et al. 2021). In Wysin-1, XRMI images (Pasternacki 2017) were reinterpreted to identify "breakout"-type structures, on the basis of which it was possible to determine the azimuth of maximum horizontal stress. The breakouts are borehole failure features that are characterized by their fixed, perpendicular orientation with respect to the direction of the maximum stress, normal to the axis of the well (Bell & Gough 1979, Zoback 2010). Figure 5 shows the distribution of failure azimuths in the Silurian-Ordovician interval in the Wysin-1 well. The red line indicates the interpreted SH_{max} direction, whose azimuth is 150°N ±15°, because it is assumed to be perpendicular to the breakout azimuth.

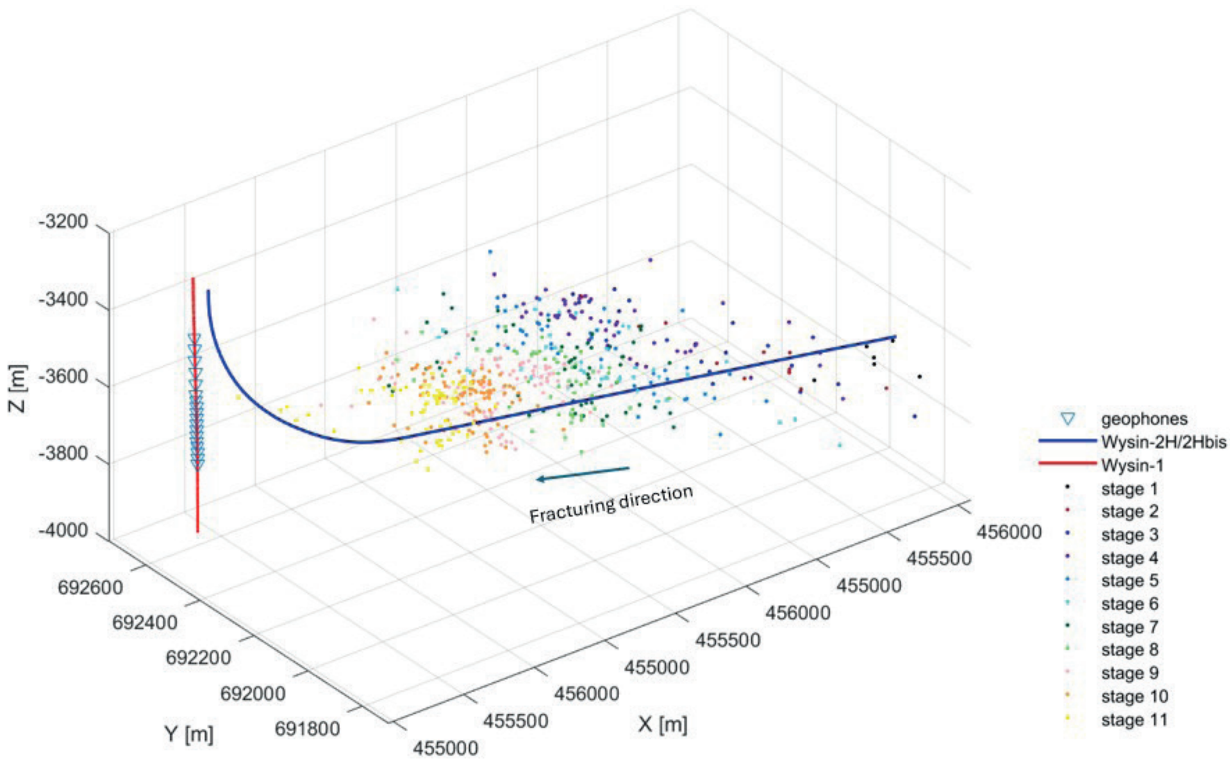

Fig. 4. *Location of 18 geophones in the monitoring well, the trajectory of the injection well, and localized seismic events in the various stages of fracturing*

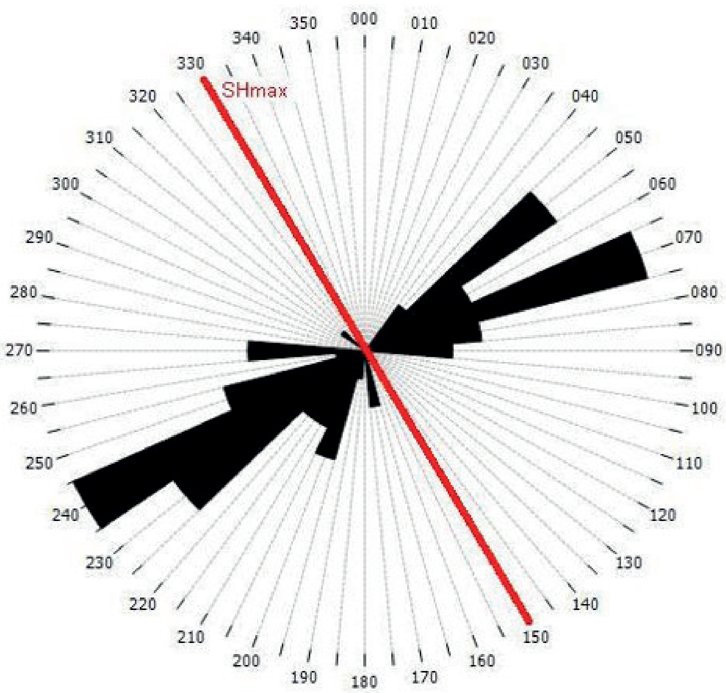

Fig. 5. *Distribution of azimuths of breakout features directions in the Silurian-Ordovician interval in Wysin-1 borehole (black); the red line indicates estimated* SH_{max} *direction*

METHODS USED TO MAP LINEAR STRUCTURES

To identify structures that could be potential induced hydraulic fractures, the authors proposed a three-step procedure for separating linear structures. Each of the three methods used has an important function in identifying structures. The collapsing method involves minimizing the scattering of events created by localization errors. The HDBSCAN algorithm applied as the second step in the procedure can find groups of points with increased intensity of occurrence in relation to their surroundings. The last step of the procedure, the calculation of scatter ellipsoids for each cluster detected by HDBSCAN, makes it possible to determine the dominant direction of each structure for comparison with the direction of regional stress. Below is a description of each of the three methods used. A flowchart describing identification of linear structures is presented in Figure 6.

Collapsing

The locations of seismic events are generally subject to error, which is due to a simplified velocity model or errors in first-break picking. This results in the locations in the seismic cloud being scattered. To discover the pattern of seismicity, the dispersion of events must be minimized. To identify fractures created by hydraulic fracturing, a collapsing method (Jones & Stewart 1997) was used to increase the resolution of the seismic cloud.

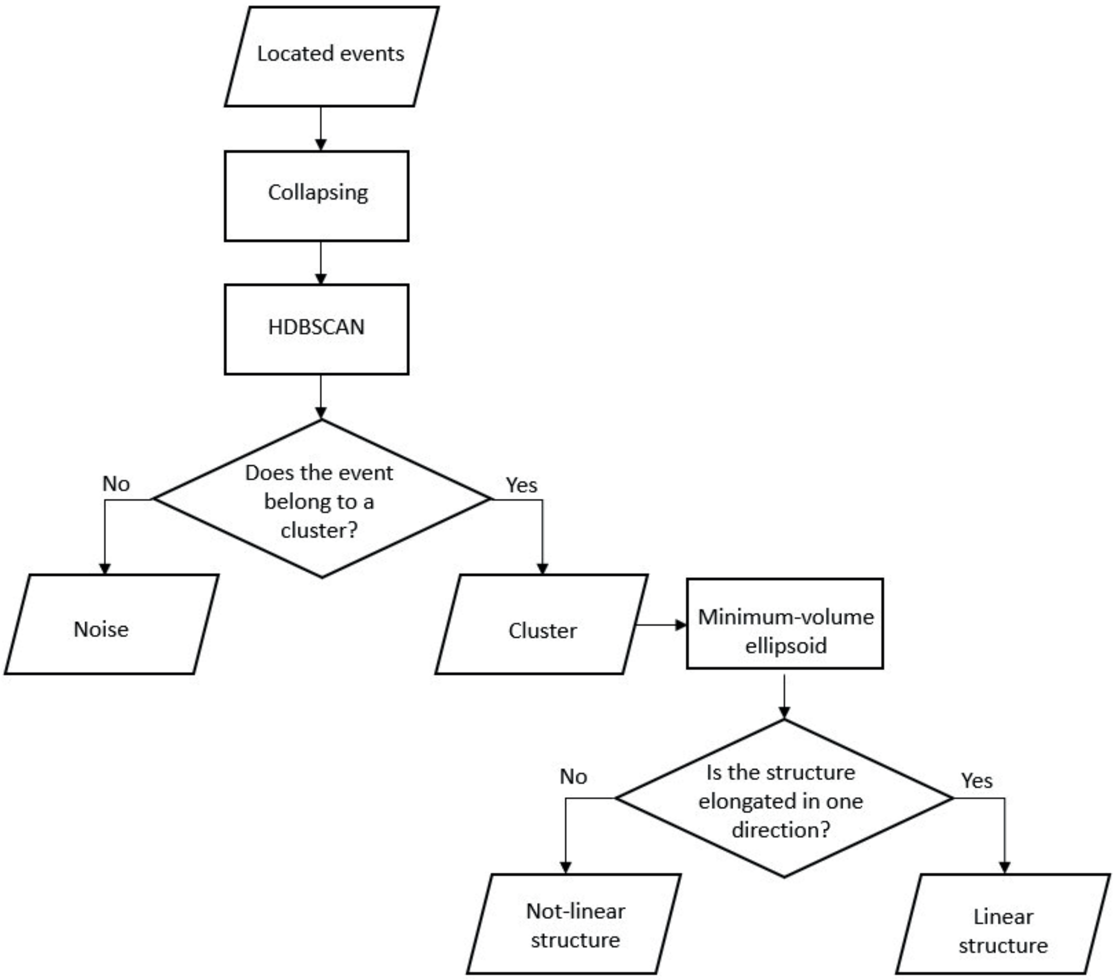

Fig. 6. *Flowchart describing linear structures identification*

This method enables a more tightly clustered character to be obtained from scattered event locations, thus allowing seismogenic structures to be identified. These structures can be pre-existing features related to tectonic deformation, such as cracks or fissures in the rock mass and associated with seismic emissions.

The first step required in the collapsing method is to determine the error ellipsoid for each seismic event. Under the assumption that errors are random and have a normal distribution, the error ellipsoids can be determined for each event by assuming a statistical significance level. The collapsing algorithm involves the gradual relocation of emission sources in the direction of local centers' densities. The relocation of each event takes place only inside its error ellipsoid. Relocation is performed iteratively until the translation population takes the form of an χ^2 distribution. This allows new locations of events to be obtained that are equivalent to original locations in a statistical sense. All the details of the algorithm's operations are described in more detail by its authors (Jones & Stewart 1997). While the collapsing method was originally presented for seismological data (Jones & Stewart 1997), it has also been adapted for microseismic data, e.g. (Evans et al. 2005, Leśniak et al. 2020, Węglińska & Leśniak 2021, 2024).

HDBSCAN algorithm

The HDBSCAN (Campello et al. 2013) automatic cluster detection method was used to identify structures formed or reactivated by hydraulic fracturing. The algorithm was used on the seismic cloud after the collapsing procedure. In this method, like in all algorithms in the group of density-based clustering algorithms, e.g., (Ester et al. 1996, Ankerst et al. 1999), clusters are groups of events whose density is higher than that of points outside clusters (Kriegel et al. 2011). The algorithm identifies so-called cluster cores as seismic sources in whose vicinity (closer than the predetermined epsilon value (ε) – the radius of the neighborhood) there is a minimum number of neighboring hypocenters. New hypocenters that are within eps distance of any of the core sources are attached to the cluster cores. Hypocenters that are not included in any of the clusters are defined as noise. HDBSCAN has the advantage over other algorithms in the group of density-based clustering algorithms that it requires only one parameter, which is the minimum number of points forming a cluster. HDBSCAN builds a hierarchy of all possible clusters for different values of neighborhood distance and extracts clusters with the best stability. This method was chosen from other clustering methods because of its ability to identify noise and find clusters of different shapes, and it does not need to assume the number of clusters.

Mapping linear clusters on the basis of HDBSCAN

To check which clusters identified by HDBSCAN might correspond to linear structures, scatter ellipsoids were calculated, i.e., minimum-volume ellipsoids containing all points in each cluster. This method makes it possible to determine the directions of structures based on the length of the ellipsoid's semi-axis (l_1, l_2, l_3). To investigate whether a structure is elongated in one direction, an elongation coefficient (E) (Zhou et al. 2019) is calculated on the basis of the lengths of the ellipsoids' semi-axes. Assuming that for each ellipsoid the lengths of the semi-axes fulfill the condition $l_1 \geq l_2 \geq l_3$, the elongation coefficient is defined as:

$$E = \frac{l_2}{l_1}.$$

RESULTS

The first step of the scattering reduction procedure was an evaluation of the error ellipsoids for all hypocenters. The spatial orientation of each ellipsoid is determined by the relative position of the event location and the geophones. The size of the ellipsoid depends on the error in determining the location for the chosen confidence level. The error ellipsoids for the location of the hypocenters of two sample events at a significance level of 99.8% are shown in Figure 7. The collapsing procedure involves iteratively moving events toward the center of gravity inside the ellipsoid until the translation vector achieves a χ^2 distribution with three degrees of freedom. In each iteration, the Kolmogorov–Smirnov test of the correspondence of the empirical distribution with the theoretical distribution χ^2 is performed.

In the fourth iteration, the goodness of fit of empirical and theoretical distributions was obtained. The goodness of fit of theoretical and empirical distribution for the first and the last iteration is shown in Figure 8A and B respectively. If, for the entire cloud, the source displacement fulfills this condition, the seismic cloud after relocation statistically corresponds to the original cloud before relocation. The relocated seismic cloud illustrates the spatial distribution of sources allowed within the location error. The relocated seismic cloud after using the collapsing algorithm is shown in Figure 9.

It can be noted that the distribution of collapsed events is more heterogeneous than before the procedure. A clustering of points along linear structures is evident. On the basis of collapsed events, the unsupervised HDBSCAN machine learning method was used to identify clusters that could correspond to induced hydraulic fractures. From the cloud of seismic events, the algorithm extracted clusters with an increased density of events relative to the surroundings. A minimum number of 10 events per cluster was imposed. The number of events needed to form a cluster was chosen based on tests of different values of this parameter.

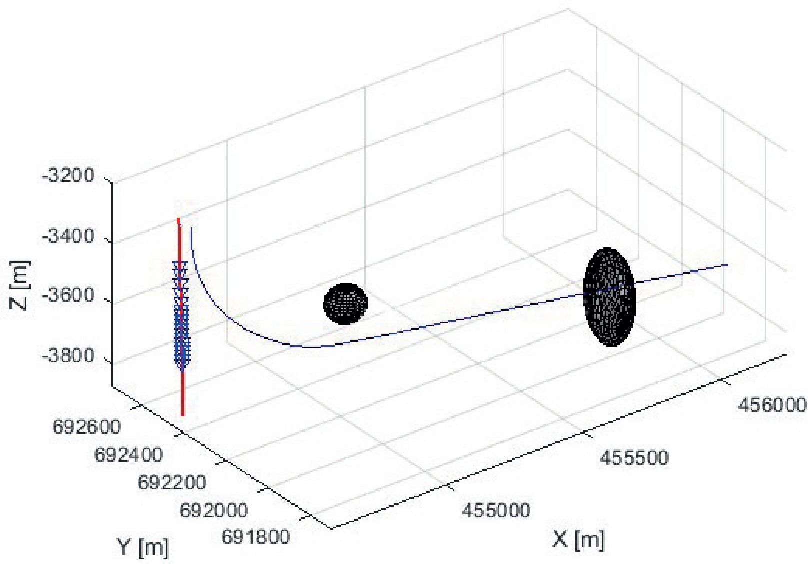

Fig. 7. *Error ellipsoids used in the collapsing procedure for the two selected events*

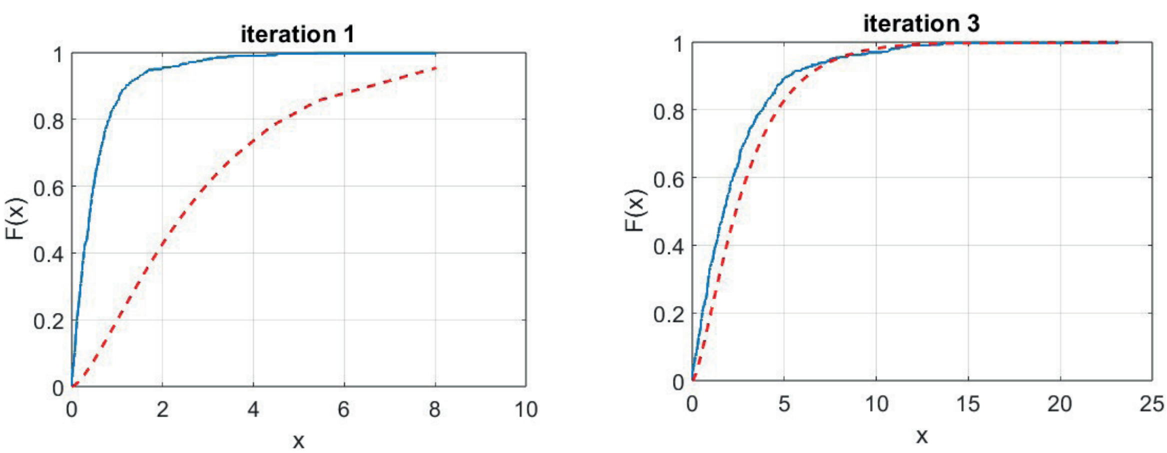

Fig. 8. *Comparison of theoretical (blue solid curve) and empirical (red dashed curve) distribution: A) first iteration; B) last iteration*

A larger number of events results in mutual aggregation of clusters, while with a smaller number the algorithm did not find linear clusters. The result of the HDBSCAN algorithm is a hierarchical representation of all possible clustering, i.e., for all potential radius values (ε). The HDBSCAN hierarchy is presented in Figure 10 in a simplified form; it shows cluster-wide changes depending on the eps value, and the most stable clusters are outlined in red. HDBSCAN identified 12 clusters and 212 noise points. These clusters have different shapes, dimensions, and population sizes. The population in each cluster is listed in Table 1.

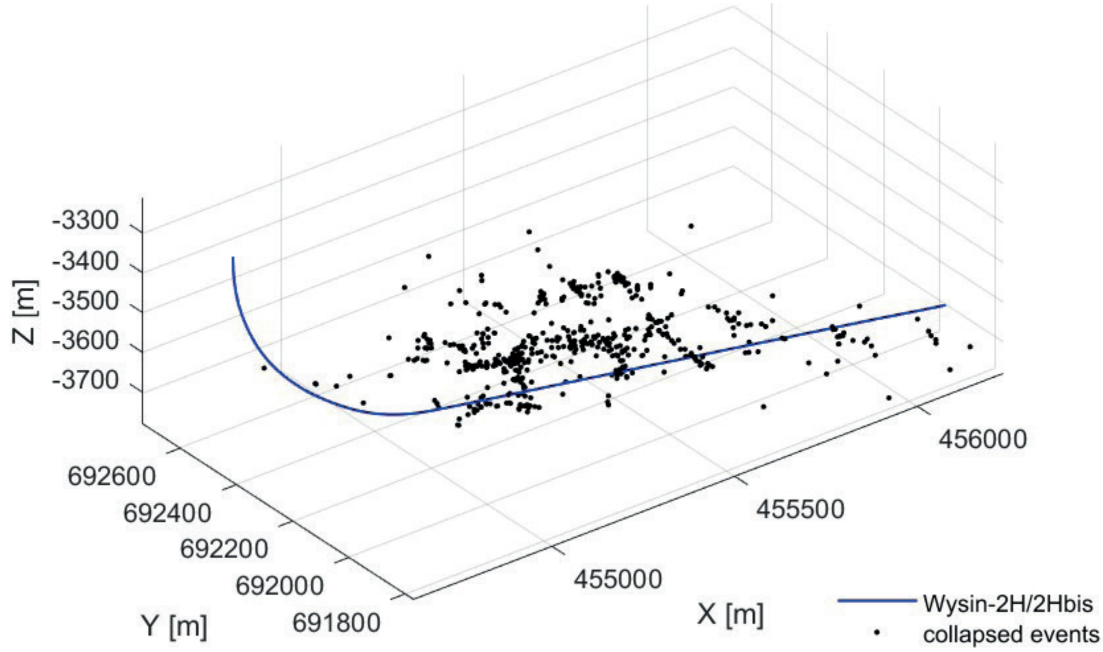

Fig. 9. *Result of applying the collapsing method to the microseismic cloud*

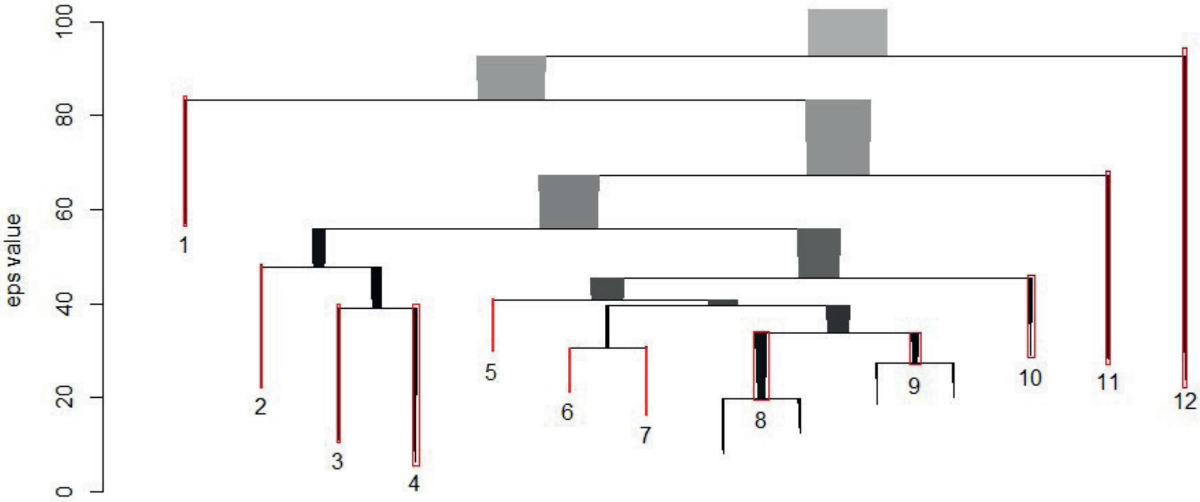

Fig. 10. *Cluster hierarchy after applying the HDBSCAN algorithm for all possible radius values. The most stable clusters are outlined in red*

Table 1
Events population in each cluster

Cluster number	1	2	3	4	5	6	7	8	9	10	11	12
Number of events	19	14	19	10	23	44	36	11	14	59	91	13

The result of applying the HDBSCAN algorithm to the set of microseismic events after the collapsing procedure is shown in Figure 11. The hypocenters marked in grey represent noise, while the hypocenters in other colors indicate individual clusters. To illustrate the need to apply the collapsing procedure, the Figure 12 shows the result of the detection of clusters in the original seismic cloud using the same parameters as for the collapsed cloud. Clusters identified in this point cloud do not present any obvious structures due to dispersion of events.

In the case of a normal stress regime, the direction of crack development and propagation should follow the direction of SH_{max} (Zoback 2010) that is observed for the distribution of events in the seismic clouds before (Fig. 13) and after applying the collapsing procedure (Fig. 14). The results after collapsing are characterized by organization into discrete clusters. The directions of these clusters are more consistent with SH_{max}. On the other hand, the asymmetry of fracture development, which was not evident in the distribution of events before collapsing, increased significantly. After reprocessing, the single-wing nature of the fracture network development in the NNW direction is visible. In particular, this is best seen for later stages of hydraulic fracturing.

The identified clusters are considered as possible structures that developed in the fracturing area. In Figure 15, each identified clusters' scatter ellipsoid is presented, which is a minimum-volume ellipsoid that contains all points in the cluster.

It was assumed that the structure should be elongated in one direction to indicate a potential fracture, i.e., the length of one half-axis must be greater than the other half-axes.

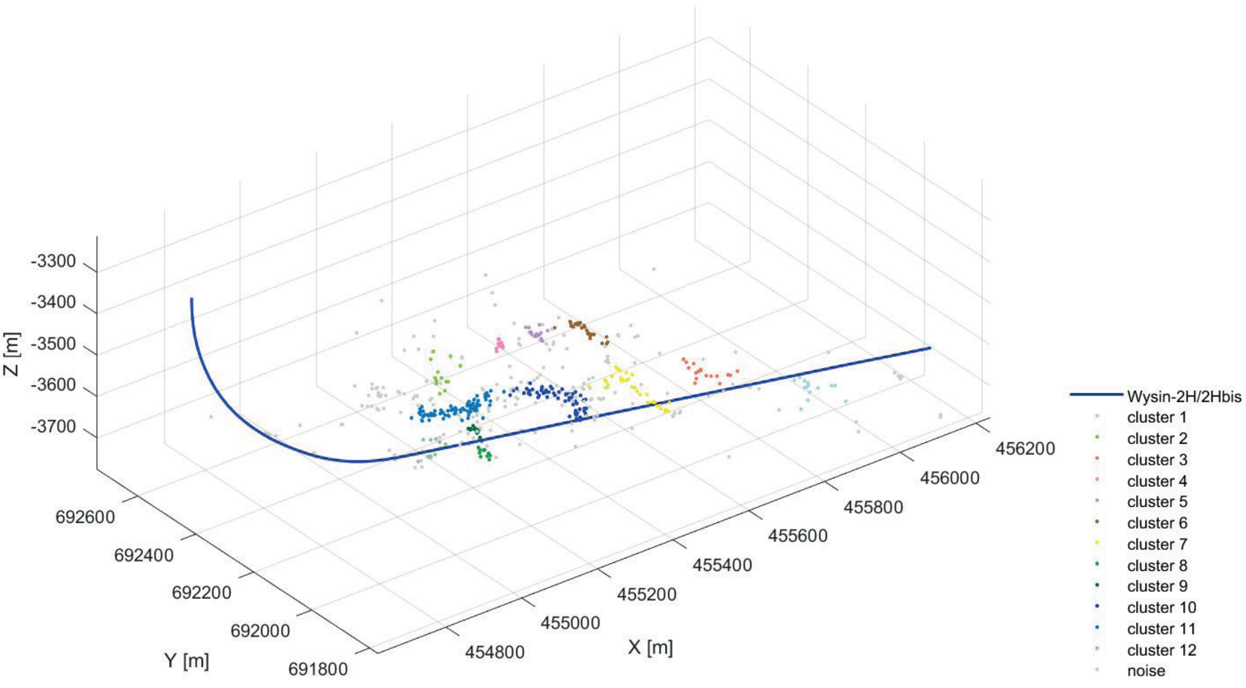

Fig. 11. *Results of applying the HDBSCAN clustering algorithm to the locations of collapsed events*

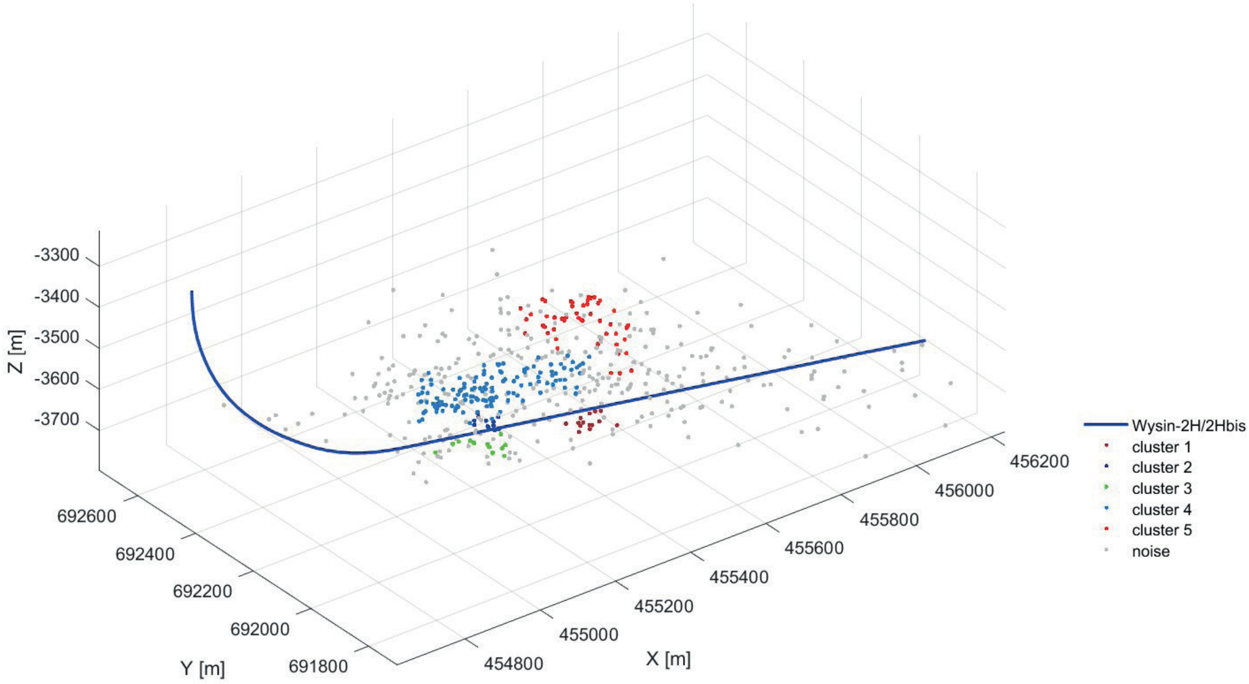

Fig. 12. *Results of applying the HDBSCAN clustering algorithm to the original locations of seismic events*

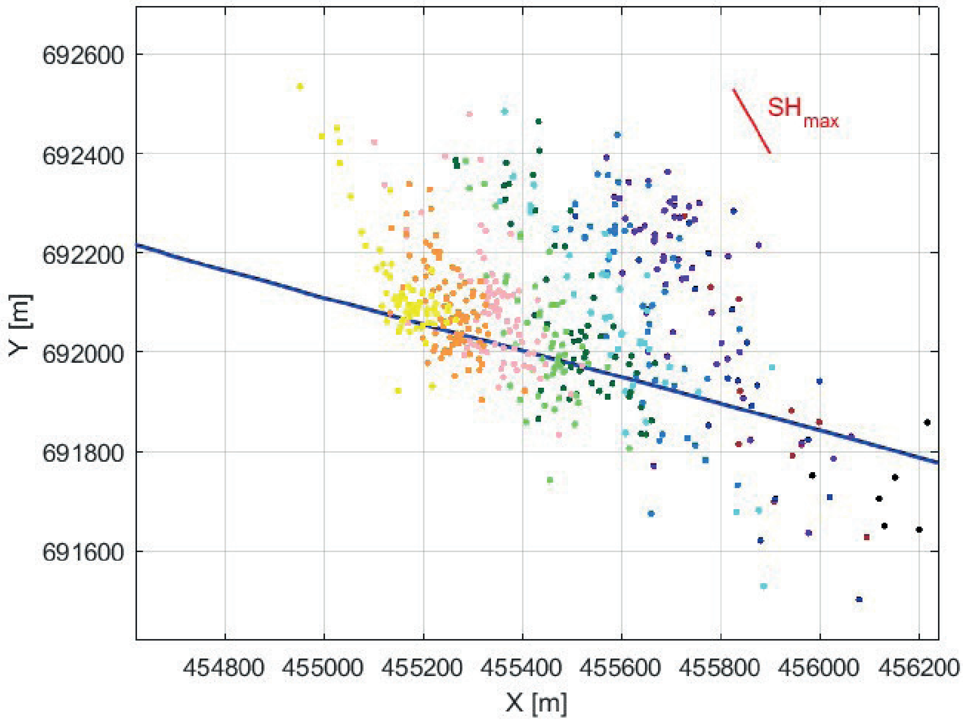

Fig. 13. *Distribution of seismic events before the collapsing procedure against the direction of regional horizontal maximum stress. The events are colored by stages*

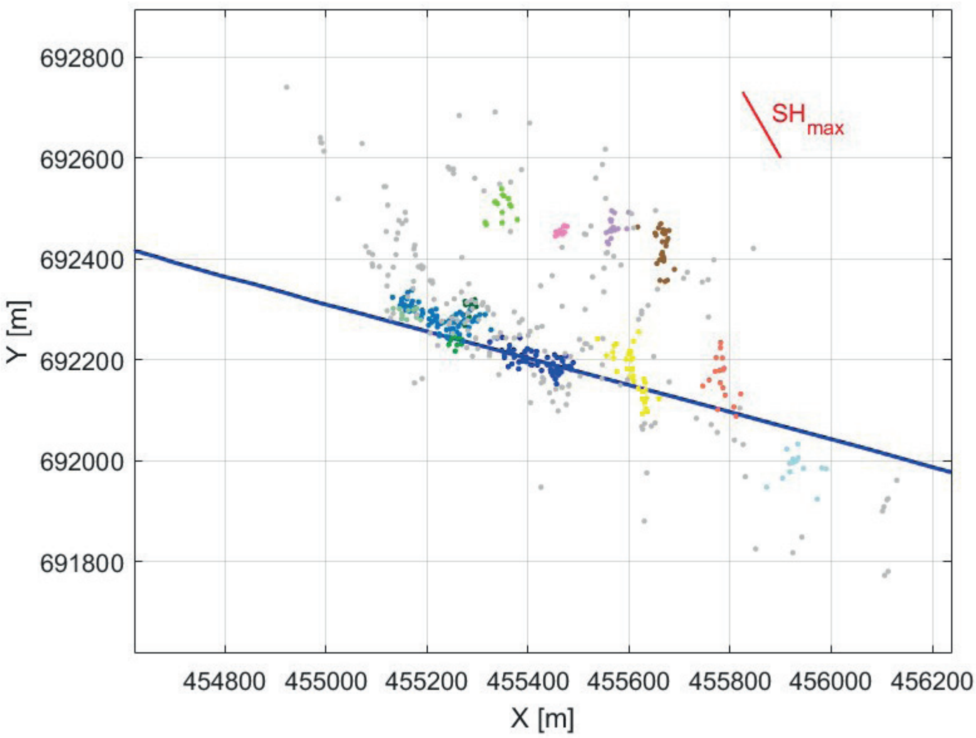

Fig. 14. Distribution of seismic events after the collapsing procedure against the direction of regional horizontal maximum stress. Grey represents points identified as noise; other colors indicate the separated clusters

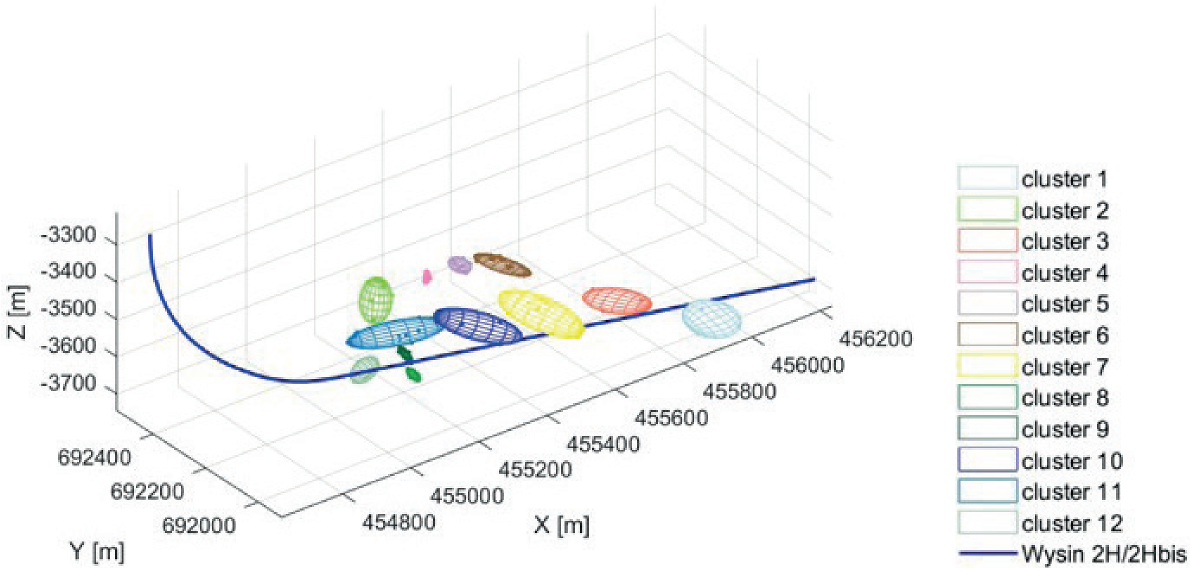

Fig. 15. Minimum-volume ellipsoids containing all events in each cluster

Based on the elongation ratio of the structures (see Table 2), it was concluded that the potential fractures might correspond to cluster numbers 3, 6, 7, 9, 10, 11, 12. To compare the directions of the ellipsoids for each cluster with the regional maximum horizontal stress, the projection of clusters described by the ellipsoids in the horizontal plane is shown in Figure 16.

Table 2
Lengths of the semi-axes and the elongation coefficient for each ellipsoid

Parameter	Cluster number											
	1	**2**	**3**	**4**	**5**	**6**	**7**	**8**	**9**	**10**	**11**	**12**
l_3	10.415	37.230	18.368	7.596	4.591	2.970	31.163	3.838	6.354	32.782	25.145	14.166
l_3	68.108	44.988	44.991	16.880	25.219	34.711	52.849	18.310	13.890	41.127	43.540	27.353
l_3	72.193	55.598	95.766	18.038	42.486	77.680	111.661	21.646	36.948	114.633	120.630	39.010
E	0.943	0.809	0.4698	0.936	0.594	0.447	0.473	0.846	0.376	0.359	0.361	0.701

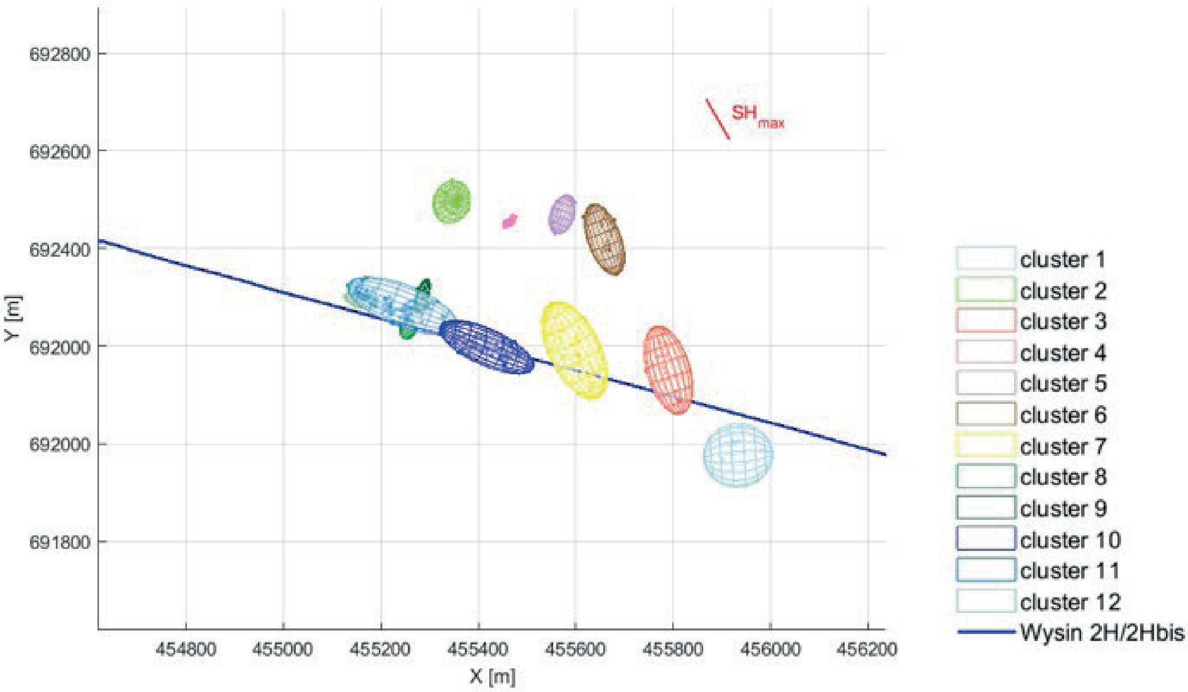

Fig. 16. *Minimum-volume ellipsoids containing all events in each cluster and the direction of the regional maximum horizontal stress (top view)*

DISCUSSION

The results presented above illustrate an attempt to identify linear structures based on seismic event locations. To perform a validation of our results using the proposed procedure, the results were compared with the 3D seismic image, which has a much higher resolution than seismicity cloud. The seismic data before and after collapsing were compared against the Wysin 3D seismic survey (a full description of the processing and the interpretation can be found in the unpublished PhD thesis by Pasternacki (2017)). The data were subjected to a standard seismic processing procedure that applied pre-stack time migration. These results made it possible to perform simultaneous pre-stacking inversion (Pendrel & Dickson 2003), thus the Z_P (P-wave impedance) and Z_S (S-wave impedance) attributes could be obtained. A detailed discussion of the operation of simultaneous inversion is presented by Veeken (2007) or Ma (2002). Simultaneous inversion provides information on rock properties, i.e., porosity, water saturation, and lithology. The resolution of the results of such an inversion is higher than in the original seismic image due to the broadening of the spectrum in the higher frequency range based on acoustic profiling measurement data. Simultaneous inversion is used directly to determine the physical properties of rocks based on estimates of their elastic parameters. For surface seismic, these are acoustic impedance (Z_P), Poisson's ratio, density (ρ), and S-wave impedance (Z_S). Density estimation from seismic sections requires the use of a seismic volume containing good-quality seismic reflections from the 40–55° angle range. Due to the limited range of offsets in the data in question, it was not possible to perform seismic inversion to identify the density-defining factor. In recent years, a number of benchmark cross-plots have been developed that estimate the relationship between elastic moduli and lithological formation based on seismic reflection data (Goodway et al. 1997, Perez 2013). Transformation of obtained volumes after prestack seismic inversion Z_P ($Z_P = V_P\rho$, where V_P is compressional velocity, ρ is density) and Z_S ($Z_S = V_S\rho$, where V_S is share wave velocity) to the λρ-μρ space (where λ and μ are Lame parameters) allows the partial interpretation of these parameters, even in the present situation, where the pre-stack inversion failed to produce a ρ volume due to above mentioned quality concerns in reflection angles beyond 40°. LMR (λρ-μρ) analysis provides quantitative information determining lithology, porosity, or reservoir fluid filling (Goodway et al. 1997). The analysis of P-wave impedance with respect to the ratio of P-wave velocity to S-wave velocity can be used to interpret geomechanical parameters. However, interpretation of changes in these parameters is more easily done with LMR analysis.

To test the effectiveness of the collapsing method for localized events in the Wysin-2H/2Hbis experiment, the hypocenters were plotted against a 3D seismic image. Based on the results of geomechanical parameter calculations for geophysical measurements in the Wysin-1 borehole (Poisson coefficient, Young modulus, geomechanical brittleness coefficient) (Perez & Marfurt 2013), the probability classes of the brittleness index in the LMR parameter domain were determined (Boyd et al. 2010) based on the borehole data. Based on the Z_P and Z_S attributes, the probability of a given brittleness index was estimated for the whole space. Figures 17 and 18 show the probability classes of a given range of the brittleness index on a color scale, where 1 indicates rocks with low susceptibility to fracturing, and 4 indicates brittle rocks with higher susceptibility to fracturing. Brittleness maps are shown for 4 depth sections, labeled A-D. Above each map, the depth range of events is shown. The first value refers to the minimum depth of event occurrence, the middle value is the depth cut by the parametric model, and the last is maximum depth of event occurrence. The map labeled A covers the deepest area, while the letter D labels the shallowest surface. Brittleness maps are shown for the original event locations and the relocated event locations at cross-sections of the same depth. It can be noted that for the original locations of events, we are unable to determine whether they occur in more brittle or ductile zones. The distribution of collapsed events, some of which coincide with regions identified as more brittle shows that there is a tendency for rock to fracture preferentially in these areas. In a seismological context, low brittleness index values can also be characterized as areas where less earthquakes will be generated, but more energy accumulation will occur there. In areas with higher brittleness indices, more small earthquakes can be expected. Comparing the two results before and after the collapsing procedure, it can therefore be assumed that the observed asymmetry of later stages of hydraulic fracturing may be related to the transition of the Wysin-2H/2Hbis well to a zone less prone to fracture development. In particular, anomalies "b" and "c" can be interpreted as barriers to fracture development in the south direction, while anomaly "a" is bypassed by microseismic events.

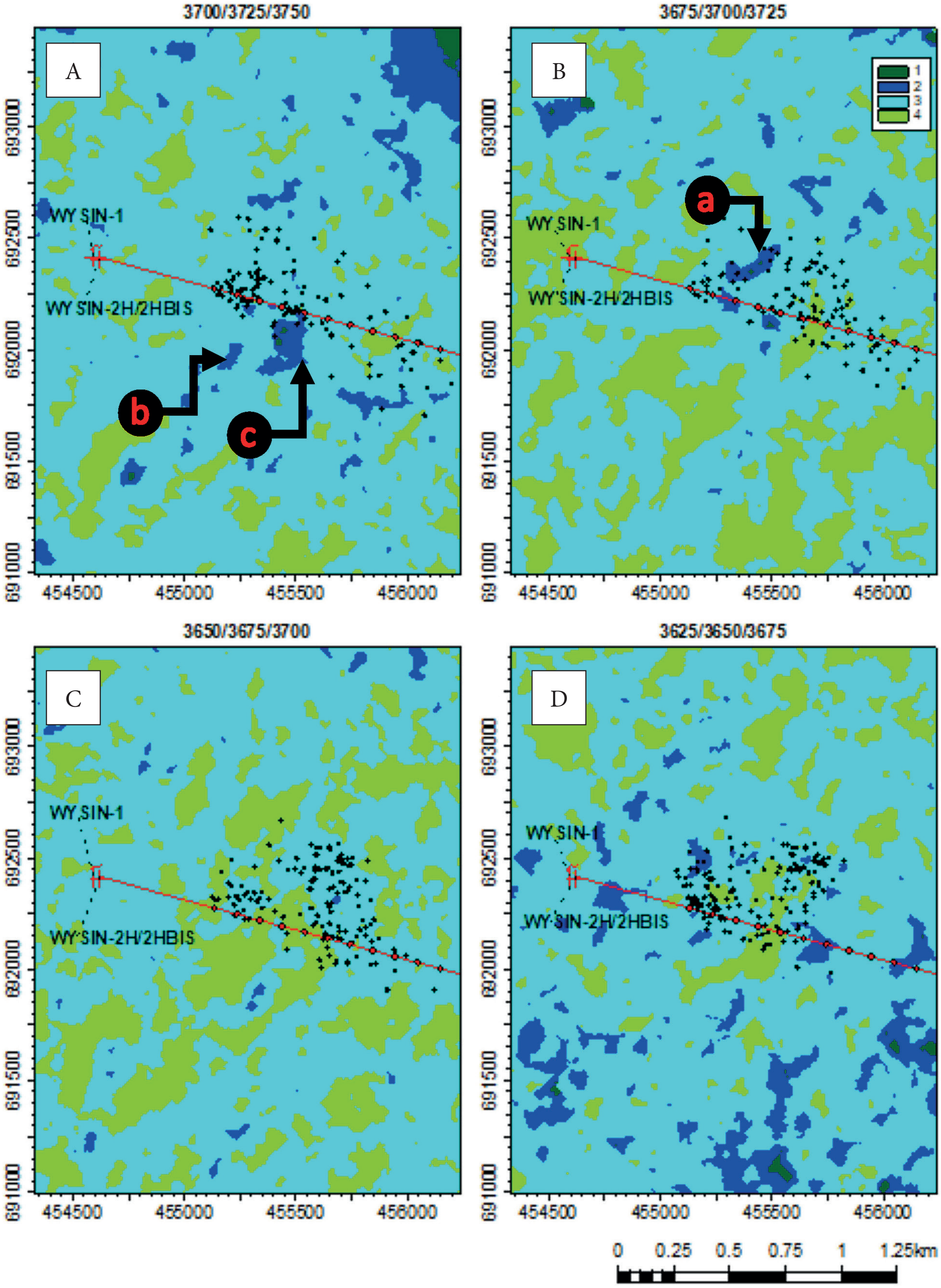

Fig. 17. *Probability classes of the brittleness index on microseismic location data before the collapsing procedure: a, b, c – anomalous index values (description in the text). The numerical values above each map refer to minimum depth of event occurrence, depth cut by the parametric model, and maximum depth of event occurrence. Event locations contained within the specific depth interval are shown with black dots. The class 1 indicates rocks with low susceptibility to fracturing, while 4 indicates brittle rocks with higher susceptibility to fracturing*

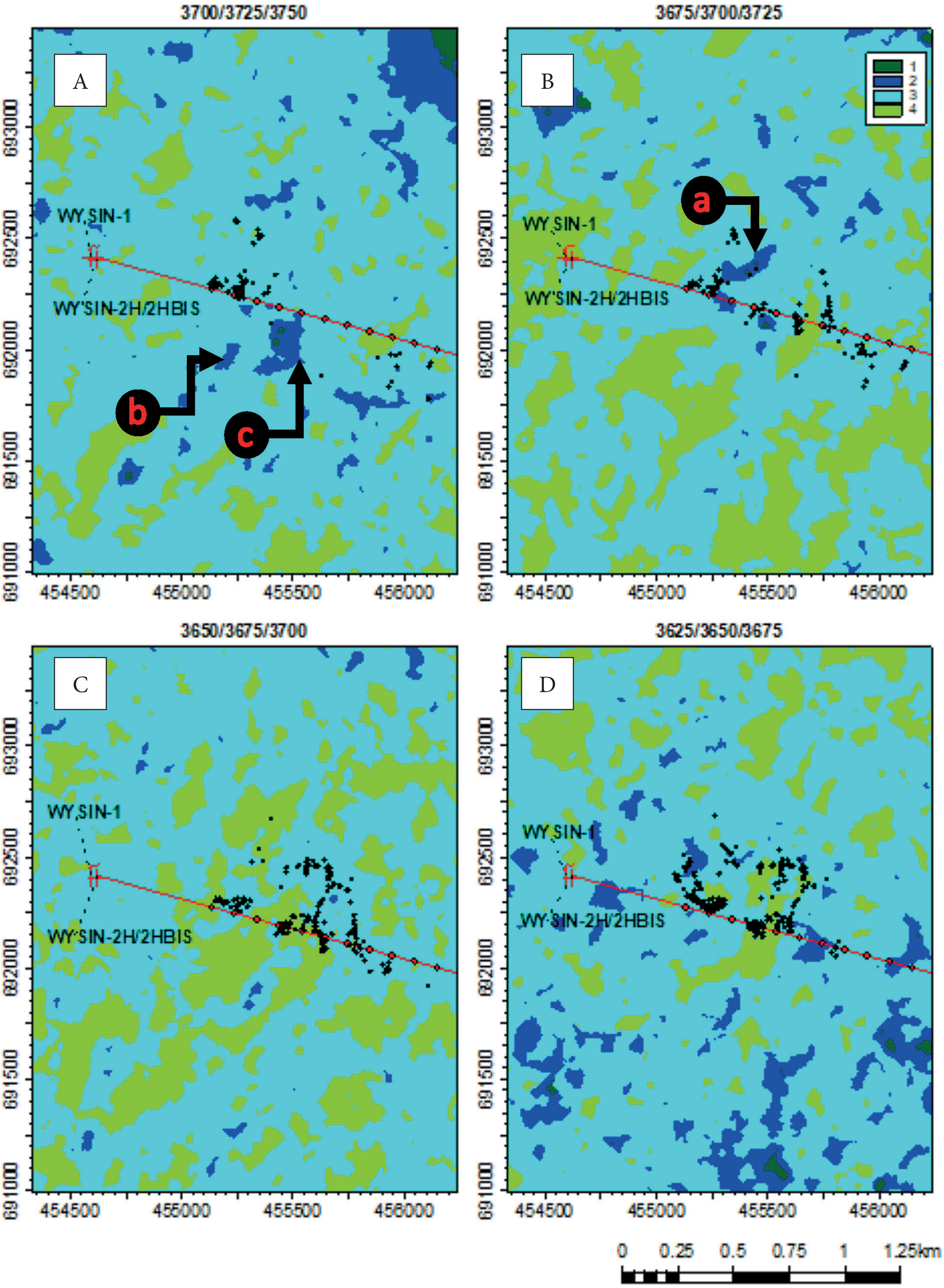

Fig. 18. *Probability classes of the brittleness index superimposed on microseismic location data after the collapsing procedure: a, b, c – anomalous index values (description in the text). The numerical values above each map refer to minimum depth of event occurrence, depth cut by the parametric model, and maximum depth of event occurrence. Event locations contained within the specific depth interval are shown with black dots. The class 1 indicates rocks with low susceptibility to fracturing, while 4 indicates brittle rocks with higher susceptibility to fracturing*

CONCLUSIONS

Precise imaging of fractures in a scattered seismic cloud is difficult due to event location errors. To identify fractures created during HF, the authors proposed an integrated approach comprising the collapsing method, HDBSCAN clustering, and delineating the linear structures based on the elongation coefficient. These methods were demonstrated on microseismic events located during the fracturing of the Wysin-2H/2Hbis well. The use of the collapsing method made it possible to reduce the dispersion of the cloud of seismic events that results from location errors. Clustering made it possible to separate the areas with increased intensity of events relative to the surrounding area and noise. Determination of the scatter ellipsoid for each separated cluster enabled calculation of the elongation factor, on the basis of which the linear structures were identified. Of the 12 detected clusters, 8 of them can be considered linear structures. The direction determined by the longest semi-axis of the ellipsoid for each structure was contrasted with the direction of maximum horizontal stress. These structures were identified in the earlier stages of fracturing. This approach made it possible to distinguish structures suspected of transporting shale gas. It is important to note that the identified structures do not need to be individual fissures; they can include a series of smaller ones. However, they are located close enough to each other that clustering methods identify them as one large structure. Distinguishing the structures that may be responsible for fluid flow is key to estimating the effectiveness of fracturing. The probability of a given brittleness index was estimated as a technique for recognizing brittle and ductile regions. Comparing the brittleness maps with the seismic cloud before and after collapsing, there appears to be some correlation where the locations after applying the algorithm appeared in more rigid regions. These are areas where we expect more energy release. The results presented in this paper have significant implications for the interpretation of induced seismicity resulting from hydraulic fracturing. Accurate delineation of structures based on the location of microseismic events is key to determining the extent of fracturing. The integrated approach proposed by the authors for fracture identification can be applied to any induced seismicity data.

This study is part of the project "Appraisal of microseismic monitoring techniques of hydraulic fracturing and development of optimal processing and interpretation methodologies" (SHALEGASMICROS), funded by the Polish National Center for Research and Development within the Program Blue Gas. The authors are grateful to PGNiG SA for generously providing downhole data and seismic data for research purposes. We are very much indebted to the Schlumberger and the Halliburton Landmark Solutions companies for provision of geophysical data interpretation and processing software through the University Software Grants Programs. This research was supported by AGH University of Krakow, Faculty of Geology, Geophysics and Environmental Protection as a part of the statutory project.

REFERENCES

Ankerst M., Breunig M.M., Kriegel H.P. & Sander J., 1999. OPTICS: Ordering points to identify the clustering structure. [in:] *Proceedings of the 1999 ACM SIGMOD International Conference on Management of Data: SIGMOD '99, Philadelphia, PA, USA, June 1–3, 1999: Vol. 28*, Association for Computing Machinery, New York, 49–60. https://doi.org/10.1145/304182.304187.

Bell J.S. & Gough D.I., 1979. Northeast-southwest compressive stress in Alberta evidence from oil wells. *Earth and Planetary Science Letters*, 45(2), 475–482. https://doi.org/10.1016/0012-821X(79)90146-8.

Boyd N.K., Cardenas M. & Galarraga M., 2010. Improved reservoir characterization using prestack analyses, Eden Yuturi field, Ecuador. [in:] *SEG Technical Program Expanded Abstracts 2010*, Society of Exploration Geophysicists, 2265–2269. https://doi.org/10.1190/1.3513301.

Campello R.J.G.B., Moulavi D. & Sander J., 2013. Density-based clustering based on hierarchical density estimates. in advances in knowledge discovery and data mining. [in:] Pei J., Tseng V.S., Cao L., Motoda H. & Xu G. (eds.), *Advances in Knowledge Discovery and Data Mining: PAKDD 2013*, Lecture Notes in Computer Science, 7819, Springer, Berlin, Heidelberg, 160–172. https://doi.org/10.1007/978-3-642-37456-2_14.

Ester M., Kriegel H.P., Sander J. & Xu X., 1996. A density-based algorithm for discovering clusters in large spatial databases with noise. [in:] Simoudis E., Han J. & Fayyad U. (eds.), *KDD'96: Proceedings of the Second International Conference on Knowledge Discovery and Data Mining*, AAAI Press, Portland, Oregon, 226–231.

Evans K.F., Moriya H., Niitsuma H., Jones R.H., Phillips W.S., Genter A., Sausse J., Jung R. & Baria R., 2005. Microseismicity and permeability enhancement of hydrogeologic structures during massive fluid injections into granite at 3 km depth at Soultz HDR site. *Geophysical Journal International*, 160(1), 388–412. https://doi.org/10.1111/j.1365-246X.2004.02474.x.

Goodway B., Chen T. & Downton J., 1997. Improved AVO fluid detection and lithology discrimination using Lamé petrophysical parameters: "λρ", "μρ", and "λ/μ fluid stack": from P and S inversions. [in:] *SEG Technical Program Expanded Abstracts 1997*, Society of Exploration Geophysicists, 183–186. https://doi.org/10.1190/1.1885795.

Jones R.H. & Stewart R.C., 1997. A method for determining significant structures in a cloud of earthquakes. *Journal of Geophysical Research: Solid Earth*, 102(B4), 8245–8254. https://doi.org/10.1029/96JB03739.

Kriegel H.P., Kröger P., Sander J. & Zimek A., 2011. Density-based clustering. *WIREs Data Mining and Knowledge Discovery*, 1(3), 231–240. https://doi.org/10.1002/widm.30.

Leśniak A., Śledź E. & Mirek K., 2020. Detailed recognition of seismogenic structures activated during underground coal mining: A case study from Bobrek Mine, Poland. *Energies*, 13(18), 4622. https://doi.org/10.3390/en13184622.

Lopez-Comino J.A., Cesca S., Jaroslawski J., Montcoudiol N., Heimann S., Dahm T., Lasocki S., Gunning A., Capuano P. & Ellsworth W.L., 2018. Induced seismicity response of hydraulic fracturing: results of a multidisciplinary monitoring at the Wysin site, Poland. *Scientific Reports*, 8, 8653. https://doi.org/10.1038/s41598-018-26970-9.

Ma X.Q., 2002. Simultaneous inversion of prestack seismic data for rock properties using simulated annealing. *Geophysics*, 67, 1877–1885. https://doi.org/10.1190/1.1527087.

Maxwell S.C., 2013. Unintentional seismicity induced by hydraulic fracturing. *CSEG Recorder*, 38(08), 40–49.

Maxwell S.C., 2014. *Microseismic Imaging of Hydraulic Fracturing: Improved Engineering of Unconventional Shale Reservoirs*. Distinguished Instructor Series, 17, Society of Exploration Geophysicists. https://doi.org/10.1190/1.9781560803164.

Maxwell S.C., Mack M., Zhang F., Chorney D., Goodfellow S.D. & Grob M., 2015a. Differentiating wet and dry microseismic events induced during hydraulic fracturing. [in:], *SPE Unconventional Resources Technology Conference 2015: San Antonio, Texas, USA, 20–22 July 2015*, https://doi.org/10.15530/urtec-2015-2154344.

Maxwell S.C., Chorney D. & Goodfellow S.D. 2015b. Microseismic geomechanics of hydraulic-fracture networks: Insights into mechanisms of microseismic sources. *The Leading Edge*, 34(8), 904–910. https://doi.org/10.1190/tle34080904.1.

Pasternacki A., 2017. *Ocena efektywności procesu szczelinowania hydraulicznego w eksploatacji gazu ziemnego z łupków ilastych na podstawie badań mikrosejsmicznych* [*Appraisal of hydraulic fracturing effectiveness in the shale gas exploration based on microseismic monitoring*]. Akademia Górniczo-Hutnicza, Kraków [PhD thesis, unpublished].

Pendrel J. & Dickson T., 2003. Simultaneous AVO inversion to P impedance and Vp/Vs. [in:] *CSEG Annual Meeting Abstracts 2003*, Canadian Society of Petroleum Geologists, Calgary, 417S0131. https://old.cseg.ca/assets/files/resources/abstracts/2003/417S0131.pdf.

Perez R., 2013. Brittleness estimation from seismic measurements in unconventional reservoirs: Application to the Barnett Shale. [in:] *SEG Technical Program Expanded Abstracts 2013*, University of Oklahoma, Oklahoma, 2258–2263. https://doi.org/10.1190/segam2013-0006.1.

Perez R. & Marfurt K., 2013. *Calibration of brittleness to elastic rock properties via mineralogy logs in unconventional reservoirs* [conference poster]. AAPG International Conference and Exhibition. https://www.searchanddiscovery.com/documents/2013/41237perez/ndx_perez.pdf.

Poprawa P., 2010. Potencjał występowania złóż gazu ziemnego w łupkach dolnego paleozoiku w basenie bałtyckim i lubelsko-podlaskim [Shale gas potential of the Lower Palaeozoic complex in the Baltic and Lublin-Podlasie basins]. *Przegląd Geologiczny*, 58(3), 226–249.

U.S. Energy Information Administration (EIA), 2013. *Technically recoverable shale oil and shale gas resources: An assessment of 137 shale formations in 41 countries outside the United States*. U.S. Department of Energy, Washington. https://www.eia.gov/analysis/studies/worldshalegas/pdf/overview.pdf [access: 18.04.2024].

Veeken P.C.H., 2007. *Seismic Stratigraphy, Basin Analysis and Reservoir Characterisation*. Elsevier, Amsterdam.

Wandycz P., 2022. *Wyznaczenie współczynnika dobroci Q na podstawie zdarzeń mikrosejsmicznych indukowanych podczas procesu szczelinowania hydraulicznego oraz ocena możliwości jego wykorzystania w przetwarzaniu danych mikrosejsmicznych* [*Determination of the quality factor Q from microseismic events induced during the hydraulic fracturing process and evaluation of its applicability in microseismic data processing*]. Akademia Górniczo-Hutnicza, Kraków [PhD thesis, unpublished].

Wandycz P., Święch L., Eisner L., Pasternacki A., Wcisło M. & Maćkowski T., 2019. Estimation of the quality factor based on the microseismicity recordings from Northern Poland. *Acta Geophysica*, 67, 2005–2014. https://doi.org/10.1007/s11600-019-00362-7.

Węglińska E. & Leśniak A., 2021. Induced seismicity and detailed fracture mapping as tools for evaluating HDR Reservoir Volume. *Energies*, 14(9), 2593. https://doi.org/10.3390/en14092593.

Węglińska E. & Leśniak A., 2024. A novel approach to identifying seismogenic structures and estimating reservoir volume based on synthetic cloud of seismicity induced by hydraulic fracturing. *Acta Geodaetica et Geophysica*. https://doi.org/10.1007/s40328-024-00442-1.

Williams-Stroud S. & Billingsley R.L., 2010. Techniques to estimate fracture effectiveness when mapping low-magnitude microseismicity. [in:] *SEG Technical Program Expanded Abstracts 2010*, Society of Exploration Geophysicists, Houston, 2075–2079. https://doi.org/10.1190/1.3513253.

Zaręba M. & Danek T., 2018. VSP polarization angles determination: Wysin-1 processing case study. *Acta Geophysica*, 66, 1047–1062. https://doi.org/10.1007/s11600-018-0200-8.

Zaręba M., Danek T. & Stefaniuk M., 2021. P-wave-only inversion of challenging walkaway VSP data for detailed estimation of local anisotropy and reservoir parameters: A case study of seismic processing in Northern Poland. *Energies*, 14(8), 2061. https://doi.org/10.3390/en14082061.

Zhou C., Zhang M., Li Y., Lu J. & Chen J., 2019. Influence of particle shape on aggregate mixture's performance: DEM results. *Road Materials and Pavement Design*, 20(2), 399–413. https://doi.org/10.1080/14680629.2017.1396236.

Zoback M.D., 2010. *Reservoir Geomechanics*. Cambridge University Press, Cambridge.